Technische Universität Braunschweig

institut für thermodynamik ift

# Experimental and numerical analysis of a two-stage turbo compressor system for industrial superheated steam drying

## Masterarbeit

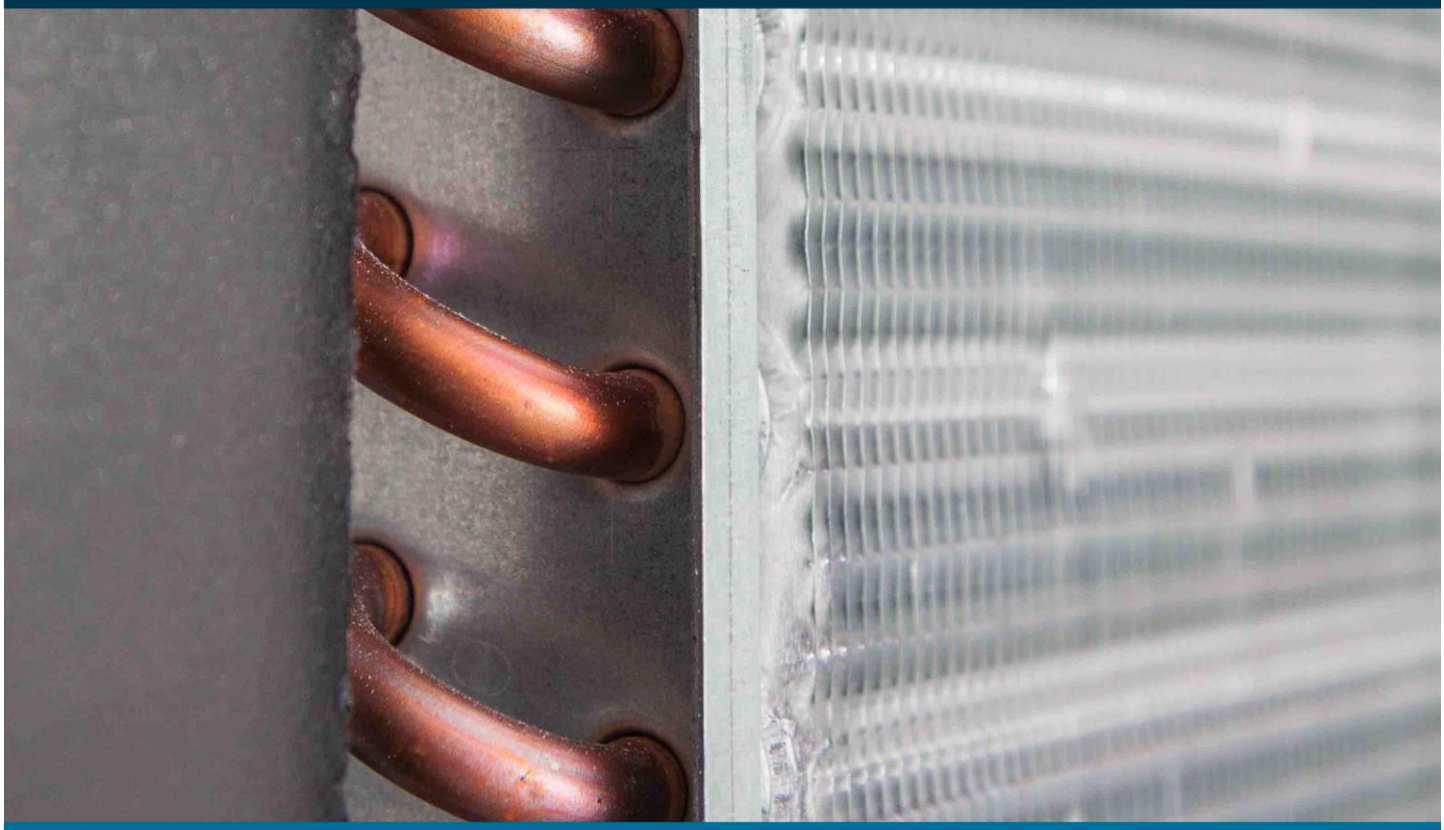


Autor: B. Sc. Marcel Ulrich Ahrens

Betreuer: M. Sc. Maximilian Hebeler

Prüfer: Prof. Dr.-Ing. Jürgen Köhler


10.07.2018

Technische Universität Braunschweig

institut für thermodynamik ift

# Masterarbeit

für Herrn Marcel Ulrich Ahrens

Matrikelnummer 4310389

## Experimental and numerical analysis of a two-stage turbo compressor system for industrial superheated steam drying

### Background and objective

Industrial drying and dehydration processes require intensive use of energy, and estimates show that 12-25% of the national industrial energy consumption in developed countries is attributable to industrial drying. Currently, most of this energy is based on the use of fossil fuels with no utilization of waste heat streams. Hence, there is a great potential for more efficient and environment-friendly technologies within industrial drying processes. Heat pump system can be applied in drying processes in order to reduce energy consumption and increase the share of renewable energy.

A newly developed compressor technology enables heat pumps working at high temperatures (i.e. up to 150°C). In order to evaluate the performance of the turbo compressors a test system was developed. This system is used in the Master Thesis to evaluate the compressor performance. The performance maps enable to analyse the overall mechanical vapour recompression (MVR)-system performance for a superheated steam dryer.

The objective of the Master Thesis is to analyse the thermodynamic perfomance of the turbo compressor technology experimentally, validate existing compressor models and evaluate the system performance of a two-stage turbo compressor MVR-system.

**The following tasks are to be considered:**

- Literature review of turbo compressor models covering high rotational speeds a wide operation range
- Uncertainty analysis of turbo compressor performance test facility at SINTEF Energy
- Conduct performance tests of turbo compressors
- Identify, select and validate compressor model
- Evaluating system performance using the validated compressor model
- Analyze and discuss model results
- Make proposal for further work

Prof. Dr.-Ing. Jürgen Köhler

# Preface and Acknowledgements

## Preface

Hiermit versichere ich, dass ich die vorliegende Masterarbeit selbstständig angefertigt, keine anderen als die mir erlaubten Hilfsmittel benutzt habe und die Stellen der Masterarbeit, die in Wortlaut oder im wesentlichen Inhalt aus anderen Werken entnommen wurden, mit genauen Quellenangaben versehen habe.

I declare that I have authored this thesis independently, that I have not used other than the declared sources / resources, and that I have explicitly marked all material which has been quoted either literally or by content from the used sources.

*Braunschweig, den 10. Juli 2018*

Marcel Ulrich Ahrens

## Acknowledgements

I would like to acknowledge SINTEF Energy Research for the support and opportunity to use facilities and expertise during the elaboration of my master's thesis.

The project has received funding from the European Union's Horizon 2020 programme for energy efficiency and innovation action under grant agreement No. 723576.

# Abstract

Industrial drying and dehydration processes require intensive use of energy and account for a large proportion of national industrial energy consumption in industrialized countries. Currently, a high share of this energy is based on the use of fossil fuels with limited utilization of waste heat streams. This leads to a great potential for improvement in order to reduce energy consumption and $CO_2$ emissions. For example, heat pump systems can be applied in drying processes to reduce energy consumption and increase the share of renewable energy while replacing the consumption of fossil fuels. A newly developed compressor technology enables the cost-effective use of heat pumps working at supply temperatures of up to 150 °C.

The aim of this master's thesis was the experimental analysis of the turbo compressor technology performance as well as the development of a numerical turbo compressor model and the evaluation of the two-stage turbo compressor performance.

To analyse the performance of the turbo compressors technology, experiments were performed at the test facility developed by SINTEF Energy Research. A suitable numerical turbo compressor model was identified and validated for the development of a system model. The achieved results and experiences were used for the evaluation of the two-stage turbo compressor performance.

The experiments demonstrated a stable operation of the two-stage turbo compressor system. The compressor maps have been created which allow an analysis of the performance and operating range of the turbo compressor. The numerical models were able to reproduce the results in a good approximation and allowed the estimation of further operating points. During this elaboration, the system was able to compress superheated steam from atmospheric pressure to above 3.0 bar, where it can be condensed at a saturation temperature of 133.5 °C. The COP of the performed investigation was 5.9, when the achievable condensation energy is compared to the total amount of energy supplied to the system.

# Table of Contents

# List of Figures

# List of Tables

# Nomenclature

**Latin letters**

| | | | | | |
|---|---|---|---|---|---|
| $A$ | Area | $(\mathrm{m}^2)$ | $\dot{m}$ | Mass flow | $\left(\frac{\mathrm{kg}}{\mathrm{s}}\right)$ |
| $c$ | Velocity | $\left(\frac{\mathrm{m}^2}{\mathrm{s}}\right)$ | $N$ | Impeller speed | (rpm) |
| $c_P, c_v$ | Specific heat capacity | $\left(\frac{\mathrm{J}}{\mathrm{kg} \cdot \mathrm{K}}\right)$ | $p$ | Pressure | (bar) |
| $C$ | Discharge coefficient | $(-)$ | $P$ | Power | (W) |
| $C_v$ | Coefficient of variation | $(-)$ | $\dot{Q}$ | Heat flow | (W) |
| $d$ | Inner diameter | (m) | $Re$ | Reynolds number | $(-)$ |
| $D$ | Outer diameter | (m) | $s$ | Specific entropy | $\left(\frac{\mathrm{kJ}}{\mathrm{kg} \cdot \mathrm{K}}\right)$ |
| $E$ | Energy | (W) | $T$ | Temperature | (K) |
| $h$ | Specific enthalpy | $\left(\frac{\mathrm{kJ}}{\mathrm{kg}}\right)$ | $\dot{V}$ | Volume flow | $\left(\frac{\mathrm{m}^3}{\mathrm{s}}\right)$ |
| $l$ | Length | (m) | $\dot{W}$ | Work flow | (W) |

**Greek letters**

| | | | | | |
|---|---|---|---|---|---|
| $\alpha$ | Heat transfer coefficient | $\left(\frac{\mathrm{W}}{\mathrm{m}^2 \cdot \mathrm{K}}\right)$ | $\Pi$ | Pressure ratio | $(-)$ |
| $\epsilon$ | Expansibility factor | $(-)$ | $\rho$ | Density | $\left(\frac{\mathrm{kg}}{\mathrm{m}^3}\right)$ |
| $\eta$ | Efficiency | $(-)$ | $\sigma, s$ | Standard deviation | $(-)$ |
| $\kappa$ | Isentropic exponent | $(-)$ | $\omega, \bar{X}$ | Sample mean | $(-)$ |
| $\mu$ | Dynamic viscosity | $\left(\frac{\mathrm{kg}}{\mathrm{m} \cdot \mathrm{s}}\right)$ | | | |

**Subscripts**

| | | | |
|---|---|---|---|
| 1 | First stage | *in* | Inlet |
| 2 | Second stage | *ins* | Instrument |
| *amb* | Ambient | *inverter* | Inverter |
| *c* | Cold | *isen* | Isentropic |
| *cal* | Calculated | *lift* | Lift |
| *carnot* | Carnot | *m* | Mean |
| *comp* | Compressor | *max* | Maximum |
| *cond* | Condensation | *out* | Outlet |
| *cool* | Cooling | *red* | Reduced |
| *design* | Design point | *ref* | Reference |
| *dif* | Diffuser | *sat* | Saturation |
| *dyn* | Dynamic | *set* | Set |
| *el* | Electrical | *surface* | Surface |
| *h* | Hot | *st* | Static |
| *hl* | Heat losses | *steam* | Steam |
| *imp* | Impeller | *t* | Total |

**Abbreviations**

| | | | |
|---|---|---|---|
| COP | Coefficient of performance | R.F. | Recovery factor |
| DAQ | Data acquisition system | SHS | Superheated steam |
| DryF | DryFiciency | TIL | TLK IfT Library |
| IfT | Institut für Thermodynamik – TU Braunschweig, Germany | TLK | TLK-Thermo GmbH, Germany |
| MVR | Mechanical vapour recompression | | |

# 1 Introduction

The following master's thesis deals with the experimental and numerical analysis of a two-stage turbo compressor system for industrial superheated steam drying.

The topic of this master's thesis is part of the DryFiciency (DryF) project which has received funding from the European Union's Horizon 2020 programme for energy efficiency and innovation action under grant agreement No. 723576[1]. The goal of the DryF project is to develop and demonstrate two types of high-temperature industrial heat pump systems for waste heat recovery in industrial drying processes. (AIT Austrian Institute of Technology GmbH, 2018)

## 1.1 Motivation

According to (Sannan, et al., 2016, p. 4), industrial drying and dehydration processes require intensive use of energy, and estimates show that 12 % to 25 % of the national industrial energy consumption in developed countries is attributable to industrial drying. Currently, a high share of this energy is based on the use of fossil fuels with limited utilization of waste heat streams. There is an accordingly large potential for more efficient and environment-friendly technologies within industrial drying processes. Heat pump systems can be applied in drying processes to reduce energy consumption and increase the share of renewable energy. (Sannan, et al., 2016, p. 4)

The goal of the integration of the novel high-temperature heat pump systems in industrial drying processes is to recover the waste heat streams, in order to reduce the specific energy demand as much as 60 % to 80 % in relation to the current demand (Sannan, et al., 2016, p. 4). In many industrial fields, hot steam is produced and used. If the energy of hot steam can be reused, the reduction of input energy and the increase

[1] https://www.cordis.europa.eu/project/rcn/205646_en.html

of efficiency for the industrial process can be expected. One of the ways to reuse hot steam is to use latent heat recovery technology using steam compression, also known as Mechanical Vapour Recompression (MVR). (Kang, et al., 2016, p. 1)

The newly developed turbo compressor technology is considered as a potentially cost-effective and efficient alternative to conventional compressors (Weel, M., et al., 2013). In addition, heat pumps / MVR-systems can be operated at working temperatures of up to 150 °C. (Bantle, 2017) demonstrated that the operating conditions were stable for superheated steam compression. To evaluate the performance of the turbo compressors a two-stage turbo compressor test facility was developed at SINTEF Energy Research. This system is used in the master's thesis to evaluate the turbo compressor performance. The performance maps enable to analyse the overall MVR-system performance for a superheated steam dryer.

The performances that can be demonstrated and measured at a test facility, are however limited to the specific application. It does not allow to draw conclusions for other applications or operating conditions that were not tested during the experiments. The development of validated numerical models enables to estimate the performance also for operating conditions that were not specifically tested.

Therefore, numerical models of the turbo compressor as well as the entire system are a good complement or extension of the experimental work. Experimentally validated models can be used for comprehensive analysis of the turbo compressor technology and the overall drying system performance in different operating conditions. This leads to a lower number of experiments that must be carried out. Further, new turbo compressors can be validated more effectively. In addition, the variation and analysis of various conditions is easier to realize. A functional model can be used for the application, e.g. MVR-systems and steam compression cycles and can be implemented in various process simulations, as pointed out by (Bantle, et al., 2016).

## 1.2 Objective and structure

The objective of the master's thesis is to analyse the thermodynamic performance of the turbo compressor technology experimentally, select and validate an existing compressor models and evaluate the system performance of a two-stage turbo compressor mechanical vapour recompression system for industrial superheated steam drying.

In the first part of the master's thesis, an introduction to the state of the art in industrial steam drying will be given to classify the present work thematically. Subsequently, in Chapter 2 the experimental setup used for the conduction of the performance tests will be explained. This includes the presentation of the two-stage turbo compressor test facility, the turbo compressors and measuring instruments used as well as the processes for preparation and follow-up for operating the system.

Chapter 3 deals with the execution and processing of measurements for the experimental analysis of the thermodynamic performance and discusses the entire process from the planning of the experiments to the final determination of the turbo compressor performance and the measurement uncertainties. Chapter 4 analyzes and discusses the experimental results obtained with respect to the turbo compressors performance and the performance of the two-stage turbo compressor system.

The consideration of the numerical part of the master's thesis is covered in the Chapters 5 and 6. Chapter 5 focuses on the development of the turbo compressor model. This includes the entire process from the literature research to the final validation of the model compared to the experimental performance test results. Chapter 6 deals with the development of a system model and the evaluation of the system performance.

The master's thesis concludes with a summary of the discussed topic as well as a discussion of the achieved results and improvements. Furthermore, recommendations for further work are proposed based on the results obtained.

As part of this master's thesis, a conference paper was published for the 13th IIR GUSTAV LORENTZEN CONFERENCE ON NATURAL REFRIGERANTS 2018, in Valencia, Spain[2], which is attached to the work (see Appendix C).

[2] GL2018 Conference - www.gl2018.upv.es

## 1.3 State of the art in industrial superheated steam drying

This section covers an overview of the state of the art in industrial superheated steam drying. At the beginning, the focus is on the general concept of industrial superheated steam drying. Subsequently, the focus is tuned towards the possible application of turbo compressors in the field of Mechanical Vapour Recompression (MVR). Finally, the theory of the analysis of the turbo compressor performance is discussed.

**Concept of industrial superheated steam drying**

Drying is one of the oldest preservation technologies and made it possible for humans to store food for extended periods of time. Thus, drying has been a crucial technology in the evolution of human cultures. To this day drying is still one of the dominating industrial preservation processes for innumerable products. Industrialization helped to optimize processes of drying, which are conducted under varying, but controlled conditions. The Handbook of Industrial Drying (Mujumdar, 2015) gives at least 15 different dryer types and identifies more than 20 different industrial drying sectors, which makes it rather difficult to generalize drying technologies. For every product a certain drying process is characterized by the type of dryer, the quality of the final product, the extended product shelf-life, additional needed processing, the ease of handling, sanitation, cost/energy effectiveness, and investment. However, the basic principle of drying is the same as it used to be thousands of years ago, and the most common dryer type is based on convective drying. (Sannan, et al., 2016, p. 5) The Figure 1.1 shows the simplified process of convective drying with superheated steam (SHS).


Figure 1.1: Simplified process visualization of convective drying with superheated steam

The hot SHS hits the wet product and heats it up. After the first surfaces reach the evaporation temperature of the contained water, the water begins to evaporate and is carried along by the SHS flow. This evaporated water is called excess steam. The process continues until the product reaches the defined moisture content. The temperature of

the SHS decreases continuously, due to the heat transferred to the product, the mixing with the vaporized water from the product and heat losses in the process. Since the temperature of the cold steam is during the drying process above the condensation temperature (superheated), the process is called superheated steam drying (SHS drying).

For the use of industrial SHS drying, the product must withstand temperatures above 100 °C. If so, the SHS drying may offer advantages in comparison to air drying. The energy consumption is 15 % to 20 % less compared to air drying. Due to the high specific heat capacity and low viscosity of steam, pasteurizing or sterilising of the product is possible. Because of the SHS atmosphere at nearly atmospheric pressure no air/oxygen is present in the drying chamber and the risks of fire/auto ignition or oxidation of the product is minimized. Superheated steam can also use for conveying without any risk of condensation, therefore no problem of salmonella growth exists (Sannan, et al., 2016, p. 5). In the following, the layout and conditions of a SHS dryer will be discussed.

**Superheated steam dryer with an open-loop heat pump**

The Figure 1.2 shows a simplified schematic layout of a SHS dryer with an open-loop heat pump to heat up the process steam with the recompressed excess steam from the drying process.

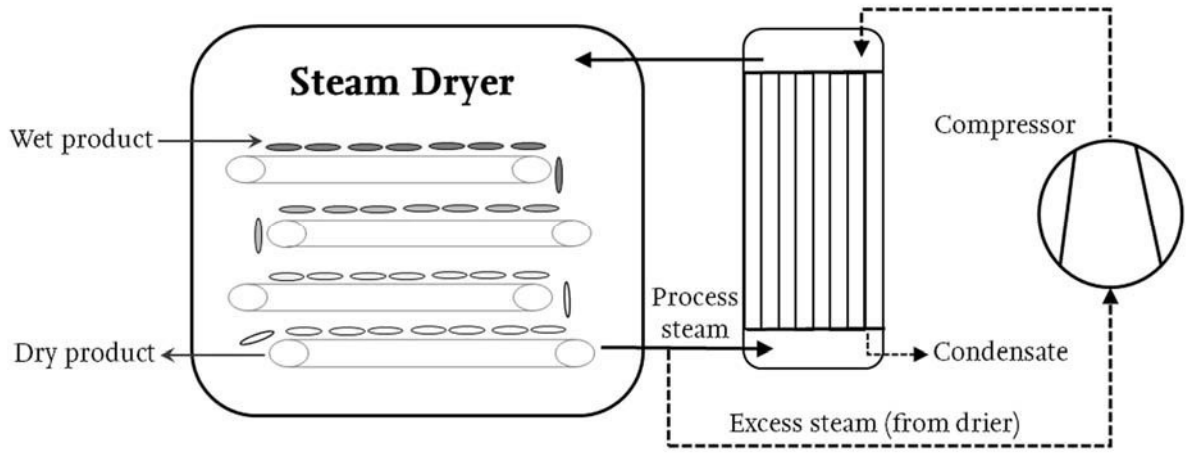


Figure 1.2: Simplified schematic layout for superheated steam dryer with energy recovery through mechanical vapour recompression (Bantle, 2017, p. 2)

The wet product is fed into the drying chamber and transported through a superheated steam atmosphere, e.g. by belts. The drying chamber is open at the bottom and the steam is close to atmospheric pressure. As schematically shown in Figure 1.1, the product is dried due to the superheat of the steam and the evaporated moisture of the wet product is heated up to SHS conditions. The superheated steam in the drying chamber is cooled

down during drying from around 150 °C to 180 °C at the inlet to 110 °C (10 K overheat) at the outlet of the dryer. It is important to mention that the superheated condition need to be sustained at any time, with e.g. 10 K safety margin, to prevent condensation. An open-loop heat pump is compressing the excess steam from the dryer to a higher-pressure level. Subsequently, downstream heat exchanger can be applied to condense the recompressed SHS and hereby re-heating the process steam of the dryer. In this case, the dryer functions as the evaporator of the heat pump. One of the main advantages of SHS drying is this possibility to recover the excess product steam through open-loop heat pump and use this heat as thermal energy source to heat up the process steam. Otherwise the removed water from the product in the form of excess steam is wasted because it is too cold to be utilized further. Open-loop heat pumps with R718 (water) as working fluid are often called Mechanical Vapour Recompression (MVR). (AIT Austrian Institute of Technology GmbH, 2018)

Depending on the SHS flow rate and the pressure ratio of the compression, several compressors systems are available including screw compressors, 5…10 stage blowers systems or two to three stage turbo compressor systems.

**Mechanical Vapour Recompression (open-loop heat pump)**

To achieve a higher-pressure level and condensation temperature through the Mechanical Vapour Recompression (MVR) a two-stage compression system is useable. The Figure 1.3 shows a simplified schematic layout for a two-stage compression system with water injection to de-superheat the working fluid between the stages.

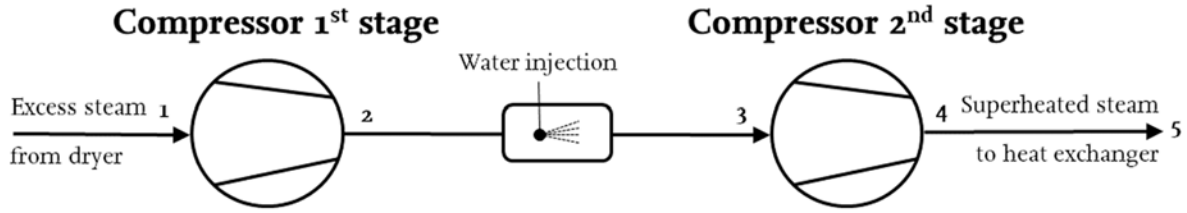


Figure 1.3: Simplified schematic layout for the two-stage compression system with water injection

Excess steam from the dryer reaches the first compressor stage (1) and is compressed to a higher pressure and temperature (2). Before entering the second compressor stage (3) the steam is de-superheated through the injection of liquid water. After the compression in the second compressor stage (4), the superheated steam is passed to a downstream heat exchanger (5), where the energy can be transferred to the process steam.

Figure 1.4 shows a log p-h and T-s diagrams of the two-stage compression system with de-superheating between the first and second compressor stage for an exemplary case.

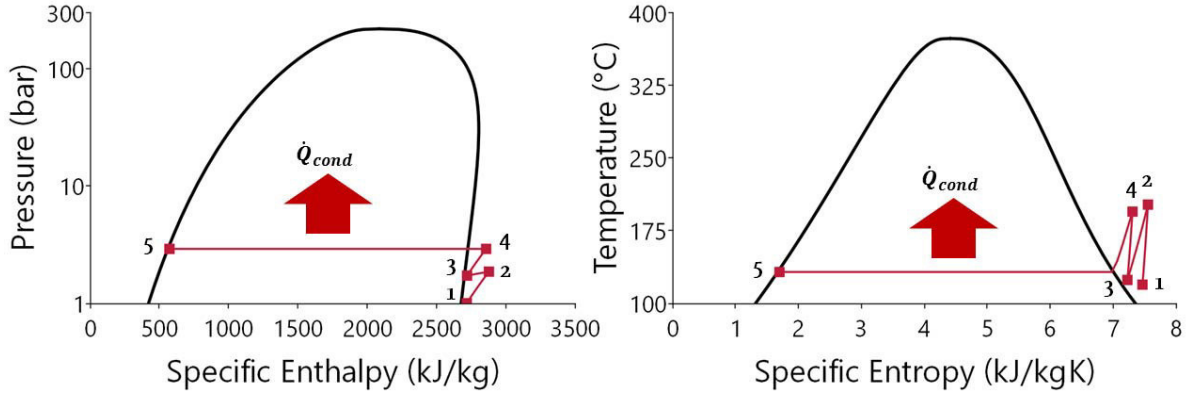


Figure 1.4: Log p-h and T-s diagram for the process in the MVR system including energy flow

The two-stage compression system for SHS consists of the following ideal process steps:

1 – 2: Isentropic compression of the excess steam from dryer in compressor 1

1 – 2: Isobaric cooling of the SHS through water injection via the de-superheater

3 – 4: Isentropic compression of the SHS in the compressor of the second stage

4 – 5: Isobaric cooling and condensation of the steam in the following heat exchanger

Based on (Weigand, et al., 2013), the Coefficient of performance (COP) for the two-stage compression system is defined as the ratio of the condensation heat flow transferred from the condenser to the process steam $\dot{Q}_{cond}$ and the electrical power $P_{el}$ consumed by both compressors and the auxiliary consumers, e.g. as water pumps.

$$COP = \frac{\dot{Q}_{cond}}{P_{el}} \tag{1.1}$$

In the context of this work, the condensation heat flow describes the achievable condensation heat flow calculated from the product of mass flow rate and evaporation enthalpy at the respective pressure. In accordance to (Weigand, et al., 2013), the ideal Carnot efficiency $\eta_{carnot}$ describes the maximum thermal efficiency that a heat pump cycle can achieve as permitted by the Second Law of Thermodynamics. Here, $T_c$ describes the cold temperature at the inlet and $T_h$ the hot at the outlet of the system.

$$\eta_{carnot} = \frac{T_h}{T_h - T_c} \tag{1.2}$$

The most cost-intensive part of an MVR-system is the compressor for the compression of the working fluid. Different types of turbomachines are available for this use.

**Turbomachinery**

According to (Dixon & Hall, 2014, p. 1), turbomachines are classified as machines that transfer energy to a fluid or extract energy from a fluid. The impacted working fluid moves continuously through the turbomachinery in a dynamic process. There are two main subcategories to classify turbomachines depending upon whether they increase or decrease the energy of the fluid. Those that extract energy from the fluid and lower its pressure are called wind, hydraulic, steam or gas turbines. Those that add power to the fluid are called pumps, compressors and blowers, depending on the state of the working fluid and level of the pressure ratio. Normally, both types are connected to a rotating shaft that transfers energy to or from the turbomachinery to a generator or motor. Moreover, turbomachines are divided into more categories depending on the fluid passage design. Those categories are axial flow, radial flow, and mixed flow turbomachines. The Figure 1.5 shows different types of turbomachines. Based on (Dixon & Hall, 2014, p. 1).

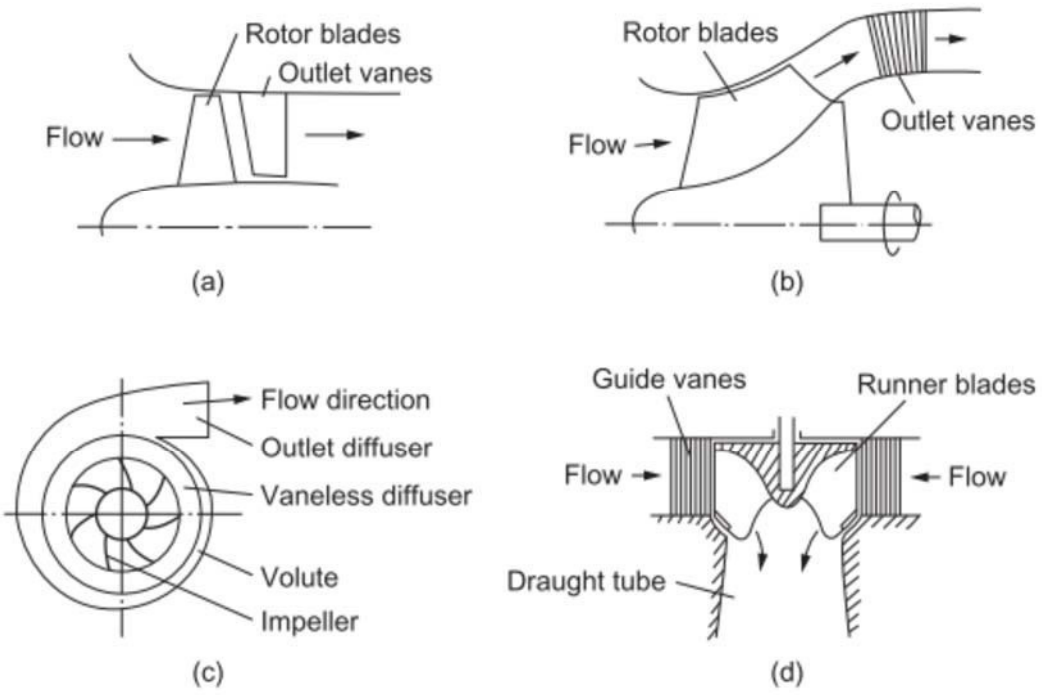


Figure 1.5: Different types of turbomachines (Dixon & Hall, 2014, p. 2)

Centrifugal compressors (c) can be operated in wide range of operating conditions with high efficiencies and high stage pressure ratios (Kus, 2013, p. 30). Due to the specific conditions of the MVR-system, the centrifugal compressor offers a good opportunity. In the following, the centrifugal compressor will be explained in more detail.

### Centrifugal compressor

A centrifugal compressor consists essentially of a rotating impeller followed by a diffuser, which can be constructed with or without vanes. At the center of the centrifugal compressor is the impeller with a series of blades mounted on it. After the working fluid has entered the compressor through the eye, it reaches the fluid passage. This is located between the impeller vanes and the working fluid moves due to the rotation of the impeller. The energy level of the fluid is increased by means of the impeller that acts on the fluid with angular momentum. During this process, the velocity and the static pressure of the fluid are increased. The following diffuser is a non-rotating device that has an increased flow area over the flow passage. Therefore, the role of the diffuser is to convert the kinetic energy or reducing the excess flow velocity to increased pressure. The collector scroll gathers the fluid leaving the diffuser and directs it to the outlet pipe. (Dixon & Hall, 2014, p. 268) The Figure 1.6 shows a simplified representation of a centrifugal compressor stage including the main components.

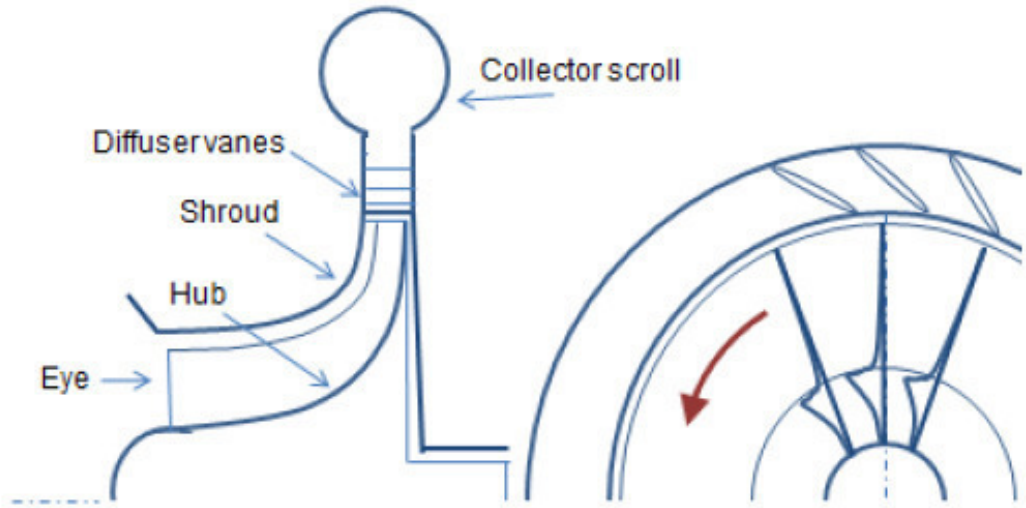


Figure 1.6: Schematic representation of a centrifugal compressor stage (Kus, 2013, p. 31)

The MVR-system requires high compressing technology, and high reliability and durability. Thus, the centrifugal compressor is used for the MVR to satisfy these requirements. Since many variables of the centrifugal compressor design need to be considered, it is complex to predict its performance. Extending the limit causes the compressor to become noisy and vibrate and can even break. Therefore, it is important to examine the characteristics of the compressor and determine a way to predict its performance. (Kang, et al., 2016, p. 1)

### Compressor isentropic efficiency and compressor performance map

The isentropic efficiency allows a statement about the performance of a turbo compressor. In addition to other operating parameters, the determination of the isentropic efficiency forms the basis for the creation of a compressor performance map. In the following, both the determination of the isentropic efficiency and the structure of a compressor performance map are discussed.

Based on (Moran & Shapiro, 2006, p. 247), an isentropic compression process is adiabatic and reversible, meaning that the process can return to initial state. On the other hand, an actual process is irreversible and cannot reach the initial state due to occurring losses, e.g. friction, heat losses, leakage and more. Figure 1.7 shows the comparison of an actual and an isentropic compression process in a simplified h-s diagram.

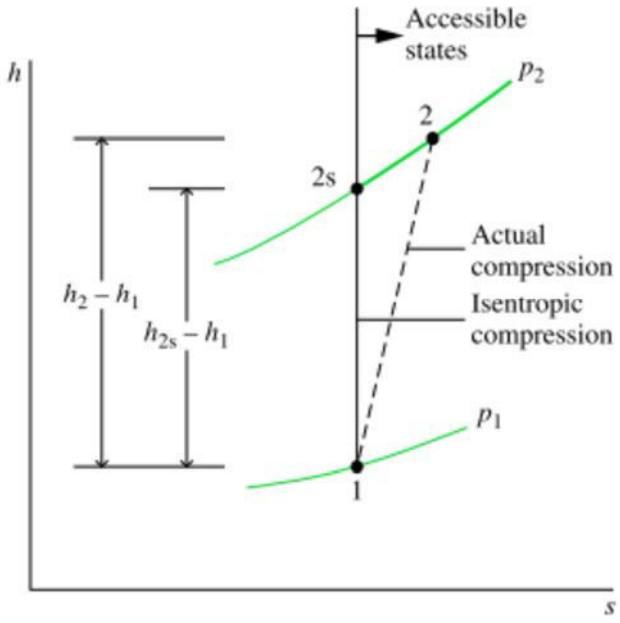


Figure 1.7: Representation of the processes of the actual und isentropic compression in a simplified h-s diagram (Moran & Shapiro, 2006, p. 247)

The green curves are isobaric lines, meaning that the pressure is constant. The isentropic compression process moves vertically upwards along the specific enthalpy scale without any changes in specific entropy. The specific enthalpy difference is $h_{2s}$ - $h_1$. An actual compression process experiences irreversibility and therefore the specific entropy of the working fluid increases. During this process, the system remains on the same isobaric line and provides the same output pressure. For the actual compression process, the specific enthalpy difference is $h_2$ - $h_1$ and larger compared to the isentropic process. Therefore, the actual compression requires more work done by the compressor.

According to (Moran & Shapiro, 2006, p. 247), the compressor isentropic efficiency $\eta_{isen}$ is calculated by the ratio of the isentropic and actual compression. Therefore, the isentropic efficiency is an evaluation parameter for the effectiveness of the actual compression process compared to the isentropic compression process.

$$\eta_{isen} = \frac{Isentropic\ compressor\ work}{Actual\ compressor\ work} = \frac{h_{2s} - h_1}{h_2 - h_1} \tag{1.3}$$

The determined isentropic efficiency and the operating behaviour of a centrifugal compressor can be visualized in a compressor performance map. This compressor map can be used to display and evaluate achieved operating points of the compressor. Figure 1.8 shows a schematic representation of a compressor performance map.

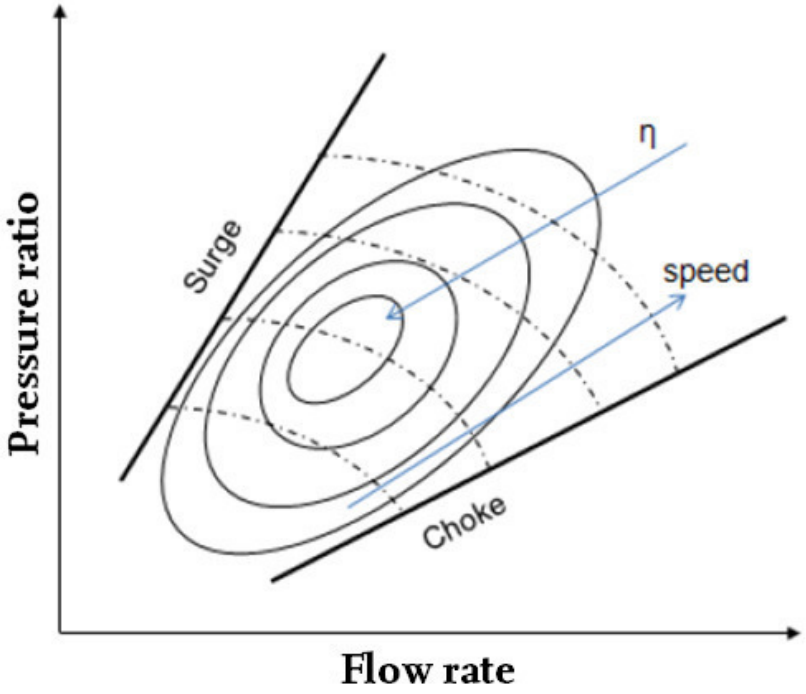


Figure 1.8: Schematic representation of a compressor performance map (Kus, 2013, p. 32)

To create the compressor map, the pressure ratio is displayed above the flow rate using the mass flow rate or volume flow rate. In addition, the representation considers lines of constant impeller speed and isentropic efficiency. An increasing impeller speed leads to an increase of achievable flow rates and pressure ratios. The maximum of the isentropic efficiency lies in the middle of the operating range. Based on the description of (Bergstrøm & Leufven, 2007, p. 25), the compressor map can be divided into three different ranges. In the middle between the surge and choke line is the normal operating range for the operation of the compressor. The best operating range is identified and shown by the efficiency contours.

In the lower right of the compressor map is the choke area. The flow chokes, when the flow reaches sonic velocity at some sections of the compressor (Gravdahl & Egeland, 1999, p. 162). Choking of the compressor means that the mass flow rate is too large and the flow rate through the compressor stays constant even when the pressure ratio decreases further. Reaching these two ranges is not dangerous to the compressor, even though choke is often not desired. (Bergstrøm & Leufven, 2007, p. 25)

To the left is the compressor map limited by the surge line. When the compressor travels beyond this line, surge will occur. This is because the compressor is unable to maintain flow lines and therefore the flow breaks down. This breakdown of flow lines causes uneven distributed load on the compressor blades and bearings and can damage the compressor. When the flow collapses completely, a reversal of the mass flow is possible. The compressor now acts like a turbine. Furthermore, the reverse mass flow causes a reduction in the pressure ratio until the compressor can again maintain a positive mass flow. Subsequently, the pressure ratio increases again. Without any changes to the system the compressor enters a new surge cycle. (Bergstrøm & Leufven, 2007, p. 25)

According to (Kurzke, 2011, pp. 1-2), the creation of a realistic compressor map is the basis for high-quality performance calculations and analysis. There are several approaches to transferring and adapting a compressor map to a desired application and working fluid. The problem with most of the purely mathematically based methodologies is that they pay no heed to the laws of physics. This leads to deviations during the adaption of the speed and isentropic efficiency lines. Therefore, calculating a compressor map requires knowledge of the detailed geometry and operating behaviours of a compressor. Only when a model used for the calculation has been calibrated with experimental data it can get sufficiently accurate results be obtained for slightly different compressor designs. For this reason, experimental data and experiences for the evaluation of the performance and the later development of the numerical turbo compressor model are generated at the test facility. (Kurzke, 2011, pp. 1-2)

# 2 Experimental Setup

This chapter covers the presentation of the experimental setup used for the performance tests. At the beginning, the test facility and turbo compressor prototype used are described in detail. Subsequently, the measuring system used is defined and the start-up and shutdown procedures are discussed.

## 2.1 Presentation of the test facility at SINTEF Energy

For the experimental setup the two turbo compressors were installed in a open loop heat pump/ mechanical vapour recompression (MVR) unit. The idea for the design of the test facility is based on the previously explained schematic layout of a superheated steam dryer (see Figure 1.2). For the further analysis, the focus is on the two-stage turbo compressor system and not the total SHS dryer system. The Figure. 2.1 shows the defined system boundaries for the developed test facility at SINTEF Energy Research.

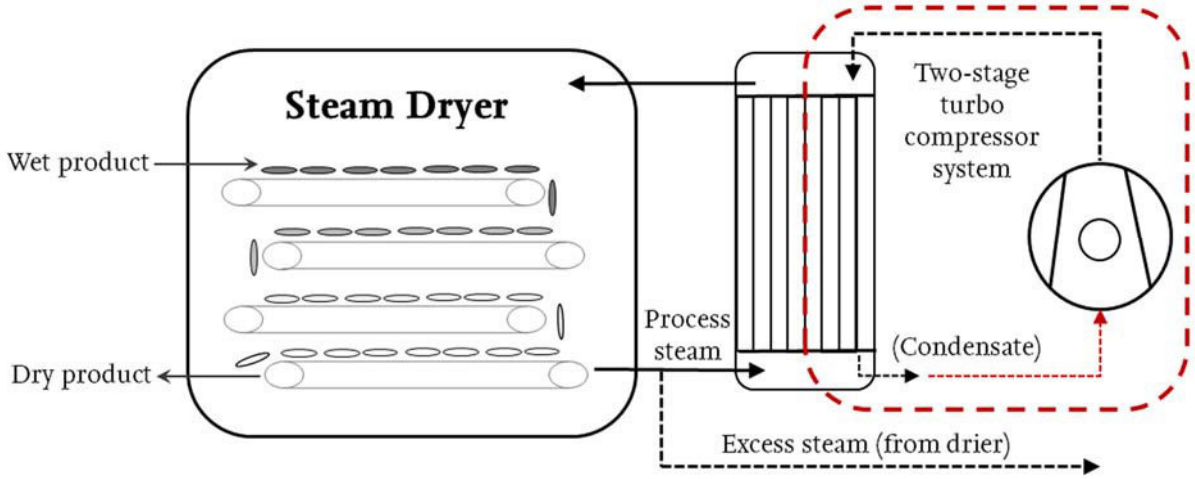


Figure 2.1: Simplified schematic layout for superheated steam drier with defined system boundaries for the test facility at SINTEF Energy based on (Bantle, 2017, p. 2)

The system boundaries were defined after the separation of excess steam from the dryer at the inlet and through the heat exchanger at the outlet for the two-stage turbo compressor system. This means that the actual steam dryer is not displayed.

For the operation of the test facility, the open-loop two-stage turbo compressor system was transformed into a closed-loop. For this purpose, the heat exchanger was replaced by a steam generator and the previously open outlet (condensate) was connected to the inlet of the first turbo compressor stage. The Figure 2.2 shows the principle setup of the test facility at SINTEF Energy Research.

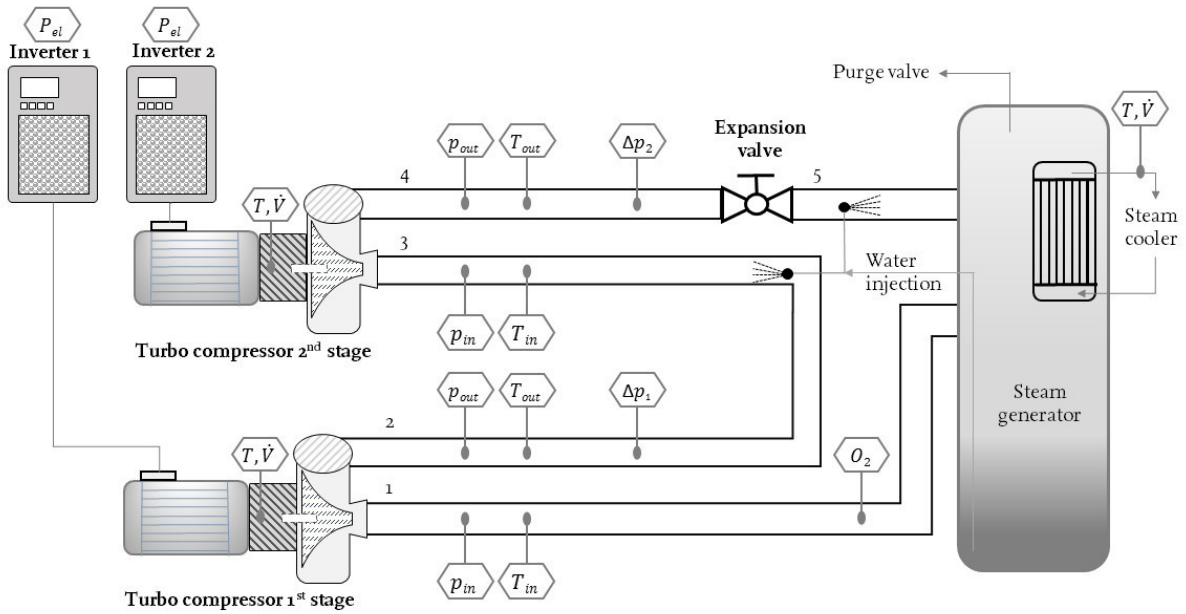


Figure 2.2: Principle setup of the two-stage turbo compressor test facility consisting of turbo compressors units, de-superheaters, expansion valve, steam generator and measurement points

The inlet of the first turbo compressor stage is connected to the steam generator which is operated as steam supply unit. After the compression in the first stage (1-2) a controlled amount of water is injected via an installed de-superheater to de-superheat the working fluid before entering the second stage with an approximately superheat of 20 K (2-3). Subsequently, after the compression in the second stage (3-4) the expansion valve decreases the pressure of the superheated steam (SHS) to atmospheric conditions (4-5). A second de-superheater is used to de-superheat the SHS after the expansion valve to reduce the thermal stress to the steam generator.

A steam cooler connected to the steam generator cools the total system by de-superheating the working fluid before the inlet to the first stage (5-1). The pressure in the steam generator is approximately at atmospheric condition since the purge valve is open to the ambient. Therefore, the SHS reaches the inlet of the first stage at atmospheric pressure and 20 K superheat. The system is fully automated and controlled by a self- developed software program. (see Appendix C)

The Figure 2.3 illustrates the described close-loop process of the test facility in a logarithmic p-h and T-s diagram. The respective process steps of the corresponding points in the diagrams (1-5) were explained before.

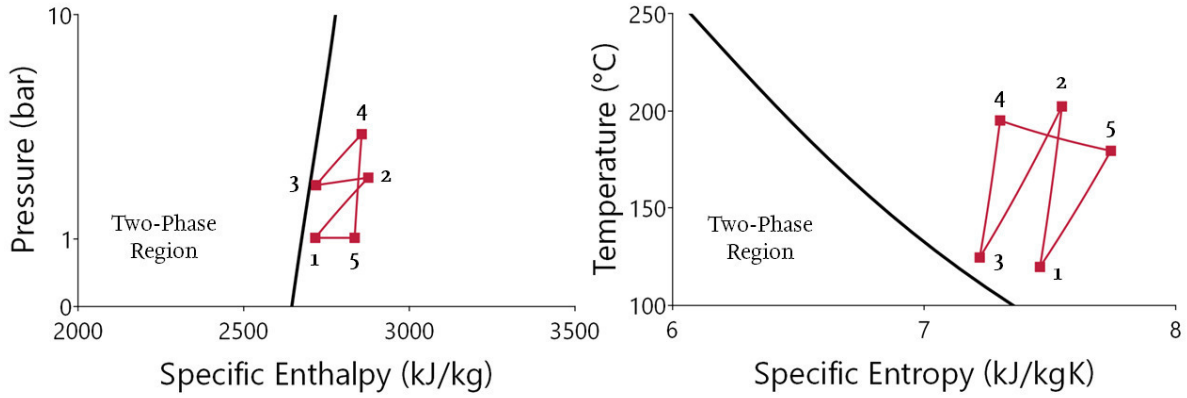


Figure 2.3: Representation of the close-loop process of the test facility in a logarithmic p-h and T-s diagram for water

All piping work was constructed in a way that the thermal expansion is compensated during start-up and operation, so that the mechanical stress to the turbo compressor is reduced to a minimum. The piping is insulated by 50 mm mineral wool. Both turbo compressors are controlled by type AC30 variable speed drives with an estimated efficiency of 98 % (Parker Hannifin A/S, 2017) and 3-phase power meters were installed upstream each inverter. Gearbox and motor of the turbo compressors are cooled by water and the required cooling is calculated by measuring temperature and volume flow. The energy flow for the steam cooler is also calculated by measuring temperature and volume flow. (see Appendix C)

Temperature and pressure measurements are performed before and after both compressor stages. Each measuring point is equipped with a pair of temperature sensors and an absolute pressure sensor connected to a pair of horizontally aligned pressure tapings. The mass flow rate of each stage is calculated by using an orifice plate and differential pressure sensor to measure the differential pressure according to DIN 5167:2003. The differential pressure sensors are measuring the differential pressure across the orifice plate via two horizontal aligned corner tapings in the flanges.

Based on the results of (Bantle, 2017) and (Johannesson, 2017), the test facility has been extended by an oxygen sensor. The measured oxygen content in the steam was always lower than 0.1 %. As a result, the uncertainty of the fluid composition could be eliminated.

## 2.2 Description of the turbo compressor prototype used

The turbo compressors used for both stages during the experiments are a further development of a conventional radial turbocharger from the automotive industry. The patented design has been adapted by the manufacturer Rotrex A/S[3] for use in superheated steam compression. Figure 2.4 shows a section view through the prototype of the turbo compressor including the DC-motor and gearbox.

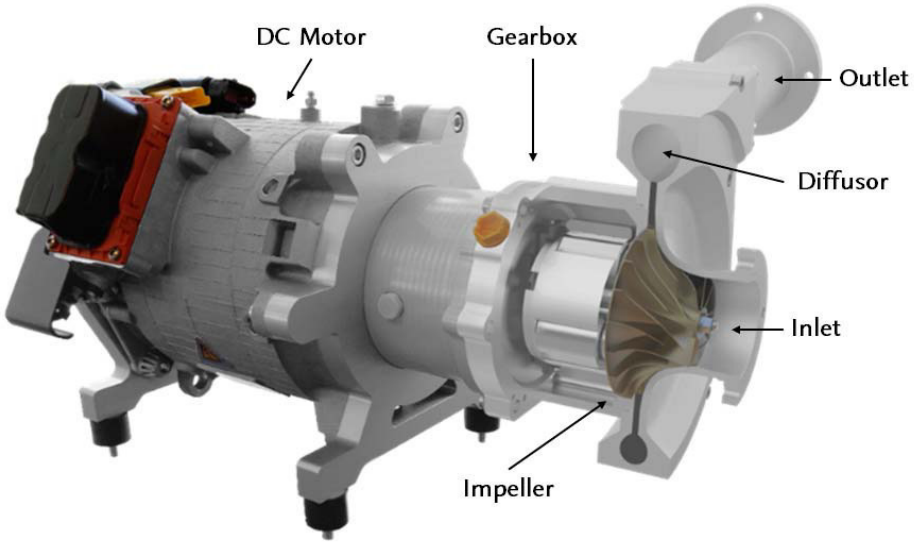


Figure 2.4: Section view through the prototype of the turbo compressor (Bantle, 2017)

For the further development, the impeller was designed in titanium. The rest of the casting is done in aluminium. The carbon sealing between the compression chamber and the planetary traction drive was reinforced to ensure a better sealing. The aim of these modifications was to increase the achievable pressure ratio at a high efficiency and to improve the durability for long-term, continuous operation. (see Appendix C)

The turbo compressor is designed to achieve a pressure ratio of 2.5 and a mass flow rate of 450 to 550 kg/h at atmospheric pressure at the inlet. The isentropic efficiency of the compressor was calculated to be 74.5 %. Depending on the temperature and pressure of the steam on the low-pressure side at the inlet, it will be possible to achieve a thermal power of up to 300 kW while achieving a temperature lift of approximately 25 K between high and low-pressure saturation temperatures. (see Appendix C)

[3] Rotrex A/S, Copenhagen, Denmark - www.rotrex.com

On the drive shaft of the turbo compressor, a planetary traction gearbox is mounted that enables a high transmission ratio of 7.5 at a mechanical efficiency of 98 % under full load. The planetary gearbox is lubricated by means of an internal cooling oil. The cooling oil is pumped by an internal oil pump and cooled against a cold tap water stream using a plate heat exchanger. (see Appendix C)

On the drive shaft of the gearbox, a 650 Volt DC-motor is placed which can deliver up to 12,000 rpm directly, thus a rotational speed of up to 90,000 rpm can be achieved at the impeller. The motor is driven by an inverter that delivers up to 59 kW. The total weight of the entire unit out of turbo compressor, gearbox and DC-motor is about 40 kg. The dimensions are 50 cm in length, 40 cm in width and 35 cm in height, which illustrates the compact and light weighted design. (see Appendix C)

Figure 2.5 shows an overview of the main components of the turbo compressor setup discussed above.

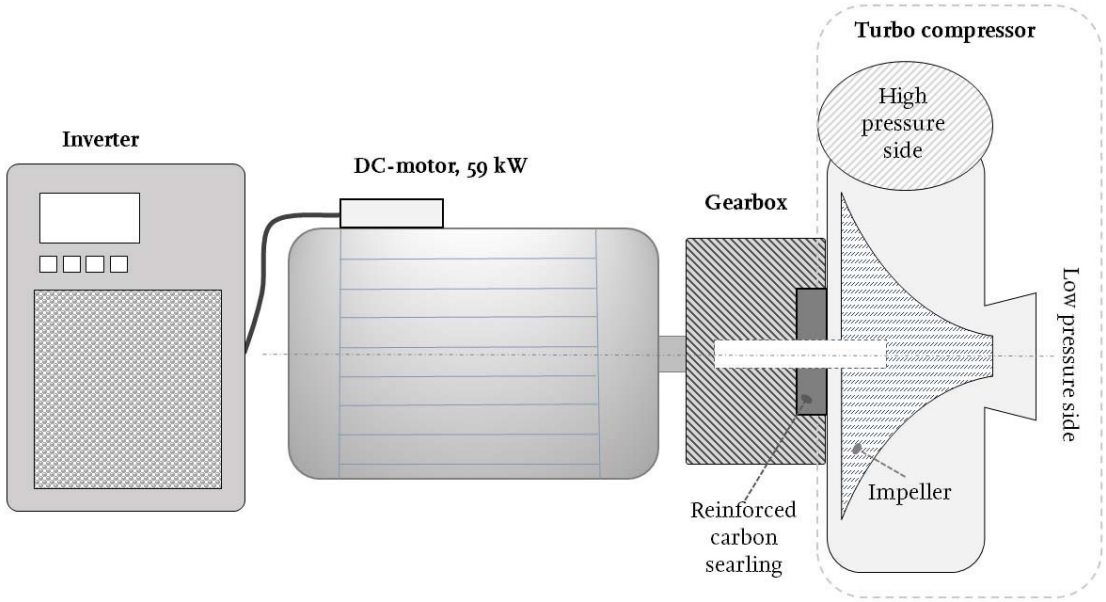


Figure 2.5: Overview of the main components of the turbo compressor setup (Bantle, 2017)

## 2.3 Definition of the measuring system used

This section defines the measuring system used. The Figure 2.6 shows a simplified structure of the measuring system including the placement of instruments.

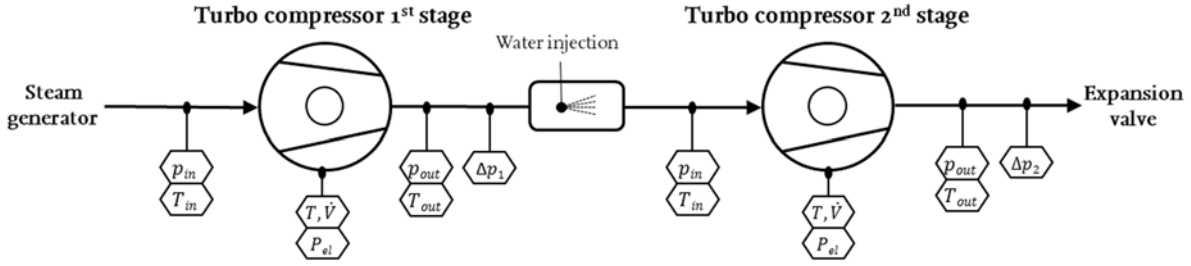


Figure 2.6: Simplified structure of the measuring system including the placement of instruments

The measuring instruments are distributed over both stages to determine all important parameters for the further analysis of the performance of the turbo compressors as well as the total test facility performance. In the following, the measuring instruments and the respective accuracy are discussed.

**Temperature sensors**

The temperature sensors are thermocouple sensor of type Pt100 B 1/3 DIN with a 3-wire connection. The sensors transmit current in the range of 4-20 mA and can be used for a temperature range from 0 °C to 300 °C. The accuracy is according to the manufacturer ± 0.75 °C. (Jensen Electric A/S, 2016) The temperature sensors in the suction line have a length of 150 mm and in 200 mm in the discharge line. This provides for a larger distance of the sensors to the hotter pipe on the discharge line. However, the measuring depth is identical for all sensors and extends to the middle of the pipe cross-section.

**Pressure sensors**

The absolute pressure sensors are pressure transmitter of type 528 with a 2-wire connection and transmit current in the range of 4-20 mA. Depending on the position at the test facility the pressure sensors have different pressure ranges. The pressure sensor in the first stage suction line can measure a pressure range from 0.0 bar to 1.6 bar. The pressure sensors in the first stage discharge line and second stage suction line can measure a pressure range from 0.0 bar to 4.0 bar. The pressure sensor in the second stage discharge line can measure a pressure range from 0.0 bar to 10.0 bar. The accuracy is according to the manufacturer ± 0.75 % of full scale. (Huba Control AG, 2017a)

**Differential pressure sensors**

The differential pressure sensors are pressure transmitter of type 692 with a 2-wire connection. The sensors transmit current in the range of 4-20 mA and can measure a differential pressure range from 0.0 bar to 0.2 bar. The accuracy is according to the manufacturer ± 0.75 % of full scale. (Huba Control AG, 2017b)

**Orifice Plates**

The orifice plates of type ISB/1 have a concentric square-edged hole. The outer diameter is 98 mm and the plate thickness 3 mm. The orifice diameter for the first stage is 55 mm and 50 mm for the second stage. The accuracy is according to the manufacturer ± 0.6 %. (Emco Controls A/S, 2018)

**Power Meters**

The power meters of type OMNIPOWER CT (current transformer) are 3-phased current transformer electricity meter for registration of electric energy. The accuracy is according to the manufacturer below 0.5 %. (Kamstrup A/S, 2016)

**Combined flow and temperature sensors**

The combined flow and temperature sensors of type MULTICAL® 403 are based on the ultrasonic principle and consists of a calculator, a flow sensor and two temperature sensors. The MULTICAL® 403 calculates energy based on the formula given in EN 1434-1 and is intended for energy measurement in systems where water is used as the energy-conveying medium. (Kamstrup A/S, 2017)

**Data acquisition system**

All Signals from the previously discussed measuring instruments are collected in the data acquisition (DAQ) system. The DAQ system consists of an Advantech ADAM 5000 L/TCP with 3 analogue input modules each having 8 channels and one counter/frequency module with 4 channels in counter mode. The accuracy is according to the manufacturer below ± 0.2 %. (Advantech Co, Ltd., 2018)

The measuring instruments in the system send an analog output signal to the data sampling system. The sampling system is connected to a router that serves as a data bridge between the data system to transfer real-time data to the operating computer and the data collection viewer respectively. All measurement data during the experiment are put into an CSV file and contains information about the timing of each measurement for the further analysis.

## 2.4 Start-up and shutdown of the test facility

Due to the complexity of the two-stage turbo compressor test facility, it is important to define and follow a start-up procedure as well as a subsequent shutdown procedure before the conduction of planned performance tests. The focus here is the actual control of the test facility, the preparation and post-processing of the system is not further treated, for example by the connection of the power supply.

**Start-up procedure**

The impeller of the turbo compressor is quite sensitive to particle or droplet impact at higher speed and the inlet conditions of the working fluid need therefore to be superheated to avoid liquid droplets. Hence the system cannot be started with saturated steam and needs therefore to be pre-heated to above 100 °C before water/steam is injected. Since the turbo compressors are originally designed for air the start-up or preheating of the system can therefore be performed with air as working fluid.

The turbo compressors are hereby started when the system is dry and filled with ambient air. The system is then heated up by the excess heat of the compressors until the coldest point (inlet at the first stage) reaches a stable temperature above 100 °C. Then water is injected through the de-superheaters which is immediately evaporated and filling up the system with superheated steam by replacing the air through the purge valve of the steam generator. The start-up procedure takes around 45 minutes and after that the system is filled with steam and ready for the normal operation. The oxygen content is below 0.1 % at this point. (see Appendix C)

**Shutdown procedure**

The aim of the shutdown procedure is to shut down the test facility safely and prepare the system for the next use. The first step is to bring the system as far as possible from the surge line to a safe and stable operating point by opening the expansion valve. Subsequently, the impeller speed of turbo compressors is gradually decrease to a low operating point at around 40 % of the maximum speed. At the same time, the amounts of water for the injection via the de-superheaters are proportionally reduced and the heater of the steam generator is switched off. Then the drain valves are opened, and the system is cooled with the incoming ambient air and dried out. In the last step, the turbo compressors are switched off.

# 3 Execution and Processing of Measurements

This chapter deals with the execution of measurements and processing of the measured data through the conduction of performance tests. At the beginning, the planning of the experiments is discussed. Subsequently, the performing of experiments including all performed calculation steps based on the selection of measurement data is explained. Finally, the turbo compressor performance is determined based on the final data and the determination of the measurement uncertainties is carried out in the context of an uncertainty analysis. These steps will be explained in more detail during this chapter.

The Figure 3.1 visualizes the sequence of the performed steps from the planning of the experiments to the final data for the following analysis of the experimental test results.

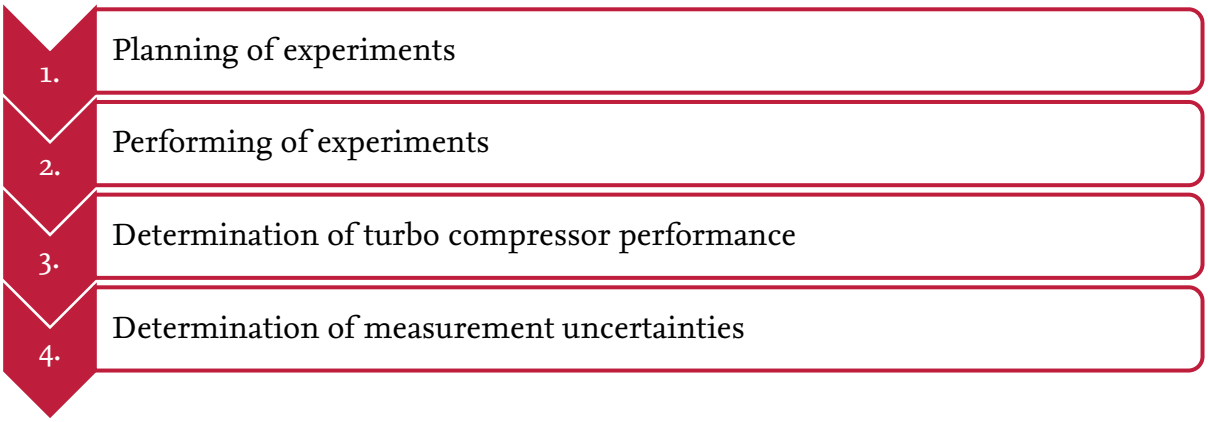


Figure 3.1: Sequence of the correction and calculation steps performed

All calculation steps were implemented and calculated in Microsoft EXCEL and the relevant superheated steam properties were calculated by using REFPROP version 9.

## 3.1 Planning of experiments

This section describes the planning of experiments and use of the previously discussed test facility to obtain measurement data and operational experience. The aim of the planned experiments is to generate the required database for the analysis of the turbo compressor performance as well as the two-stage turbo compressor system performance. For this reason, it is important to cover a maximum operation area of the compressor by testing a wide range of possible impeller speeds and flow rates during the planned performance tests. The variation of the operation points is possible by changing the impeller speed of both turbo compressors and changing the valve opening position of the expansion valve (see Section 2.1). Before carrying out the tests, the test facility must be put into operation and switched off again after completion. This procedure has been described in the Section 2.4.

**Operating and controlling of the system during the experiments**

During the planned experiments, the impeller speeds of the turbo compressors were either the same relative to each other or differed by 5 % or 10 % in relation to the maximum design speed. An overview of all tested constellations of the impeller speeds is attached. (see Appendix A)

When performing a test series, the turbo compressors were first brought to the desired impeller speeds. In this case, the expansion valve was fully open to operate at a maximum distance from the surge line. Subsequently, the amounts of water for the injection via the de-superheaters were adjusted. The aim was to set an overheating of 10 K to 20 K at the inlets of both turbo compressor stages. After reaching a stable operating point, the expansion valve was closed manually until a change of the pressure ratio and mass flow rate was recognizable. The aim was an even distribution of recorded operating points over the assumed speed line between the surge and choke line.

When carrying out a planned measurement series, experience has shown that a new stable operating state can be realized more quickly when operating from low speeds to higher speeds. This happens because the system takes longer to cool down than to heat up.

## 3.2 Performing of experiments

This section covers the complete process from the identification and selection of stable operating points to the final measurement data for the further analysis of the turbo compressor and total system performance (see Figure 3.1).

**Identification and selection of stable operating points for further analysis**

For a meaningful and reliable analysis, stable operating points with almost stationary measured values are needed. Therefore, the identification and selection of stable operating points is important. When a stable range is reached, various parameters for the evaluation are calculated. In the first step, the simple mean values for the interval is determined. Here, the measured values of both temperature sensors for each measuring point were analysed together. These average values will be used in the further process. To calculate the sample mean $\omega$, the sum of all values in the chosen interval is determined and divided by the number of values.

$$\omega = \bar{X} = \frac{1}{n} \cdot \sum_{i=1}^{n} X_i \tag{3.1}$$

The standard deviation $\sigma$ is a tool to measure the degree of uncertainty in a sample. A low standard deviation indicates that the data points are close to the simple mean and a high standard deviation indicates the sample is widespread.

$$\sigma = s = \sqrt{\frac{1}{n-1} \cdot \left( \sum_{i=1}^{n} X_i^2 - n\bar{X}^2 \right)} \tag{3.2}$$

The coefficient of variation $C_v$ is calculated from the ratio of the standard deviation $\sigma$ and the sample mean $\omega$. (Reddy, 2011, p. 70)

$$C_v = \frac{\sigma}{\omega} \tag{3.3}$$

The limits for the coefficient of variation $C_v$ are defined as 1.0 % for the temperature and pressure sensors and 4.0 % for the differential pressure sensors over a duration of five minutes. The limit values were defined based on the determined measurement data. The differences in the limit values are based on the higher $C_v$ in differential pressure measurement compared to the temperature and pressure measurements.

**Flow rate calculation based on the differential pressure drop over the orifice**

The flow calculation is an iterative process according to the conditions and equations mentioned in (EN ISO 5167-1:2003, 2003) and (EN ISO 5167-2:2003, 2003). Based on the geometric values for the pipe and orifice diameter (see Table 3.1), the initial values for the discharge coefficient and epsilon were estimated from Table A.5 and Table A.12 according to (EN ISO 5167-2:2003, 2003). The first calculation of the mass flow rate is based on the measured pressure drop and the determined initial values for discharge coefficient C and expansibility factor $\epsilon$. This calculated mass flow rate is used as the initial value for the following iteration steps.

$$\dot{m} = C \cdot \epsilon \cdot \frac{\pi}{4} \cdot d^2 \cdot \frac{\sqrt{2 \cdot \Delta p \cdot \rho}}{\sqrt{1 - \beta^4}} \tag{3.4}$$

$\beta$ is given by the diameter ratio of the orifice diameter $d$ and the inner pipe diameter $D$. The discharge coefficient C is determined with the Stolz equation.

$$\begin{aligned} C = {} & 0.5959 + 0.0312 \cdot \beta^{2.1} - 0.1840 \cdot \beta^8 + 0.0029 \cdot \beta^{2.5} \cdot \left(\frac{10^6}{Re}\right)^{0.75} \\ & + 0.0900 \cdot L \cdot \beta^4 \cdot (1 - \beta^4)^{-1} - 0.0337 \cdot L \cdot \beta^3 \end{aligned} \tag{3.5}$$

The relative pressure tapping spacing L is defined by the ratio of the distance of pressure tapping to orifice plate $l$ and $D$. The Reynolds number Re in the upstream is given by

$$Re = \frac{\rho \cdot c \cdot D}{\mu} \tag{3.6}$$

where ρ is the fluid density at the inlet, c is the fluid velocity, D is the inner pipe diameter and μ is the dynamic viscosity. The empirical equation is used to calculate the expansibility factor $\epsilon$ for compressible fluids.

$$\epsilon = 1 - (0.351 + 0.256 \cdot \beta^4 + 0.93 \cdot \beta^8) \cdot \left[1 - \left(\frac{p - \Delta p}{p}\right)^{\frac{1}{\kappa}}\right] \tag{3.7}$$

The fluid density $\rho$ is a function of the temperature and pressure and was determined at the inlet and outlet for both stages. Since the mass flow rate $\dot{m}$ through each turbo compressor is constant, the fluid density $\rho$ can be used to calculate the respective volume flow rate $\dot{V}$ at the inlet and outlet.

$$\dot{V} = \frac{\dot{m}}{\rho} \tag{3.8}$$

The fluid velocity $c$ is calculated from the quotient of the volume flow rate $\dot{V}$ and the pipe cross-sectional area $A$ at the measuring point:

$$c = \frac{\dot{V}}{A} \tag{3.9}$$

The Table 3.1 summarize the constant parameters which were used for the flow calculation.

Table 3.1: Summary of constant parameters for the flow rate calculation over the orifice

| Stage | $D$ (m) | $d$ (m) | $l$ (m) | $\beta$ (−) | $L$ (−) | $A$ (m$^2$) |
|---|---|---|---|---|---|---|
| 1st | 0.108 | 0.055 | 0.0254 | 0.5093 | 0.2352 | 0.0092 |
| 2nd | 0.108 | 0.050 | 0.0254 | 0.4630 | 0.2352 | 0.0092 |

**Determination of total pressure and temperature**

The temperature and pressure sensors used cannot measure the total temperature and pressure. Due to this fact, the measurement data must be corrected to total conditions of temperature and pressure to derive the performance of the turbo compressors.

$$\begin{aligned} T_t &= T_{st} + T_{dyn} \\ p_t &= p_{st} + p_{dyn} \end{aligned} \tag{3.10}$$

The temperature $T_t$ at total conditions results from the sum of the static temperature $T_{st}$ and the dynamic temperature $T_{dyn}$. The same applies to the pressure. The measured temperature considers a part of the dynamic temperature in addition to the static temperature. This dynamic part is considered by the recovery factor $R.F.$.

$$T_m = T_{st} + T_{dyn} \cdot R.F. \tag{3.11}$$

The recovery factor $R.F.$ is defined by the ratio of the temperature components.

$$R.F. = \frac{T_m - T_{st}}{T_t - T_{st}} = \frac{T_m - T_{st}}{T_{dyn}} \tag{3.12}$$

For the further calculation, the recovery factor $R.F.$ is set to 0.7. (Anthoine, et al., 2009, p. 151) By transforming the Equation 3.12, the temperatures $T_{st}$ and $T_t$ can be calculated.

$$\begin{aligned} T_{st} &= T_m - T_{dyn} \cdot R.F. \\ T_t &= T_m + (1 - R.F.) \cdot T_{dyn} \end{aligned} \tag{3.13}$$

The dynamic temperature is determined from the ratio of fluid velocity $c$ and heat capacity at constant pressure $c_p$. For simplification, an isobaric behavior is assumed.

$$T_{dyn} = \frac{c^2}{2 \cdot c_p} \tag{3.14}$$

The Calculation of the total pressure considers the static pressure multiplied by the ratio of total temperature and static temperature as well as the isentropic exponent $\kappa$.

$$p_t = p_{st} \cdot \left(\frac{T_t}{T_{st}}\right)^{\frac{\kappa}{\kappa-1}} \tag{3.15}$$

The isentropic exponent κ is calculated of the ratio of the heat capacity at constant pressure $c_p$ and the heat capacity at constant volume $c_v$. For this purpose, $c_p$ and $c_v$ are simplified assumed to be constant. (Nguyen-Schäfer, 2015, p. 21)

**Consideration of surface heat losses**

Despite the insulation of all pipes (see Section 2.1), heat losses from the measuring points to the compressor inlet and outlet must be considered due to the large area of hot surfaces with high temperature differences. At the compressor inlet, the surface heat losses reduce the actual temperature compared to the measured value. On the other side, the surface heat losses lead to a decrease of the measured temperature compared to the actual temperature at the compressor outlet. The respective change of actual temperature leads to a change of the respective enthalpy. This will be discussed in more detail below.

For the determination of the mean surface temperatures $T_{\mathrm{m\,surface}}$ for each section, seven thermocouples were installed per stage. Two of the thermocouples were installed between the inlet measuring point and the compressor inlet, one on the compressor housing and three between the compressor outlet and the outlet measuring point. The seventh was installed on the test facility to measure the ambient temperature. All type T thermocouples consist of two different wire materials that are bare wire stub welded and have an accuracy better then ± 1.0 °C (Doebelin, 1990, pp. 625-626).

During the experiments one measurement per 30 seconds was recorded. In the first step, the mean surface temperatures $T_{\mathrm{m\,surface}}$ for each section were determined. Subsequently, the mean temperature differences $\Delta T_{\mathrm{m}}$ were calculated as positive difference from the determined $T_{\mathrm{m\,surface}}$ and current ambient temperature $T_{\mathrm{amb}}$. For evaluation, the mean temperature differences $\Delta T_{\mathrm{m}}$ for each section were determined and then plotted against the respective measured total steam temperature at the inlet $T_{\mathrm{t\,in}}$ or at the outlet $T_{\mathrm{t\,out}}$ for each stage.

The following Figures 3.2 and 3.3 visualize the result diagrams. Both figures each consist of three diagrams for the previously explained sections. The axis intercepts were adapted to the determined value ranges. The red dots represent the determined mean temperature differences $\Delta T_{\mathrm{m}}$ and the drawn line represents the determined linear trend line. The corresponding equation for each linear trend line is shown in the lower right corner.

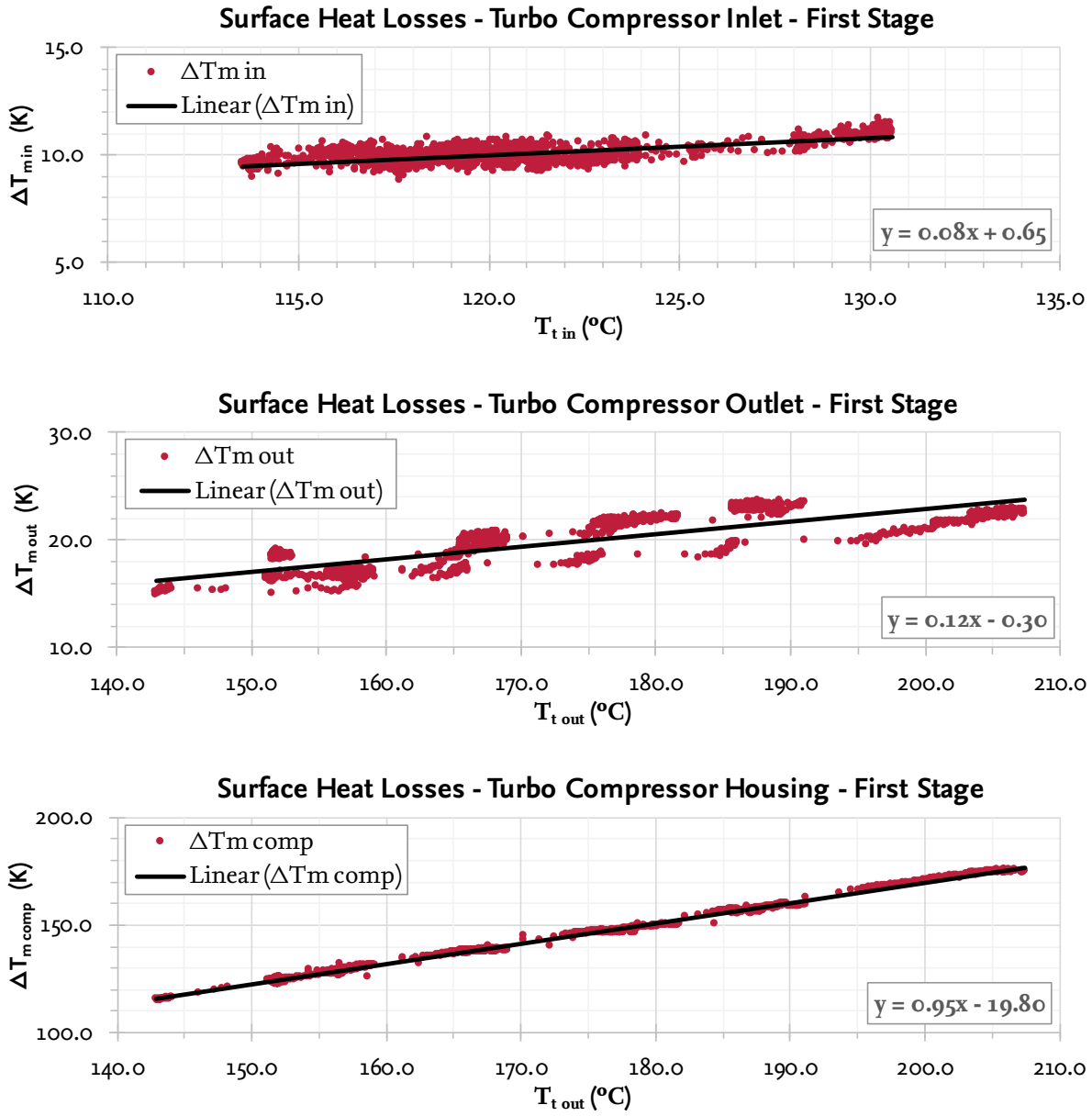


Figure 3.2: Determination of the surface heat losses at the first stage

For both stages, the axis range of the measured temperatures at the inlet is smaller than at the outlet due to the control of the inlet conditions by water injection via the de-superheaters. In addition, the temperature at the outlet depends on the set impeller speed and an increase in the impeller speed leads to higher temperatures at the outlet.

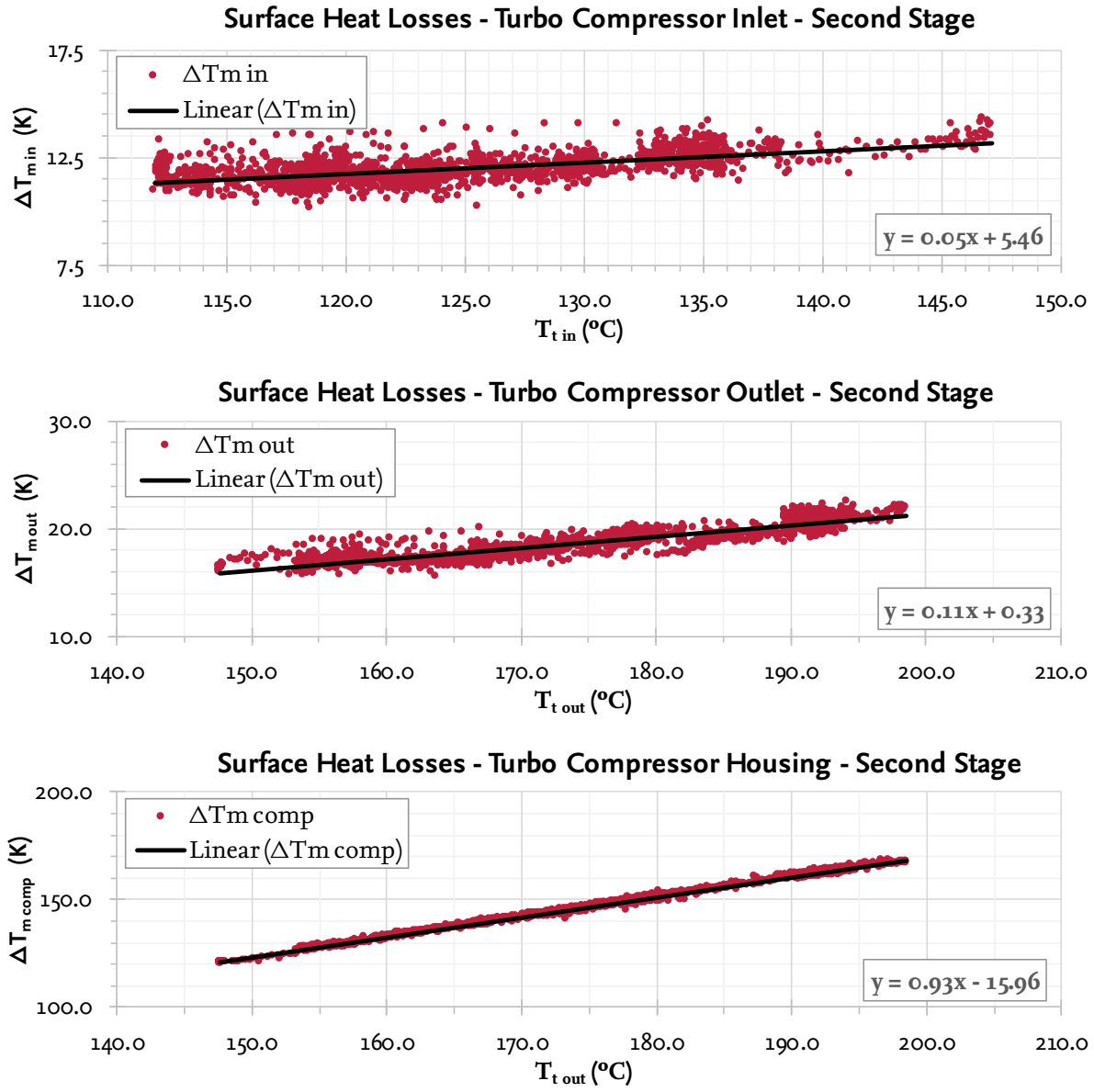


Figure 3.3: Determination of the surface heat losses at the second stage

Table 3.2 summarizes the empirically determined equations of the linear trend lines obtained from the result diagrams for each section of both stages. To further determine mean temperature differences, these equations were included in the calculation of heat losses.

Table 3.2: Equations of the linear trend lines for the mean temperature differences between surface and ambient

| Stage | $\Delta T_{m\,in} =$ | $\Delta T_{m\,comp} =$ | $\Delta T_{m\,out} =$ |
|---|---|---|---|
| 1st | $0.08 \cdot T_{t\,in} + 0.65$ | $0.95 \cdot T_{t\,out} - 19.80$ | $0.12 \cdot T_{t\,out} - 0.30$ |
| 2nd | $0.05 \cdot T_{t\,in} + 5.46$ | $0.93 \cdot T_{t\,out} - 15.96$ | $0.11 \cdot T_{t\,out} + 0.33$ |

The heat transfer coefficient at the surface for each section was calculated with the simplify Equation 3.16. That means for the surfaces of the insulation for the inlet and outlet lines as well as on the surface of the compressor housing.

$$\alpha_{surface} = a_1 + a_2 \cdot \Delta T_m \tag{3.16}$$

This simplify equation contains the constants $a_1$ and $a_2$ and applies to stationary air and considers radiation and free convection. In this case, the value for $a_1$ and $a_2$ were set to 8 ($W/m^2$) and 0.04 ($W/m^2K$) in accordance to (Verein deutscher Ingenieure VDI e.V., 2013, p. 721). After the determination of $\alpha_{surface}$ the heat flow due to heat losses $\dot{Q}_{hl}$ for each section is calculated using the following Equation 3.17.

$$\dot{Q}_{hl} = \alpha_{surface} \cdot A \cdot \Delta T_m \tag{3.17}$$

In this equation $\alpha_{surface}$ is the heat transfer coefficient at the surface, A is the surface and $\Delta T_m$ is the mean temperature difference (Verein deutscher Ingenieure VDI e.V., 2013, p. 33). The surfaces of the different sections were assumed to be $A_{in} = 0.8\ m^2$ for the first, $A_{in} = 0.6\ m^2$ for the second, $A_{out} = 1.0\ m^2$ and $A_{comp} = 0.2\ m^2$ equal for both stages. The emitted $\dot{Q}_{hl}$ leads to a reduction of the steam temperature and thus to a reduction of the specific enthalpy. The specific enthalpy difference due to the heat losses $\Delta h_{hl}$ is calculated from the ratio of $\dot{Q}_{hl}$ and the mass flow rate at total conditions $\dot{m}_t$.n

$$\Delta h_{hl} = \frac{\dot{Q}_{hl}}{\dot{m}_t} = c_p \cdot \Delta T \tag{3.18}$$

The specific enthalpy difference $\Delta h_{hl}$ can also be determined by the product of the specific heat capacity $c_p$ and temperature difference $\Delta T$. For this purpose, an isobaric change of state is assumed. (Nguyen-Schäfer, 2015, p. 22) This relation is used for the calculation of the specific enthalpy $h_{hl}$ and temperature $T_{hl}$ considering the surface heat losses for each section. Table 3.3 summarizes the equations used for the calculation.

Table 3.3: Equations for the calculation of the specific enthalpies and temperatures considering the surface heat losses for each section

| Stage | $h_{hl\,in} =$ | $T_{hl\,in} =$ | $h_{hl\,out} =$ | $T_{hl\,out} =$ |
|---|---|---|---|---|
| 1st | $h_{t\,in} - \frac{\dot{Q}_{hl\,in}}{\dot{m}_t}$ | $T_{t\,in} - \frac{\dot{Q}_{hl\,in}}{\dot{m}_t \cdot c_{p\,in}}$ | $h_{t\,out} + \frac{\dot{Q}_{hl\,out}}{\dot{m}_t}$ | $T_{t\,out} + \frac{\dot{Q}_{hl\,out}}{\dot{m}_t \cdot c_{p\,out}}$ |
| 2nd | $h_{t\,in} - \frac{\dot{Q}_{hl\,in}}{\dot{m}_t}$ | $T_{t\,in} - \frac{\dot{Q}_{hl\,in}}{\dot{m}_t \cdot c_{p\,in}}$ | $h_{t\,out} + \frac{\dot{Q}_{hl\,out}}{\dot{m}_t}$ | $T_{t\,out} + \frac{\dot{Q}_{hl\,out}}{\dot{m}_t \cdot c_{p\,out}}$ |

## 3.3 Determination of turbo compressor performance

For the determination of the turbo compressor performance the creation of a compressor map is suitable since different operating points at off-design conditions can be compared and evaluated. For the creation of the compressor map, the isentropic efficiency $\eta_{isen}$, the pressure ratio $\Pi$, the mass flow rate $\dot{m}$ or volume flow rate $\dot{V}$ and the impeller speed $N$ are required. In the following, the determination of the necessary parameters for the compressor map is discussed.

As previously discussed in Section 1.3, the isentropic efficiency is calculated from the ratio of the differences of the specific enthalpy at the outlet for the isentropic process and the actual specific enthalpy at the outlet to the specific enthalpy at the inlet.

$$\eta_{isen} = \frac{h_{out\,s} - h_{in}}{h_{out} - h_{in}} \tag{3.19}$$

The pressure ratio $\Pi_t$ is defined as the pressure increase across the compressor and is calculated from the quotient of the pressure at the outlet and the pressure at the inlet.

$$\Pi_t = \frac{p_{t\,out}}{p_{t\,in}} \tag{3.20}$$

For a better comparability of the operating points at different inlet conditions, the mass flow rate $\dot{m}_t$ is reduced to defined reference conditions for the temperature and the pressure at the turbo compressor inlet. (Essen, H. A. van, 1998, p. 143)

$$\dot{m}_{red} = \dot{m}_t \cdot \frac{\sqrt{(T_{hl\,in}/T_{ref})}}{(p_{t\,in}/p_{ref})} \tag{3.21}$$

The reference conditions at the inlet were set to $T_{ref} = 120$ °C and $p_{ref} = 1.03$ bar due to the achievable inlet conditions during the experiments at the test facility. To calculate the reduced volume flow rate $\dot{V}_{red}$, the reduced mass flow rate $\dot{m}_{red}$ is divided by the density at reference conditions with $\rho_{ref} = 0.565\ kg/m^3$.

$$\dot{V}_{red} = \frac{\dot{m}_{red}}{\rho_{ref}} \tag{3.22}$$

Due to different inlet conditions, the set impeller speed $N_{set}$ must be reduced to the reference temperature as well. (Hafaifa, et al., 2014, p. 633)

$$N_{red} = \frac{N_{set}}{\sqrt{(T_{hl\,in}/T_{ref})}} \tag{3.23}$$

For the determination of the speed lines at reference conditions, the reduced parameters were set in relation to the set impeller speed. Therefore, the parameters were multiplied with the quotient of the set impeller speed $N_{set}$ and the reduced impeller speed $N_{red}$.

$$\begin{aligned} \Pi_{rel} &= \Pi_t \cdot \frac{N_{set}}{N_{red}} \\ \dot{m}_{rel} &= \dot{m}_{red} \cdot \frac{N_{set}}{N_{red}} \\ \dot{V}_{rel} &= \dot{V}_{red} \cdot \frac{\mathrm{N_{set}}}{N_{red}} \end{aligned} \tag{3.24}$$

The reduction to reference conditions as well as the speed correction ensure a simplification of the presentation and valuation of operating points at different inlet conditions. Without these adjustments, the respective inlet parameters must be specified for each operating point. The effects of the conducted steps will be shown in the next chapter.

The energy balance $\Delta E$ for each turbo compressor stage was determined to double check the measured and calculated performance results. A large deviation of the energy balance from zero can indicate a faulty measurement or calculation. For this purpose, the energy inputs and outputs were accounted for each stage.

$$\Delta E = P_{el} \cdot \eta_{inverter} - \dot{Q}_{cool} - \dot{Q}_{hl\,comp} - \dot{W}_{steam} \tag{3.25}$$

The consumed electrical power $P_{el}$ for both stages is calculated from the measured power before the inverters multiplied by the efficiency of the inverters. The heat flow due to the cooling of the motor and gearbox $\dot{Q}_{cool}$ is caused by losses occurring in the motor and gearbox and heats the cooling water. Therefore, the amount also provides information about the efficiency of the motor and gearbox. The heat flow $\dot{\mathrm{Q}}_{\mathrm{hl\,comp}}$ describes the surface heat losses through the compressor housing between the inlet and outlet, which were not consider in the cooling flow. Both, the heat flow due to the cooling of the motor and gearbox $\dot{Q}_{cool}$ and the heat flow due to surface heat losses through the turbo compressor housing $\dot{\mathrm{Q}}_{\mathrm{hl\,comp}}$ reduce the energy balance. $\dot{W}_{steam}$ describes the energy transferred by the work of the turbo compressor to the working fluid. Therefore, $\dot{W}_{steam}$ is determined from the actual specific enthalpy difference between the outlet and the inlet of the turbo compressor multiplied by the mass flow rate. See Figure 2.5 for a schematic overview of the turbo compressor unit.

## 3.4 Determination of measurement uncertainties

Experiments always contains certain measurement uncertainties. The basis for the determination of measurement uncertainties is the conduction of an uncertainty analysis for the two-stage turbo compressor test facility. According to (Moffat, 1988), the uncertainty analysis relates to the process of estimating how great the effects of the uncertainties on the individual measurement are on the calculated result. Besides its obvious role in publishing, uncertainty analysis provides the experimenter a rational way of evaluating the significance of the scatter on repeated trails. (Moffat, 1988, p. 1)

The measured values do not necessarily correspond to the truth value. However, the true value is most likely within an error range that can be defined. For this definition it is important to identify the sources of uncertainties and define the impact of the measurement. (Moffat, 1988, p. 1) In the following, the calculation methods for the determination of the uncertainties for the mass flow rate and isentropic efficiency are presented and the sources of uncertainties are discussed. Here, the focus is on errors of the measuring instruments. Due to the changing inlet conditions as well as manual changes, such as the change of the opening of the expansion valve, a multiple repetition of the same operating point is unrealistic. Therefore, it is important to know how large the deviation is for each recorded operating point.

**Mass flow rate**

The method of estimating the relative uncertainty of the mass flow rate is in accordance to ISO-5167-1:2003 and combines relative uncertainties from different parameters via the following equation. (Reddy, 2011, p. 86)

$$\frac{\delta \dot{m}}{\dot{m}} = \sqrt{\left(\frac{\delta C}{C}\right)^2 + \left(\frac{\delta \epsilon}{\varepsilon}\right)^2 + \left(\frac{2\beta^4}{1-\beta^4}\right)^2 \cdot \left(\frac{\delta D}{D}\right)^2 + \left(\frac{2}{1-\beta^4}\right)^2 \cdot \left(\frac{\delta d}{d}\right)^2 + \frac{1}{4}\left(\frac{\delta \Delta p}{\Delta p}\right)^2 + \frac{1}{4}\left(\frac{\delta \rho}{\rho}\right)^2} \quad (3.26)$$

$\delta\dot{m}/\dot{m}$ is the relative uncertainty of the mass flow rate. $\delta C/C$ is the relative uncertainty of the discharge coefficient. $\delta\varepsilon/\varepsilon$ is the relative uncertainty of the expansibility factor. $\beta$ is the diameter ratio of the orifice diameter to the inner pipe diameter. $\delta D/D$ is the relative uncertainty of the inner pipe diameter. $\delta d/d$ is the relative uncertainty of the orifice plate diameter. $\delta\Delta p/\Delta p$ is the relative uncertainty of the pressure drop over the orifice plate. $\delta\rho/\rho$ is the relative uncertainty of the fluid density. (EN ISO 5167-1:2003, 2003).

The Table 3.4 summarizes the relative uncertainties used for the calculation of the relative uncertainty of the mass flow rate. These values are based on experience of (Bantle, 2017) and (Johannesson, 2017) in previous tests with similar instruments.

Table 3.4: Summary of relative uncertainties for different parameters

| Stage | $\delta C/C$ (%) | $\delta\varepsilon/\varepsilon$ (%) | $\delta D/D$ (%) | $\delta d/d$ (%) |
|---|---|---|---|---|
| 1st | 0.450 | 0.102 | 0.215 | 0.263 |
| 2nd | 0.450 | 0.102 | 0.215 | 0.263 |

The relative uncertainty of the pressure drops over the orifice plate $\delta\Delta p\ /\Delta p$ is calculated by using an error specified by the producer of the differential pressure sensor of 0.0015 bar to $\delta\Delta p\ /\Delta p\ = 0.0015/\Delta p$. The relative uncertainty of the fluid density $\delta\rho/\rho$ is a function of the temperature and pressure uncertainties.

$$\frac{\delta\rho}{\rho} = \sqrt{\left(\frac{\delta T_{hl\ out}}{T_{hl\ out}}\right)^2 + \left(\frac{\delta p_{t\ out}}{p_{t\ out}}\right)^2} \tag{3.27}$$

$\delta T_{hl\ out}/T_{hl\ out}$ is the relative uncertainty of the temperature including the surface heat losses at the outlet and $\delta p_{t\ out}/p_{t\ out}$ is the relative uncertainty of the total pressure at the outlet. (EN ISO 5167-1:2003, 2003).

**Isentropic efficiency**

As described in the previous section, the isentropic efficiency is affected by the temperatures and pressures at the inlet and outlet. For this purpose, the accumulated errors for the temperature and pressure were determined considering the largest sources of error. The accumulated temperature error $\delta T$ consists of an instrument error $\delta T_{ins}$, a dynamic temperature error $\delta T_{dyn}$ and a heat loss error $\delta T_{hl}$.

$$\delta T = \delta T_{ins} + \delta T_{dyn} + \delta T_{hl} \tag{3.28}$$

The instrument error $\delta T_{ins}$ is the instrument measurement accuracy given by the producer. The dynamic temperature error $\delta T_{dyn}$ is assumed to be 20 % of the calculated value of the dynamic temperature. The heat loss error $\delta T_{hl}$ is assumed to be 20 % of the determined temperature difference value caused by the surface heat losses.

The accumulated pressure error $\delta p$ consists of an instrument error $\delta p_{ins}$ and a dynamic pressure error $\delta p_{dyn}$ since the surface heat losses have only a negligible influence.

$$\delta p = \delta p_{ins} + \delta p_{dyn} \tag{3.29}$$

The instrument error $\delta p_{ins}$ is the instrument measurement accuracy given by the producer. The dynamic pressure error $\delta p_{dyn}$ is assumed to be 20 % of the calculated value of the dynamic pressure. The assumed values for the temperature and pressure errors are based on experience of (Bantle, 2017) and (Johannesson, 2017) in previous tests with similar instruments.

The deviations of the isentropic efficiency are calculated for temperatures and pressures at the inlet and outlet by considering the accumulated errors.

$$\begin{aligned}
\delta\eta_{Tin} &= \eta_{isen}(T_{hl\,in} \pm \delta T_{in},\ T_{hl\,out},\ p_{t\,in},\ p_{t\,out}) - \eta_{isen} \\
\delta\eta_{Tout} &= \eta_{isen}(T_{hl\,in},\ T_{hl\,out} \pm \delta T_{out},\ p_{t\,in},\ p_{t\,out}) - \eta_{isen} \\
\delta\eta_{pin} &= \eta_{isen}(T_{hl\,in},\ T_{hl\,out},\ p_{t\,in} \pm \delta p_{in},\ p_{t\,out}) - \eta_{isen} \\
\delta\eta_{pout} &= \eta_{isen}(T_{hl\,in},\ T_{hl\,out},\ p_{t\,in},\ p_{t\,out} \pm \delta p_{out}) - \eta_{isen}
\end{aligned} \tag{3.30}$$

The relative uncertainty of the isentropic efficiency is a root-sum-square of the specific relative uncertainties caused by the determined deviations of the isentropic efficiency.

$$\frac{\delta\eta_{isen}}{\eta_{isen}} = \sqrt{\left(\frac{\delta\eta_{Tin}}{\eta_{isen}}\right)^2 + \left(\frac{\delta\eta_{Tout}}{\eta_{isen}}\right)^2 + \left(\frac{\delta\eta_{pin}}{\eta_{isen}}\right)^2 + \left(\frac{\delta\eta_{pout}}{\eta_{isen}}\right)^2} \tag{3.31}$$

# 4 Analysis of the Experimental Test Results

This Chapter covers the analysis of the measured and corrected experimental test results. For this purpose, the results are presented at the beginning and then analyzed regarding the turbo compressor performance and the two-stage turbo compressor system performance. Finally, the results are discussed in detail.

## 4.1 Presentation of the performance test results

This section presents the performance test results based on the conducted calculation and corrections steps (see Chapter 3). During the tests, the turbo compressors were operated in different operating states. For the presentation, three different operation points were selected to visualize the performed correction and calculation process. The extensive database with all recorded operating points can be found in the appendix (see Appendix A).

As described in the previous chapter, stable operating points are considered for the evaluation of the test results. A stable operating point is characterized by the fact that the determined variation of the measured values for a period of at least five minutes is smaller than the defined limit for the coefficient of variation $C_v$ (see Section 3.2).

**Identification and selection of stable operating points for further analysis**

The Table 4.1 shows the determined measurement results of the conducted performance tests for three selected operating points. The selected operating points were all performed at an impeller speed of 72,000 rpm for both turbo compressors. This allows a direct comparison of the operating parameters of both turbo compressor stages due to different valve opening positions of the expansion valve at constant speed lines.

Table 4.1: Measured performance test results for selected operating points

| Stage | | $N_{set}$ (rpm) | $T_{in}$ (°C) | $p_{in}$ (bar) | $T_{out}$ (°C) | $p_{out}$ (bar) | $\Delta p$ (bar) | $\Pi$ (–) | $\dot{m}$ (kg/s) | $P_{el}$ (kW) |
|---|---|---|---|---|---|---|---|---|---|---|
| 1. | 1st | 72,000 | 120.8 | 0.99 | 187.4 | 1.30 | 0.096 | 1.31 | 0.158 | 26.0 |
| | 2nd | 72,000 | 118.0 | 1.08 | 184.1 | 1.45 | 0.143 | 1.34 | 0.166 | 26.9 |
| 2. | 1st | 72,000 | 121.5 | 0.99 | 188.2 | 1.36 | 0.087 | 1.37 | 0.155 | 25.7 |
| | 2nd | 72,000 | 119.1 | 1.17 | 185.9 | 1.78 | 0.110 | 1.52 | 0.163 | 26.7 |
| 3. | 1st | 72,000 | 123.0 | 0.99 | 190.8 | 1.60 | 0.054 | 1.61 | 0.133 | 22.8 |
| | 2nd | 72,000 | 124.2 | 1.48 | 193.9 | 2.52 | 0.057 | 1.70 | 0.140 | 24.6 |

In the table, the measured values of the selected operating points are each represented as a pair from both turbo compressor stages with an impeller speed of 72,000 rpm. From the upper operating point downwards, the expansion valve was gradually closed. In addition to the set impeller speeds, the measured temperatures and pressures for the inlet and outlet as well as the measured differential pressure drops across the orifice are shown. The illustrated pressure ratio and mass flow rate were calculated based on the quotient of the measured pressures at the inlet and outlet as well as the differential pressure drops and using defined constants from the software. The electrical power consumed by the turbo compressors for each stage was measured before the inverters. All selected operation points were clear below the defined $C_v$ limit of 1.0 % for temperature and pressure and 4.0 % for differential pressure drop.

The results in Table 4.1 show that the inlet parameters of the first stage were almost constant for the different operating points. A slight increase in the inlet temperature causes a slight increase in the outlet temperatures. The changing inlet parameters of the second stage relates to the change of the outlet parameters of the first stage. Closing the expansion valve increases the outlet pressure and reduces the differential pressure drop of both stages. This leads to an increase in the pressure ratio, which is always higher for the second stage, and a reduction of the mass flow rate. The difference in mass flow rate between stages is due to water injection through the de-superheater. The electrical power requirement for the second stage is always greater and decreases for both stages with the reduction of the mass flow rate.

**Flow rate calculation**

Table 4.2 summarizes the main results of the flow rate calculation for the selected operating points. For the iterative calculation of the mass flow rates, the differential pressure drops were corrected. The fluid density is a function of the temperature and pressure and was determined at the inlet and outlet for both stages. Since the mass flow rate through each turbo compressor is constant, the fluid density can be used to calculate the respective volume flow rate at the inlet and outlet. The fluid velocities were calculated from the quotient of the volume flow rates and the cross-sectional areas.

Table 4.2: Flow rate calculation results for selected operating points

| Stage | | $N_{set}$ (rpm) | $\Delta p$ (bar) | $\dot{m}_{cal}$ (kg/s) | $\rho_{in}$ (kg/m³) | $\dot{V}_{in}$ (m³/s) | $\rho_{out}$ (kg/m³) | $\dot{V}_{out}$ (m³/s) | $c_{in}$ (m/s) | $c_{out}$ (m/s) |
|---|---|---|---|---|---|---|---|---|---|---|
| 1. | 1st | 72,000 | 0.096 | 0.158 | 0.553 | 0.286 | 0.614 | 0.257 | 14.0 | 28.1 |
| | 2nd | 72,000 | 0.143 | 0.165 | 0.606 | 0.273 | 0.693 | 0.239 | 29.8 | 26.1 |
| 2. | 1st | 72,000 | 0.088 | 0.155 | 0.552 | 0.281 | 0.645 | 0.241 | 13.8 | 26.3 |
| | 2nd | 72,000 | 0.110 | 0.163 | 0.654 | 0.249 | 0.848 | 0.192 | 27.2 | 20.9 |
| 3. | 1st | 72,000 | 0.055 | 0.134 | 0.549 | 0.240 | 0.754 | 0.178 | 12.0 | 19.4 |
| | 2nd | 72,000 | 0.057 | 0.140 | 0.823 | 0.171 | 1.188 | 0.118 | 18.6 | 12.9 |

Due to the temperature and pressure dependence, the fluid density increases with increasing temperature and pressure, resulting in a reduction of the volume flow rate. For this reason, the volume flow rate decreases from inlet to outlet for each turbo compressor stage. In addition, the volume flow rate for the second stage is always lower due to the higher temperature and pressure levels. Based on the calculation, the change of the fluid velocity is proportional to the volume flow rate and decreases from the inlet to the outlet for the second stage. Due to the larger cross-sectional area at the inlet, the fluid velocity is reversed for the first stage. When comparing the selected operating points, all parameters except fluid density decrease with the closing of the expansion valve. Thus, the values of the flow rate calculation follow the trend described in Table 4.1.

**Determination of total pressure and temperature**

Table 4.3 displays the determined total conditions for the selected operating points. For the temperatures as well as the pressures at the inlet and outlet the total and dynamic values are indicated since these are needed for the further consideration. If necessary, the static values can be calculated from the given parameters (see Section 3.2).

Table 4.3: Determined stagnation conditions for selected operating points

| Stage | | $N_{set}$ (rpm) | $T_{t\,in}$ (°C) | $T_{dyn\,in}$ (°C) | $p_{t\,in}$ (bar) | $p_{dyn\,in}$ (mbar) | $T_{t\,out}$ (°C) | $T_{dyn\,out}$ (°C) | $p_{t\,out}$ (bar) | $p_{dyn\,out}$ (mbar) |
|---|---|---|---|---|---|---|---|---|---|---|
| 1. | 1st | 72,000 | 120.9 | 0.05 | 1.00 | 0.54 | 187.4 | 0.20 | 1.30 | 2.41 |
| | 2nd | 72,000 | 118.0 | 0.22 | 1.08 | 2.66 | 184.2 | 0.17 | 1.45 | 2.33 |
| 2. | 1st | 72,000 | 121.6 | 0.05 | 0.99 | 0.52 | 188.3 | 0.17 | 1.36 | 2.21 |
| | 2nd | 72,000 | 119.1 | 0.18 | 1.17 | 2.38 | 186.0 | 0.11 | 1.78 | 1.84 |
| 3. | 1st | 72,000 | 123.0 | 0.04 | 0.99 | 0.39 | 190.8 | 0.09 | 1.60 | 1.41 |
| | 2nd | 72,000 | 124.2 | 0.08 | 1.49 | 1.40 | 193.9 | 0.04 | 2.53 | 0.97 |

The proportion of dynamic conditions in relation to the determined total conditions is low for both temperature and pressure. Therefore, dynamic pressure is given in unit millibar for a better overview. Due to the dependence on the previously determined fluid velocities, dynamic shares at the inlet are smaller than at the outlet for the first stage and vice versa for the second stage. Overall, the difference between the measured values and the calculated total conditions is not very large. However, this is an important calculation step because even small changes can affect the calculation of the turbo compressor performance.

**Consideration of surface Heat losses**

Table 4.4 summarizes the results of the consideration of surface heat losses for the selected operating points. The mass flow rate was corrected based on the determined total temperature and total pressure for both stages. As described in Section 3.2, the heat flow due to surface heat losses were calculated for the inlet, outlet and compressor housing. Considering the surface heat losses, the corrected temperatures were calculated for the inlet and outlet. The temperature difference represents the difference to the previously determined temperature in total condition. The effects of surface heat losses on the pressure are negligible. The enthalpy change can be determined using the new temperatures and the pressures in total conditions.

Table 4.4: Consideration of surface heat losses for selected operating points

| Stage | | $N_{set}$ (rpm) | $\dot{m}_t$ (kg/s) | $\dot{Q}_{hl\ in}$ (W) | $T_{hl\ in}$ (°C) | $\Delta T_{in}$ (°C) | $\dot{Q}_{hl\ out}$ (W) | $T_{hl\ out}$ (°C) | $\Delta T_{out}$ (°C) | $\dot{Q}_{hl\ comp}$ (W) |
|---|---|---|---|---|---|---|---|---|---|---|
| 1. | 1st | 72,000 | 0.160 | 71 | 120.6 | -0.3 | 191 | 188.0 | 0.6 | 360 |
| | 2nd | 72,000 | 0.167 | 66 | 117.8 | -0.2 | 168 | 184.7 | 0.5 | 350 |
| 2. | 1st | 72,000 | 0.156 | 71 | 121.3 | -0.3 | 192 | 188.9 | 0.6 | 363 |
| | 2nd | 72,000 | 0.164 | 66 | 118.9 | -0.2 | 170 | 186.5 | 0.5 | 355 |
| 3. | 1st | 72,000 | 0.135 | 72 | 122.7 | -0.3 | 195 | 191.6 | 0.8 | 371 |
| | 2nd | 72,000 | 0.141 | 68 | 124.0 | -0.2 | 178 | 194.6 | 0.7 | 380 |

The determined heat flows are greater for both stages at the outlet than at the inlet and for the first stage slightly larger than for the second stage. When comparing the heat flows at the inlet to the outlet, it becomes clear that they increase at a higher fluid temperature due to a higher temperature difference to the ambient. This also leads to a larger change in the temperatures at the outlet, represented by the amount of $\Delta T$. In comparison to all selected operating points, the reduction of the mass flow rate also leads to an increase of $\Delta T$. The temperatures are corrected downwards at the inlet and upwards at the outlet as described in Section 3.2. Despite a smaller surface and the same reference temperature, the heat flows through the compressor housing are about twice as high as at the outlet. This is due to the lack of insulation of the compressor housing.

**Determination of turbo compressor performance**

Table 4.5 displays the determined test results of the turbo compressor performance for selected operating points reduced to the defined reference conditions at the inlet. The impeller speed, mass flow rate and volume flow rate were calculated and reduced to the reference conditions as explained in Section 3.3. The illustrated temperatures and pressures at the inlet and outlet are the previously determined temperatures with considered heat losses and the pressures at total conditions. The pressure ratio and the isentropic efficiency were calculated in accordance to the Equations 3.19 and 3.20.

Table 4.5: Test results for selected operating points reduced to reference conditions

| Stage | | $N_{red}$ (rpm) | $\dot{m}_{red}$ (kg/s) | $\dot{V}_{red\ in}$ ($m^3/s$) | $T_{hl\ in}$ (°C) | $T_{hl\ out}$ (°C) | $p_{t\ in}$ (bar) | $p_{t\ out}$ (bar) | $\Pi_t$ (−) | $\eta_{isen}$ (−) |
|---|---|---|---|---|---|---|---|---|---|---|
| 1. | 1st | 71,942 | 0.163 | 0.288 | 120.6 | 188.0 | 1.00 | 1.30 | 1.30 | 0.37 |
| | 2nd | 72,200 | 0.156 | 0.277 | 117.8 | 184.7 | 1.08 | 1.45 | 1.34 | 0.41 |
| 2. | 1st | 71,878 | 0.160 | 0.282 | 121.3 | 188.9 | 0.99 | 1.36 | 1.37 | 0.45 |
| | 2nd | 72,098 | 0.142 | 0.251 | 118.9 | 186.5 | 1.17 | 1.78 | 1.52 | 0.60 |
| 3. | 1st | 71,755 | 0.138 | 0.244 | 122.7 | 191.6 | 0.99 | 1.60 | 1.61 | 0.68 |
| | 2nd | 71,639 | 0.096 | 0.171 | 124.0 | 194.6 | 1.49 | 2.53 | 1.70 | 0.74 |

The reduced impeller speeds are slightly different in both directions from the set 72,000 rpm. For the reduced mass flows rate, the ratio has reversed so that the mass flow rate at the second stage is less than at the first stage. For this purpose, the higher pressure at the inlet of the second stage is mainly responsible. The calculated values for the pressure ratio and the isentropic efficiency are always higher for the second stage. The achieved pressure ratio is in the range of 1.30 and 1.61 for the first stage and 1.34 and 1.70 for the second stage. When comparing the selected operating points, the differences in the mass and volume flow rates between the first and second stage increase with the closing of the expansion valve. For the differences in the pressure ratio and the isentropic efficiency, an initial increase and subsequent descent are observed. The appendix contains an overview of the parameters listed in Table 4.5 for all recorded operating points (see Appendix A)

The calculated energy balances for double checking and assessing the quality of the calculations is in range of -0.50 kW to 0.09 kW. Compared to the applied electric power in range of 22.8 kW to 26.9 kW, this is an indication of a good accuracy of the calculations. For better comparability of the results, the previous determined parameters for the performance analysis of the turbo compressor were corrected in relation to the set impeller speed (see Section 3.3). For this purpose, the reduced values for mass flow rate and volume flow rate as well as the pressure ratio were multiplied by the quotient of set and reduced impeller speed. For the selected operating points, adjustments in the range of -0.50 % and 0.28 % resulted. An overview of the results for the selected operating points can be found in the appendix (see Appendix A).

**Determination of measurement uncertainties**

Table 4.6 displays the determined measurement uncertainties for the selected operating points. The relative deviations due to the detected errors are given as coefficient of variation. This allows the identification of the largest source of error.

Table 4.6: Measurement uncertainties for selected operating points at set impeller speeds of 72,000 rpm

| Stage | | $\Pi_t$ (−) | $\dot{m}_t$ (kg/s) | $C_{v\,\dot{m}}$ (%) | $\eta_{isen}$ (−) | $C_{v\,\eta isen}$ (%) | $C_{v\,Tin}$ (%) | $C_{v\,Tout}$ (%) | $C_{v\,pin}$ (%) | $C_{v\,pout}$ (%) |
|---|---|---|---|---|---|---|---|---|---|---|
| 1. | 1st | 1.30 | 0.160 | 1.20 | 0.37 | 12.61 | 1.46 | 1.35 | 1.96 | 3.78 |
| | 2nd | 1.34 | 0.167 | 1.40 | 0.41 | 21.27 | 1.54 | 1.33 | 4.16 | 7.46 |
| 2. | 1st | 1.37 | 0.156 | 1.24 | 0.45 | 8.95 | 1.46 | 1.35 | 1.66 | 3.04 |
| | 2nd | 1.52 | 0.164 | 1.33 | 0.60 | 9.25 | 1.52 | 1.32 | 2.76 | 4.36 |
| 3. | 1st | 1.61 | 0.135 | 1.63 | 0.68 | 4.20 | 1.45 | 1.35 | 1.13 | 1.74 |
| | 2nd | 1.70 | 0.141 | 1.63 | 0.74 | 4.88 | 1.47 | 1.29 | 1.75 | 2.50 |

The coefficient of variation for mass flow rate and isentropic efficiency increase as the value of the reference parameter decreases. The instrumental error of the pressure sensor at the outlet is the dominate uncertainty. This leads to large relative uncertainty in isentropic efficiency, especially at low pressures at the outlet. The high uncertainty of the pressure regarding will decline for tests with higher pressure ratios.

## 4.2 Analysis of the turbo compressor performance

For the analysis of the turbo compressor performance, a compressor map was developed based on the previously presented experimental test results. As already described in Section 1.3 and 3.3, a compressor map provides a visual analysis of the compressor performance and achievable operating points. For this reason, different compressor maps were created from the determined performance test results. This includes the determined results for the previously described steps from the measured values to the values reduced to reference conditions, and finally the speed corrected reduced to reference conditions values. For each step, two compressor maps were created, which represent the pressure ratio achieved over the respective mass flow rate as well as the volume flow rate. For both, different questions and objectives, the suitable compressor map can be selected according to the respective requirements. All developed compressor maps are attached (see Appendix B).

For the analysis of the turbo compressor performance, the developed compressor map with the speed corrected pressure ratio achieved over the speed corrected reduced mass flow rate was selected. Figure 4.1 shows the developed compressor map including all 87 recorded operating points with estimated speed lines and isentropic efficiency lines.

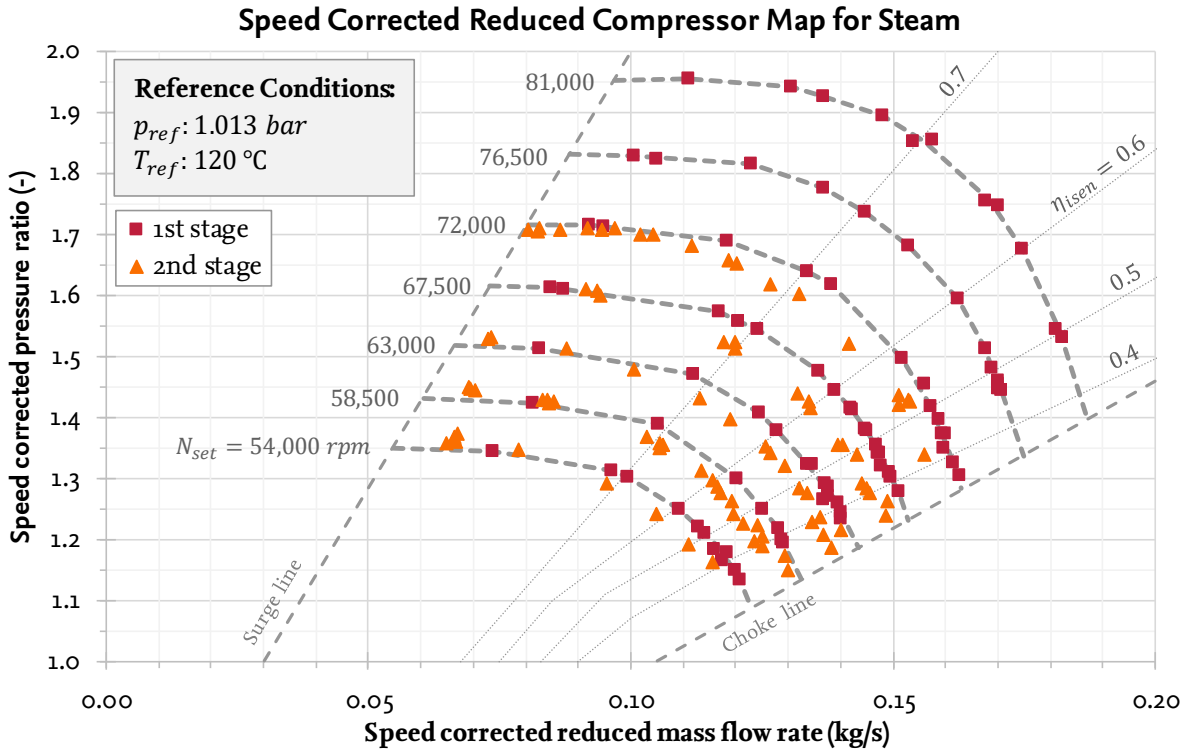


Figure 4.1: Developed compressor map including speed corrected reduced operating points for both turbo compressor stages (squares and triangles) based on experimental test results

The representation of speed corrected pressure ratio achieved over the speed corrected reduced mass flow rate allows the analysis of the turbo compressor performance. Each operating point of the first and second stages is represented by a point in the map. The system operating points are represented by a pair of first and second stage operating points. The adaptation to reference conditions as well as the speed adaptation ensure a simplification of the presentation and evaluation. Without these adjustments, the respective input parameters would have to be indicated for each point.

As previously explained in the planning of the experiments (see Section 3.1), impeller speeds below 54,000 rpm were not tested because the achieved pressure ratio and the supplied energy are too low. This leads to problems in the necessary heating of the system and the condensation of the superheated steam. During the performed experiments the impeller speed was set up to 81,000 rpm for the first stage and up to 72,000 rpm for the second stage. The Full speed of 90,000 rpm was not reachable for both stages caused by the limited factor of the cooling oil temperature of the gearboxes.

The speed lines shown are based on the results of the turbo compressor of the first stage. The curves of the speed lines between the last measurement points and the surge line as well as the choke line were estimated. The compressor map visualizes the possible operating range with achievable stable operating points. In this context, safe means with sufficient distance to the surge line. The shape of the speed lines for the first and second stage are almost identical, with the estimated speed lines for the second stage are slightly shifted to the left.

In the area near the surge line, the isentropic islands are close to each other due to the rapid decrease in isentropic efficiency in this operating field. During the performed experiments, the turbo compressors were operated in a safe distance to the surge line. This means that the real surge line is located at lower flow rates than estimated. As a result, the determined isentropic islands look more like lines because the part of the island close the surge line is not displayed. The developed isentropic efficiency lines show that the efficiency increases when approaching closer to the surge line.

The turbo compressor of the first stage reached a maximum pressure ratio of 1.95 at an impeller speed of 81,000 rpm (90 % of the maximum speed) with a determined isentropic efficiency of 0.74. The second stage turbo compressor with an identical design reached a pressure ratio of 1.70 at an impeller speed of 72,000 rpm (80 % of the maximum speed) with a determined isentropic efficiency of 0.74.

## 4.3 Evaluation of the two-stage turbo compressor system performance

Unlike the individual view of performance in the previous section, now the total system performance is considered. For this reason, the previously discussed operating points are visualized in a compressor map with the speed corrected pressure ratio achieved over the speed corrected reduced volume flow rate. The speed corrected reduced volume flow rate is calculated based on the determined speed corrected reduced mass flow rate and the defined reference fluid density. The mass flow rate is constant over the compressor and is valid for the inlet and outlet. The volume flow rate changed due to the change of fluid density. This has the advantage of making the relationships between the first and second stage more understandable, since the pressure and temperature increase lead to a visible reduction of the speed corrected reduced volume flow rate at the inlet of the second stage turbo compressor.

Figure 4.2 shows the developed compressor map including the connections (arrows) between the operating points of the first (squares) and second (triangles) turbo compressor stage.

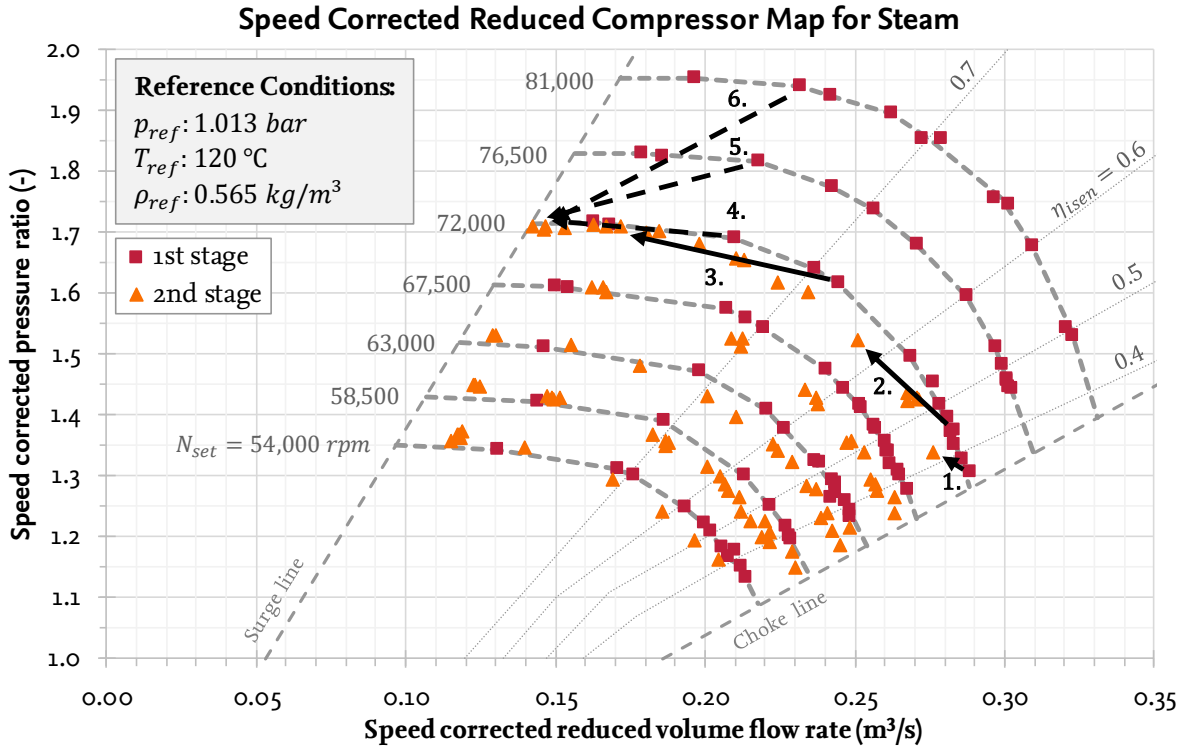


Figure 4.2: Speed corrected reduced compressor map including the previously discussed (1.-3., solid lines) and new (4.-6., dashed lines) operating points at equal and unequal impeller speeds

The three solid arrows (1.-3.) represent the connections between the first and second stage for the previously discussed operating points at equal impeller speeds (see Section 4.1). The three dashed arrows (4.-6.) represent the connections for new operating points at different impeller speeds.

For the operating points with equal impeller speeds, the operating points for the first (squares) and second (triangle) stage follow the determined speed line. With increasing pressure ratio, the difference of the speed corrected reduced volume flow rate increased due to the higher-pressure conditions at the inlet of the second turbo compressor stage. This leads to a higher correction in relation to the reference conditions for the inlet parameter of the second turbo compressor stage. In addition, the previously observed behavior of the differences in the pressure ratio and the isentropic efficiency can be seen from the consideration of the operating points in the determined compressor map. In the right part of the map, the pressure ratio and isentropic efficiency increase significantly faster due to the reduction of the volume flow rate.

For all recorded operating points, the second stage operates closer to the surge line on a lower volume flow compared to the first stage. Because of this, the second stage operates as the limitation factor for the operating area of the system. When the impeller speed of the first stage increases in relation to the second stage (5.-6.), the difference of the speed corrected volume flow rate increases as well. Additionally, the overall flow rate for the system increases, but the operating point of the second stage remains in a nearly constant position due to the changed inlet conditions. With different impeller speeds (first stage higher than second stage) it is possible to operate the system with higher pressure ratio and flow rate as well as both turbo compressors closer to the optimal operating point, that means with a higher isentropic efficiency and a safety margin to the surge line. This leads to a lower power consumption and a higher achievable total pressure ratio for the system.

For the further evaluation of the two-stage turbo compressor system performance, the Table 4.7 gives an overview of determined results for the selected and previously discussed operating points of the entire system. The operating points 1. to 3. were recorded with equal impeller speeds for both stages and decreasing flow rates due to the closing of the expansion valve. For the operating points 4. to 6., the setting of the expansion valve is almost identical, but the impeller speed of the first stage was increased. For the calculations, the respective total pressure at the inlet of the first stage with the associated saturation temperature was used. The saturation temperature $T_{sat}$ at

the outlet of the second stage is related to the achieved pressure ratio. The difference between inlet and outlet saturation temperature of the system describes the reached temperature lift $T_{lift}$. The determination of the other parameters has already been mentioned in Section 1.3.

Table 4.7: Overview of determined results for the evaluation of the two-stage turbo compressor system performance for the selected and previously discussed operating points

| # | $N_{set}$ (rpm) | $\dot{m}_t$ (kg/s) | $\Pi_t$ (−) | $T_{sat}$ (°C) | $T_{lift}$ (K) | $\dot{Q}_{cond}$ (kW) | $P_{el}$ (kW) | $COP$ (−) | $\eta_{carnot}$ (−) |
|---|---|---|---|---|---|---|---|---|---|
| 1. | 72,000 - 72,000 | 0.167 | 1.4 | 110.4 | 10.4 | 373.1 | 52.9 | 7.1 | 36.8 |
| 2. | 72,000 - 72,000 | 0.164 | 1.8 | 116.6 | 16.6 | 362.5 | 52.4 | 6.9 | 23.5 |
| 3. | 72,000 - 72,000 | 0.141 | 2.5 | 127.7 | 27.7 | 306.8 | 47.4 | 6.5 | 14.4 |
| 4. | 72,000 - 72,000 | 0.125 | 2.6 | 129.5 | 29.5 | 272.3 | 42.1 | 6.5 | 13.6 |
| 5. | 76,500 - 72,000 | 0.130 | 2.8 | 131.8 | 31.8 | 282.4 | 45.8 | 6.2 | 12.7 |
| 6. | 81,000 - 72,000 | 0.138 | 3.0 | 133.5 | 33.5 | 299.5 | 50.7 | 5.9 | 12.1 |

Closing the expansion valve reduces the total mass flow rate (1.-3.) and increases the total pressure ratio achieved. This leads to higher saturation temperatures and temperature lifts. The condensation heat flow and the supplied electrical energy are dependent on the mass flow and decrease with a reduction of the mass flow rate. The greater reduction in heat flow leads to a reduction in COP. The ideal Carnot efficiency also decreases due to the higher temperature lift. Increasing the first stage impeller speed (4.-6.) increases the total mass flow rate and the total pressure ratio achieved. As explained above, the increasing pressure ratio leads to higher saturation temperatures and temperature lifts and the rising mass flow rate to higher condensation heat flows and consumed electrical energy. The COP and ideal Carnot efficiency behave identically.

With the two-stage turbo compressor system and two identical turbo compressors it is possible to compress a superheated steam flow of 0.14 kg/s from atmospheric pressure to above 3.0 bar, where it can be condensate at a temperature of 133.5 °C. The COP of the performed investigation was 5.9 when the achievable condensation energy (299.5 kW) is compared to the total amount of energy supplied to the system (50.7 kW). The ideal Carnot efficiency is 12.1, resulting in a system efficiency of around 49 %.

## 4.4 Discussion of results

During the conducted experiments, the impeller speed was set in a range between 54,000 rpm and 81,000 rpm for the first stage and between 54,000 rpm and 72,000 rpm for the second stage. The cooling oil used in the gearbox has a maximum allowed temperature of 140 °C, which was reached during the performed experiments. Increasing the impeller speed leads to an increase in the cooling oil temperature. The Full speed of 90,000 rpm was not reachable for both stages due to the cooling oil temperature of the gearboxes. Therefore, the cooling oil temperature is currently the limiting factor of the turbo compressor system. Improved oil cooling could be achieved by a larger oil pump, which is however integrated in the gearbox causing a need of redesigning the entire turbo compressor system.

The adaptation to reference conditions as well as the speed adaptation ensure a simplification of the presentation and evaluation. Without these adjustments, the respective input parameters, e.g. temperature, pressure and volume flow, must be indicated for each point.

During all experiments, the volume flow rate in the second stage was significantly lower compared to the first stage even when the mass flow was increased by water injection by the de-superheater after the first stage. This results in the specific volume of steam which is reduced with increased pressure. Consequently, the second turbo compressor operated closer to the surge line. For a better operation, the design of the impellers should be adjusted to the targeted pressure and volume flow conditions at each stage.

The determined speed lines of the turbo compressor are flat and almost horizontal in some parts of the map. This results in a quite sensitive surge-behaviour of the turbo compressors, even when they are operated at a safe distance to the surge line in a stable point. A slight pressure change can cause the system to turn fast into the surge area, where the turbo compressors operate no longer stable. Therefore, the system should be operated closer to the choke area of the compressor map.

At equal impeller speeds, the electrical energy consumption of the second stage was slightly higher (up to 10 %) when compared to the electrical energy consumption of the first stage. This might be caused by the fact, that the two turbo compressors were operated at different areas in the compressor map and that the second compressor had an increase mass flow rate due to the water injection by the de-superheater which was in average around 6 % higher compared to the first stage mass flow rate.

During the performed experiments, an average coefficient of variation of 1.7 % for the mass flow rate and 6.0 % for the isentropic efficiency were determined. As the mass flow rate and pressure ratio increase, the coefficient of variation obtained decreases since the instrumental errors dominate and the effects decrease closer to maximum at higher conditions. The deviation between the speed lines for both stages could depend on the higher uncertainties of the pressure sensors at the second stage, uncertainties in the differential pressure sensors or uncertainties due to the correction steps.

The performed tests demonstrated that it is possible to achieve stable operation conditions with the MVR setup and with the used of identical turbo compressors, resulting in successful commissioning. The turbo compressor of the first stage reached a maximum pressure ratio of 1.95 at an impeller speed of 81,000 rpm (90 % of the maximum speed) with a determined isentropic efficiency of 0.74. The second stage turbo compressor with an identical design reached a pressure ratio of 1.70 at an impeller speed of 72,000 rpm (80 % of the maximum speed) with a determined isentropic efficiency of 0.74. The maximum impeller speed was not reached due to the above explained issue.

With the two-stage turbo compressor system and two identical turbo compressors it is possible to compress a superheated steam flow of 0.14 kg/s from atmospheric pressure to above 3.0 bar, where it can be condensate at a saturation temperature of 133.5 °C. The achieved overall pressure resulted from pressure ratios of 1.92 and 1.65 at the first and second stage, respectively. The COP of the performed investigation is 5.9, when the achievable condensation energy (299.5 kW) is compared to the total amount of energy supplied to the inverters (50.7 kW). The ideal Carnot efficiency for the investigated temperature range is 12.1, which means that the system efficiency is around 49 % of the Carnot efficiency (including losses of inverter, motor and gearbox).

The achieved temperature lifts as well as the condensation heat flow are important parameters for the use of the MVR system in a downstream heat exchanger for heating the process steam for the drying process. Both relate to the achieved total pressure ratio due to the determination of the saturation temperature and the enthalpy of vaporization. For this reason, the focus in the further numerical analysis will be on the achieved total pressure ratio in connection with the mass flow rate

# 5 Development of the Turbo Compressor Model

This chapter covers the development of the turbo compressor model for the numerical analysis. At the beginning, existing compressor models are examined and a suitable model is selected based on the defined requirements. Subsequently, the model parameters are adjusted and the simulated results are validated and discussed.

## 5.1 Turbo compressor models in the literature

In the scientific literature, compressor models exist with focus on different phenomena and degree of complexity due to different goals and motivations of the scientific work of the past decades. The developed models cover, for example, the calculation of compressor performance, associated parameters (Song, et al., 2016) or the modeling of occurrence surge phenomena in centrifugal compressors (Hafaifa, et al., 2014). The implementation of the models can be carried out in various ways, such as purely mathematical or physical based. Here, the implementation and selection of the method must be based on the requirements of the model. For example, the purely mathematically based translation of an existing compressor map to a new impeller design can lead to errors and deviations without observing the laws of physics (Kurzke, 2011, p. 2). Many models are therefore based on the Euler's equation for turbomachinery and, for example, consider geometrical input parameters such as the inner and outer diameter of the impeller (Gravdahl, 1998), (Sidorow, et al., 2011). Furthermore, there are models that additionally include information on the design point for the calculation of further operating points (Gasparovic, 1973). In this connection the design point is often defined as the operation point with the highest efficiency and consists of the pressure ratio, flow rate, impeller speed and isentropic efficiency.

## 5.2 Selection of a suitable turbo compressor model

For use in this master thesis, the turbo compressor model must meet the following defined requirements:

- Based on physical equations instead of empirical data
- Realistic representation of the turbo compressor performance map for a defined operating area oriented on the experimental test results
- Stable operation, easy handling and possible adjustments for new impeller designs

The selection of the turbo compressor model was made based on the defined requirements. In case of this work, an already developed model was chosen based on the conducted literature research. This is because the validation of the existing model achieved good results and the defined requirements were considered. Most of the models studied are only targeted to a defined operating range, working fluid or focused on the description of individual phenomena.

The selected model is based on previous results from the work of (Bantle, et al., 2016), which had discussed the "development and performance analysis of an object-oriented turbo compressor model for steam compression cycles". The developed object-oriented model was implemented in Modelica (Modelica Association, 2018) using the TIL and TILMedia libraries of the TLK-Thermo GmbH[4].

The developed TIL turbo compressor model is a further development of the efficiency-based compressor model. For this reason, the model was extended by different input parameters based on the thoughts of (Pfleiderer, 1961). These parameters can be separated in three groups: Specification of design point, efficiency and geometry.

The design point is defined as the operating point with the highest achievable pressure ratio and isentropic efficiency. In the turbo compressor model, the specification of the design point is described by the inlet volume flow rate and the impeller speed at design conditions. The specification of efficiency covers the input parameters for the impeller and diffuser as well as the mechanical efficiency. Finally, the specification of the geometry covers input parameters of the impeller, blade and flow.

[4] TLK-Thermo GmbH, Germany - www.tlk-thermo.com

The Table 5.1 gives an overview of the defined input parameters for the turbo compressor model based on the results of (Bantle, et al., 2016).

Table 5.1: Defined input parameters for the turbo compressor model based on (Bantle, et al., 2016)

| **Design point** | | |
|---|---|---|
| $\dot{V}_{design}$ – Volume flow rate at the inlet | | $N_{design}$ – Impeller speed |
| **Efficiency** | | |
| $\eta_{imp}$ – Impeller efficiency | $\eta_{diff}$ – Diffuser efficiency | $\eta_{mech}$ – Mechanical efficiency |
| **Geometry** | | |
| **Impeller specifications** | **Blade specifications** | **Flow specifications** |
| $d_{in}$ – Inner diameter | $z$ – Number of blades | $\beta_{in}$ , $\beta_{out}$ – Absolute flow angle |
| $d_{out}$ – Outer diameter | $b_{in}$ , $b_{out}$ – Edge width | $\gamma_{in}$ , $\gamma_{out}$ – Relative flow angle |
| | $c_{in}$ , $c_{out}$ – Blade thickness | |

All these input parameters may be specified by the manufacturer or estimated based on previous results in the literature or experience. The influence of the various input parameters on the calculation of the turbo compressor model performance will be discussed in detail in the next section.

## 5.3 Parameter adjustment based on the experimental test results

The aim of the turbo compressor model is a realistic simulation of the performance with the focus on the correct calculation of the pressure ratio above the mass flow rate. For this reason, the input parameter needed to be adjusted based on the experimental test results, which were discussed in Chapter 4. For the parameter adjustment as well as the validation of the turbo compressor model, a model tester was built up in Dymola – Dynamic Modeling Laboratory[5]. The model tester consists of the developed turbo compressor model between boundaries for the definition of the various inlet and outlet conditions. The Figure 5.1 shows a schematic representation of the turbo compressor model tester.

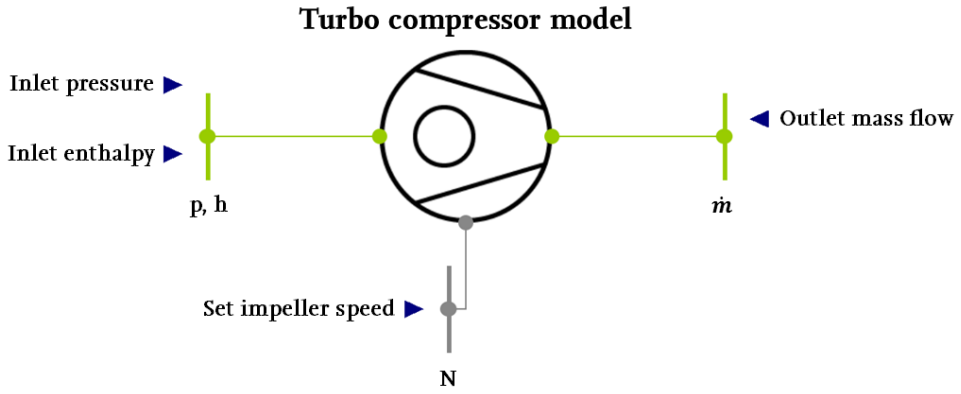


Figure 5.1: Schematic representation of the turbo compressor model tester

All values of the previously explained input parameters of the turbo compressor model as well as the displayed boundary conditions could be changed during the conduction of the simulations. The boundary at the inlet (left side of the model tester) defines the pressure and enthalpy of the inlet flow. The boundary at the outlet defines the mass flow rate achieved. Additionally, the current impeller speed of the turbo compressor can be set. Due to the defined boundary conditions the turbo compressor model calculate the conditions achieved at the outlet of the turbo compressor. To gain experience for the impact of different input parameters used in the turbo compressor model their individual influence were tested by variation of the parameter.

During the variation of the parameter, the inlet conditions were set to 1.013 bar and 120 °C as previously defined for the evaluation of the experimental data (see Chapter 4).

[5] Dassault Systèmes SE, France - www.3ds.com/products-services/catia/products/dymola

For each test run, one input parameter was changed while the others remained constant. Subsequently, test series were simulated with different impeller speeds. During each test series, the impeller speed was set constant and the mass flow rate was changed in steps of 0.01 kg/s within a defined range based on the determined performance test results.

The input parameters for the specification of the design point were set to 0.27 m³/s for the inlet volume flow rate and 90,000 rpm for the impeller speed specified by the manufacturer. During the parameter variation, the inlet volume flow rate was changed. The efficiency of the impeller and diffuser were estimated and then checked and adjusted by the results obtained. The mechanical efficiency has only impact on the energy consumption and is not important for the compressor map. All input parameters for the specification of the geometry are based on the tested impeller design and were specified by the manufacturer. These parameters were not changed during the parameter variation. The focus of the parameter variation is on the inlet volume flow rate as well as on efficiency of the impeller and diffusor.

The Figure 5.2 visualize the impact of inlet volume flow rate, impeller and diffuser efficiency of the turbo compressor performance during parameter variation performed at a set impeller speed of 81,000 rpm.

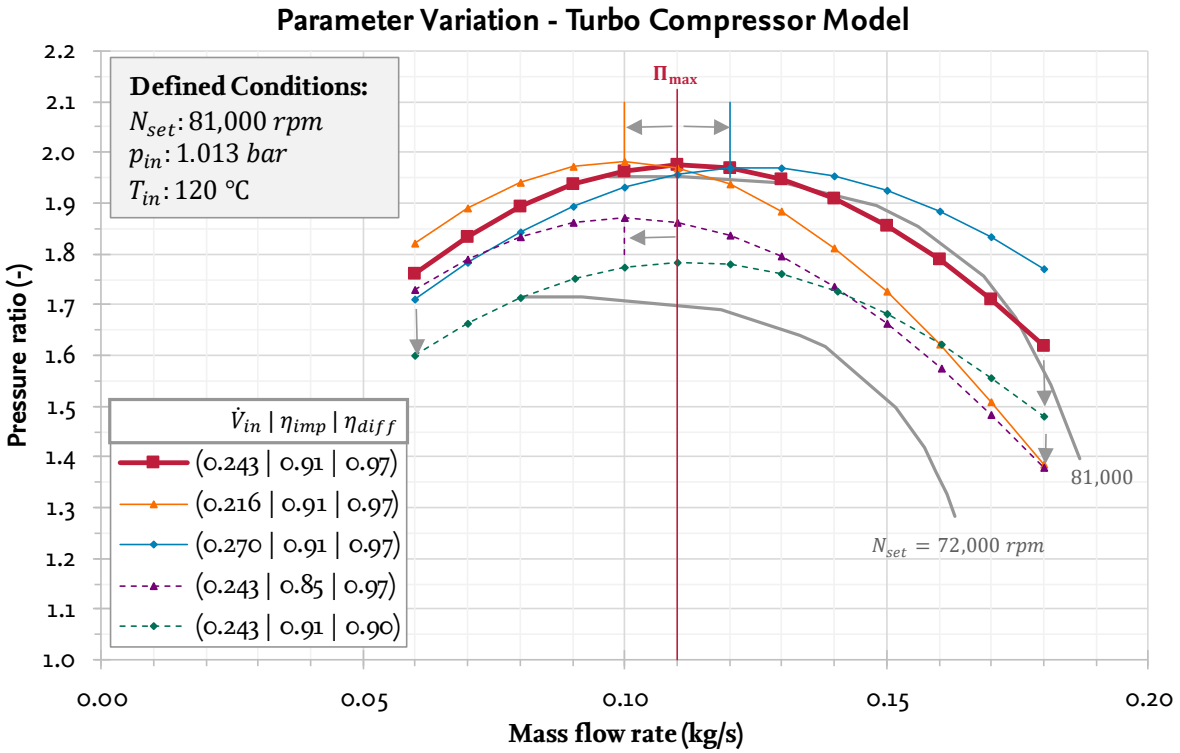


Figure 5.2: Visualisation of the impact of selected input parameters (inlet volume flow rate (solid lines), impeller and diffuser efficiency (dashed lines)) of the turbo compressor performance during parameter variation performed at a set impeller speed of 81,000 rpm

For the various simulations, the achieved pressure ratio is shown over the mass flow rate for the defined range from 0.06 kg/s to 0.18 kg/s with a step size of 0.01 kg/s. The speed lines for 81,000 rpm and 72,000 rpm obtained during the experiments are shown to evaluate the simulated results in relation to the experimental test results. Here, 81,000 rpm was chosen as this was the highest speed achieved during the experiments.

The solid red line with the squares shows the course of the optimal setting of the input parameters in relation to the determined speed lines based on the measured performance test results at the test facility. The range of the maximum pressure ratio (at 0.11 kg/s) and the course of the main operation area to the right thereof are well represented. The simulation also continues to the left in the surge area, where the operation of the turbo compressor is not possible at the test facility.

Based on the experimental test results, it was determined that the position of the maximum pressure ratio shifts for different impeller speeds. For this reason, the following relation was defined for the calculation of the actual inlet volume flow rate $\dot{V}_{actual\ inlet}$ during the variation of the set impeller speed $N_{set}$:

$$\dot{V}_{actual\ inlet} = \dot{V}_{design} \cdot \frac{N_{set}}{N_{design}} \tag{5.1}$$

Here, $\dot{V}_{actual\ inlet}$ depends on $N_{set}$ and the parameters given by the manufacturer for the specification of the design point.

The solid lines with the triangle and the rhombus represent the simulation results for a modified inlet volume flow rate. The inlet volume flow rate affects the position of the point of the maximum pressure ratio, but the amount remains the same. The position of the maximum pressure ratio shifts to the left as the inlet flow rate decreases and vice versa for an increase in the inlet flow rate.

The dashed lines with the triangle and the rhombus represent the simulation results for a modified efficiency of the impeller (triangle) and diffuser (rhombus). The impeller efficiency affects the position and amount of the point of the maximum pressure ratio. The position of the maximum pressure ratio shifts to the left and the amount decreases as the impeller efficiency decreases. In addition, the curve is rotated clockwise around the vertex. The change in diffuser efficiency leads to a vertical shift of the simulated speed line.

## 5.4 Validation of the turbo compressor model

For the validation of the turbo compressor model the defined parameters for the evaluation of the turbo compressor performance were compared with the obtained simulation results. The focus is still on the representation of the pressure ratio over the mass flow rate. The Figure 5.3 shows the simulated compressor map based on the structure of the previously developed compressor map including the operating points obtained during the simulations with different impeller speeds.

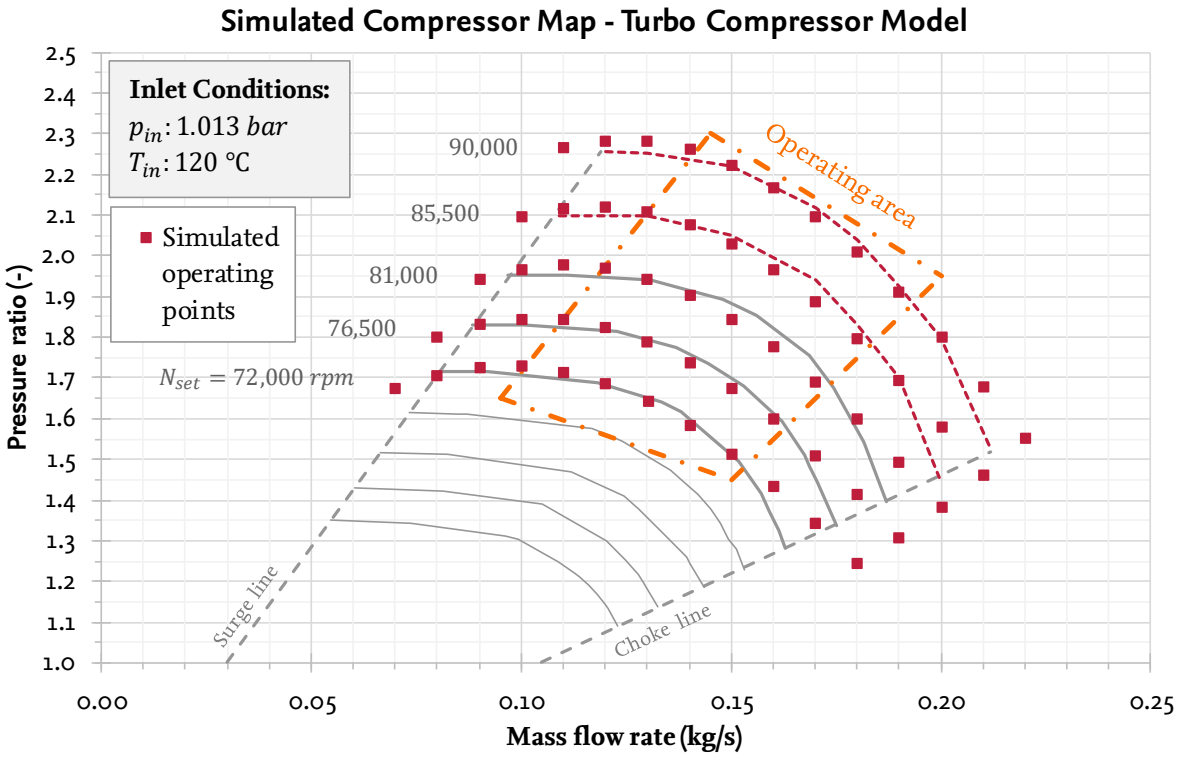


Figure 5.3: Simulated compressor map including the operating points obtained during the simulations with different impeller speeds using the developed turbo compressor model

The simulated operating points (squares) are shown compared to the previously determined speed lines (solid lines) for different impeller speeds. Additionally, the estimated speed lines (dashed lines) are shown for higher impeller speeds than the maximum 81,000 rpm achieved during the experiments based on the simulated operating points.

The operating area is defined by the area between the line near the maximum pressure ratio achieved and the position in the compressor map where the speed lines start to change the shape from horizontal to vertical. In this area, the simulated operating points represent to a good approximation the previously determined courses of the speed lines for the different speeds. The deviation between the measured and simulated data in the

right-hand area of the speed lines may depend on losses that were not or not fully considered in the turbo compressor model (Fister & Kotzur, 1982, p. 5). The Figure 5.4 shows the measured pressure ratio compared to the simulated pressure ratio using the turbo compressor model for different impeller speeds in the defined operating area.

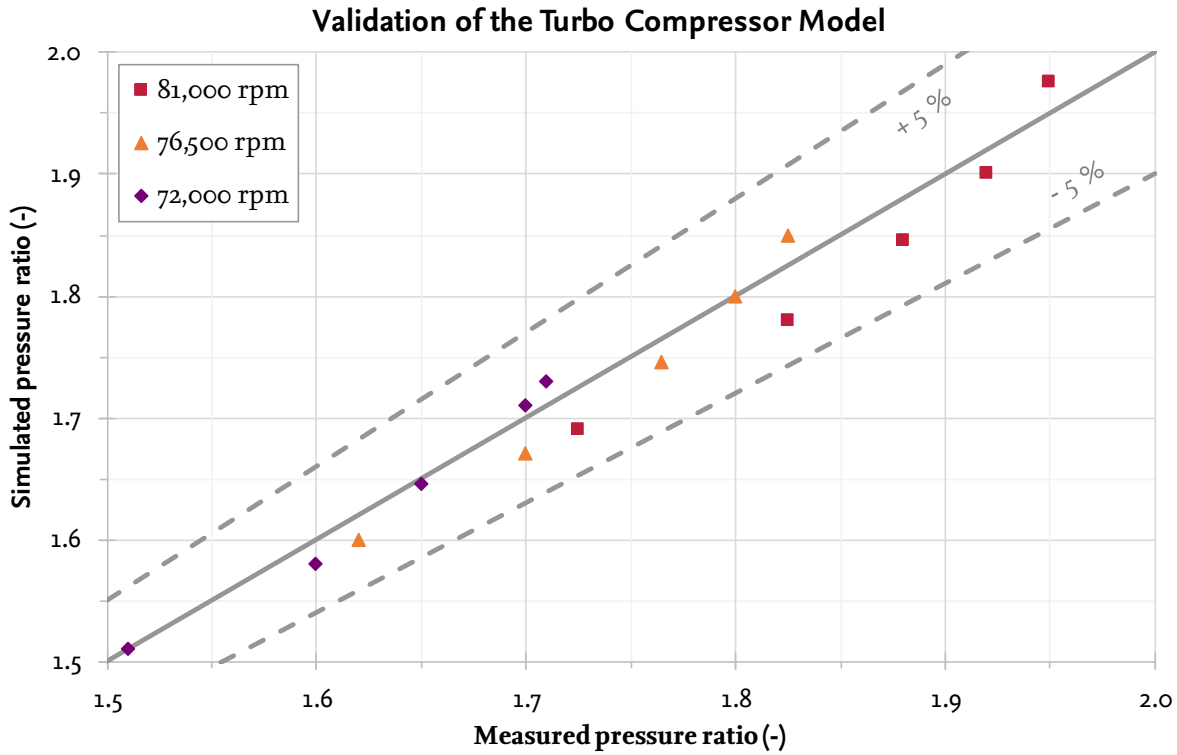


Figure 5.4: Measured pressure ratio compared to the simulated pressure ratio using the turbo compressor model for different impeller speeds in the defined operating area

The solid line represents the orthogonal, which means no deviation between the measured and simulated pressure ratio. Above and below the orthogonal are two dashed lines, which represent a deviation of ±5 % between the measured and simulated pressure ratio. In addition, the calculated deviations of the operating points are displayed for different impeller speeds (square, triangle and rhombus) in the defined operating area. All considered operating points are located within the area between the dashed lines and near the orthogonal line. This closer examination supports the previous observation that the pressure ratio in the defined operating range is shown in a good approximation.

The temperature at the outlet of the turbo compressor is up to 20 K lower compared to the experiments in the defined operating range. This leads to a lower specific enthalpy at the outlet. Furthermore, the isentropic efficiency is overestimated by up to 15 percentage points for all impeller speeds. These deviations must be considered for the further evaluation of the system model performance in the next chapter.

## 5.5 Discussion of the turbo compressor model results

The generated model results allow an estimation of the surge line based on the determination of the vertex of the speed lines. A precise definition of the choke line is difficult possible with the current model due to the given deviation. The consideration of further losses and efficiency adjustments can improve the results and enable the determination. The current deviation is acceptable due to the operation strategy, where the area near the choke line is used only for heating the system.

In the operating area, defined by the area between the line near the maximum pressure ratio and the position in the compressor map where the speed lines start to change the shape from horizontal to vertical, the simulation of pressure ratio and flow rate is possible with a low deviation to the experimental test results. These parameters are most important for the determination of the system COP by using the evaporation enthalpy and saturation temperature at the achieved pressure level.

The temperature achieved at the outlet depends on the supplied pressure work via the turbo compressor due to the defined impeller specifications. The reduced temperature at the outlet of the turbo compressor during the simulations using the developed turbo compressor model compared to the experimental results can be caused by an underestimation of the supplied pressure work. Furthermore, the lower temperature at the outlet leads to a lower specific enthalpy and influences the calculation of the isentropic efficiency. In addition, underestimation of losses may lead to an overestimation of isentropic efficiency, which depends on the losses occurring.

It is possible to complete the compressor map by using the validated turbo compressor model and estimate the speed lines for higher impeller speeds. Subsequently, these estimates should be validated in further experiments at the test facility after addressing the issue of the overheated cooling oil temperature of the turbo compressor gearboxes.

Based on the results for the turbo compressor tested, it can be assumed that the adaptation and validation of the model for a new impeller geometry will be possible with fewer measurement points. This has the advantage of faster creation of the associated compressor map with faster and less extensive experimental testing.

A possible next step is the simulation of the newly developed turbo compressor designs. Subsequently, the new impeller designs must be tested to verify the simulation results at the test facility.

# 6 Evaluation of the System Model Performance

This chapter covers the evaluation of the numerical system model performance. At the beginning, the development of the system model is presented. Subsequently, the developed system model is validated and evaluated based on the results of the simulations in comparison with the experimental test results. Finally, the system model results are discussed in detail.

## 6.1 Development of the system model

The aim of the development of the system model is the numerical performance evaluation of the two-stage turbo compressor system. The system model was built up in the same environment as the previously developed turbo compressor model (see Chapter 5). The developed system model consists of a turbo compressor model with a boundary for the set impeller speed for both stages. At the inlet and outlet are boundaries for the definition of the various inlet and outlet conditions. The section between the first and second stage contains a tube and a de-superheater. Figure 6.1 shows the schematic representation of the developed system model in Dymola.

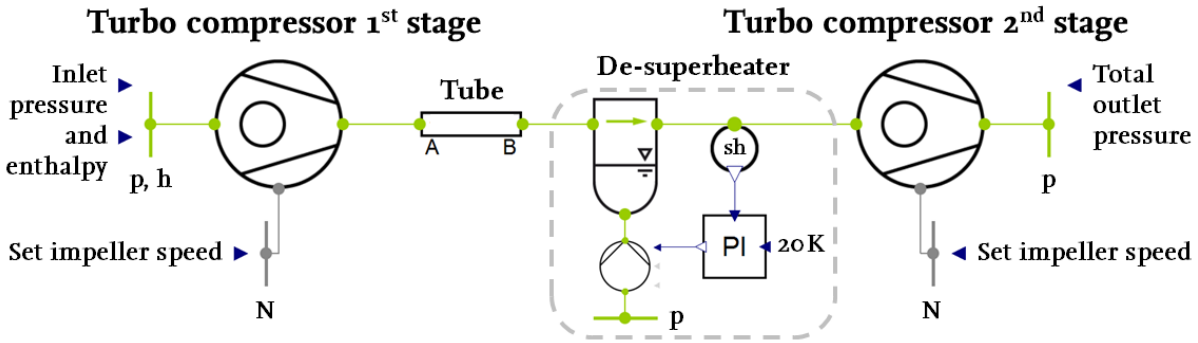


Figure 6.1: Schematic representation of the developed system model in Dymola

For both turbo compressor stages, the identical turbo compressor model was used with the previously discussed parameter settings (see Chapter 5). The boundary at the inlet defines the pressure and enthalpy of the inlet flow. At the outlet of the two-stage turbo compressor system, the boundary defines the total pressure to be achieved.

With the installed tube various aspects such as occurring pressure or heat losses can be simulated. In this case, a quadratic mass flow dependent pressure drop was defined. Furthermore, the consideration of heat losses has been omitted since the simulated temperature at the outlet of the first turbo compressor is already lower compared to the experimental results (see Section 5.4). Therefore, the heat losses at the test facility were consider due to the lower temperature at the turbo compressor outlet without the consideration of additional heat losses across the pipe surface.

The downstream de-superheater consists of different components and allows the de-superheating of the superheated steam to a defined superheat by injecting liquid water. The main part is an ideal separator, where the gas ports are connected to the superheated steam flow and the liquid port is connected to a simple pump with boundary. The filling level of the separator has been set to zero so that the water injected through the fluid port directly vaporizes and thus cools the superheated steam. The simple pump is connected to an inlet boundary with defined pressure. The mass flow through the simple pump is controlled by a PI (proportional integral) controller that controls the injected mass flow of water based on the difference between the measured superheat after the separator and the defined overheating of 20K.

At the beginning, all boundary conditions have been defined for the simulation of the system model. Subsequently, the system model calculates the achieved mass flow rate based on the set impeller speeds for both stages and the total output pressure to be achieved. In addition, the achieved pressure ratios of both turbo compressors are calculated.

## 6.2 Validation and evaluation of the system model

For the validation and evaluation of the system model, the simulated results are compared to the determined results for the performance of the turbo compressors and two-stage turbo compressor system. The inlet conditions were set to 1.013 bar and 120 °C during the simulations (see Chapter 4 and 5). The Figure 6.2 shows the simulated compressor map based on the simulated results using the developed system model.

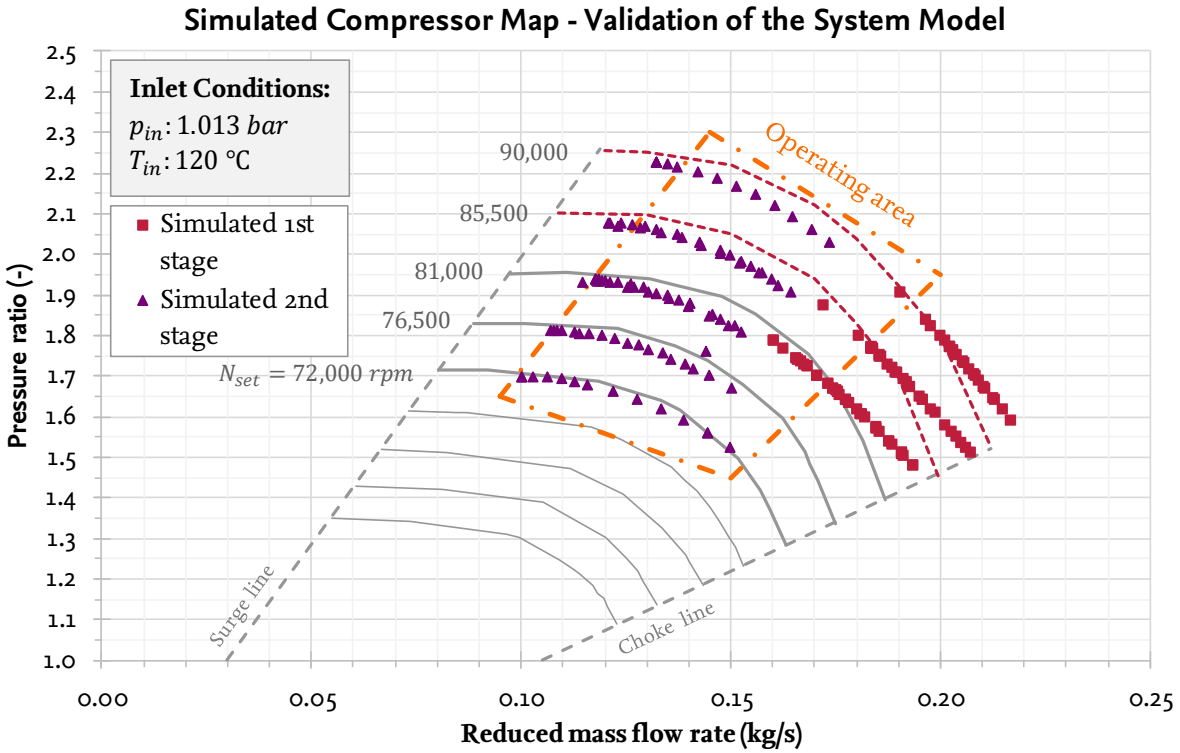


Figure 6.2: Simulated compressor map including the operating points for the first and second stage obtained during the simulations with different impeller speeds using the developed system model

The simulated compressor map displays the pressure ratio achieved over the mass flow rate reduced to the defined inlet conditions for both turbo compressor stages (see Section 3.3). The simulated operating points are represented in the diagram structure based on the simulated compressor map including the operating area, which was developed and discussed in the previous chapter (see Figure 5.3). The first stage was simulated for impeller speeds between 81,000 rpm to 90,000 rpm. The impeller speed of the second stage was set between 72,000 rpm to 90,000 rpm. Here, the impeller speed of the second stage was variated from equal speed to 5 % and 10 % lower speed compared to the first stage. The simulated operating points of the first stage begin near the choke area and show the previously discussed deviation from the speed lines for high flow rates. As the flow rate decreases, the operating points reach the operating area and

approach the speed lines. The second stage operating points begin in the operating area and follow the speed lines until the surge line. Figure 6.3 shows an operating map for the evaluation of the system model performance based on the simulated operating points using the developed system model.

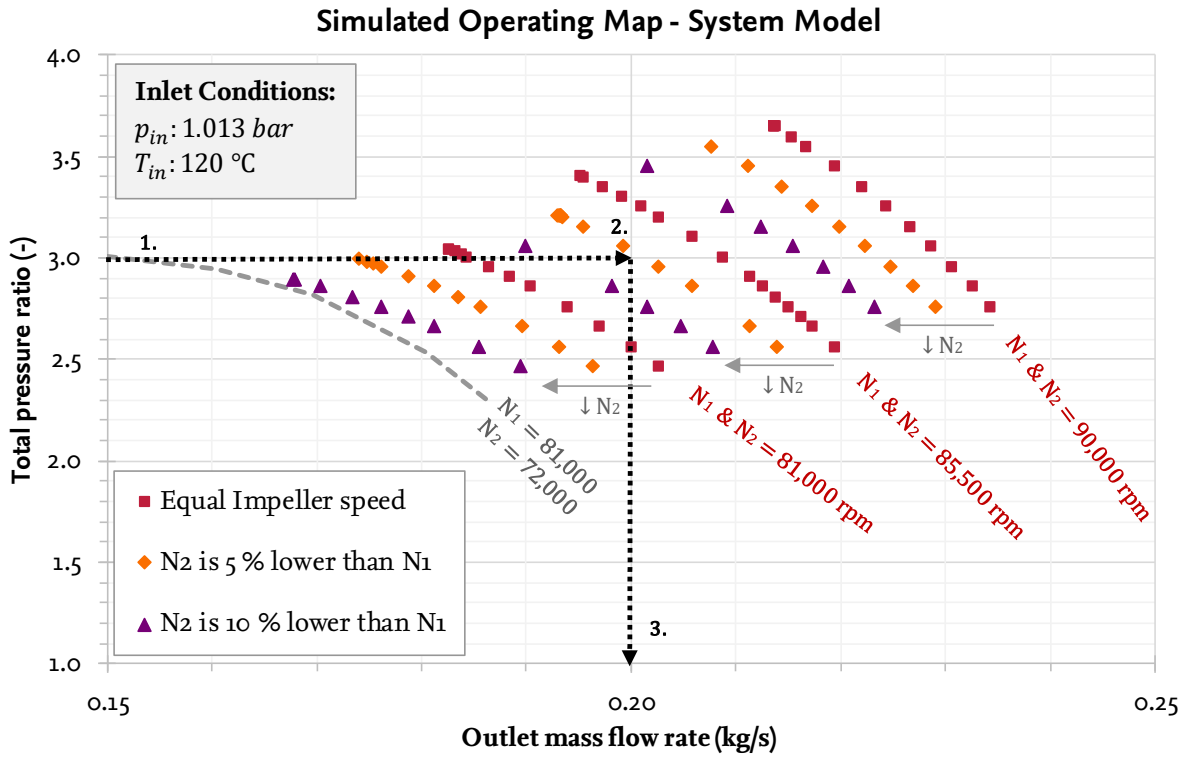


Figure 6.3: Operating map for the evaluation of the system performance including simulated operating points using the developed system model

The operating map displays the total pressure ratio achieved over the outlet mass flow after the second stage turbo compressor. Unlike the previous figures, each point represents an operating point for the entire system, including the first and second turbo compressor stages. The squares represent operating points with equal first and second stage impeller speed. The rhombuses represent operating points with a 5 % lower and the triangles with a 10 % lower second stage impeller speed compared to the first stage. For these operating points, the impeller speed of the first stage remains constant. To validate the simulated results, the highest experimental achieved test results (dashed line) are displayed. The experimental results were recorded at the same impeller speed setting as the nearby simulated operating points (lowest line of triangles). For the main operating range, the experimental test results are in good approximation to the simulated operating points. The operating map can be used to estimate possible operating points of the system. The doted arrow lines represent a possible sequence. Here, two of three parameters must be defined and the last results due to the selection.

## 6.3 Discussion of the system model results

For the development of the system model, various simplifications such as the occurring pressure drop and heat losses were assumed. In addition, the overheating of the steam at the inlet of the second stage was always accurately achieved. These assumptions lead to a greater distance between the operating points of the first and second stage displayed in the simulated reduced compressor map (see Figure 6.2) compared to the experimental results.

During the simulations, the simulated results shows the previously experimentally investigated behaviour by operating the turbo compressors with unequal impeller speeds, such as the operation of both stages closer at the optimum. The developed system model enables the testing and analysis of the system performance under changing boundary conditions. For example, the inlet pressure or enthalpy may be changed to simulate different inlet conditions. This could become important if the conditions in the superheated steam drier change or new applications should be tried out.

The developed operating map enables the calculation of the possible condensation heat flow, which can be transferred in the downstream heat exchanger for heating up the process steam before entering the drying chamber (see Section 1.3). For the achieved maximum total pressure ratio of 3.66 at a mass flow rate of 0.21 kg/s with a saturation temperature of 140.9 °C, the possible condensation heat flow is 458.3 kW. The correct calculation of the COP is not possible due to the deviation in the simulation of the consumed electrical power (see Equation 1.1). Due to the possible estimation of the achievable pressure ratio and the required setting of the impeller speeds, the structure of the operating map also enables the planning and control of the system operation.

# 7 Conclusion and Recommendations for Further Work

The aim of the master's thesis was the experimental analysis of the thermodynamic performance of the turbo compressor technology, the validation of existing compressor models and the evaluation of the system performance of the two-stage turbo compressor mechanical vapour recompression system for industrial superheated steam drying.

In the first part, an overview of the state of the art in industrial steam drying was given. Subsequently, the experimental setup used for the conduction of the performance tests was explained. This considered the presentation of the two-stage turbo compressor test facility, the turbo compressors and measuring instruments used as well as the processes for preparation and follow-up for operating the system.

The experimental setup was used for the execution and processing of measurements for the experimental analysis of the thermodynamic performance. Therefore, the entire process from the planning of the experiments to the final determination of the turbo compressor performance and the measurement uncertainties were discussed. The experimental results with respect to the turbo compressors performance and the performance of the two-stage turbo compressor system were analyzed and discussed.

For the numerical part of the master's thesis, the turbo compressor model was developed based on the results of the conducted literature research. The turbo compressor model then was validated and analyzed for performance compared to the experimental performance test results. The final step was the development of a system model and the evaluation of the system performance.

## 7.1 Summarized conclusion

The operation of a two-stage turbo compressor system for industrial superheated steam drying applications was demonstrated and stable operating conditions were documented. Suitable numerical models for the turbo compressor were identified and validated in comparison with the experimental results. A model of the two-stage turbo compressor system was developed and has shown that the numerical analysis can estimate the system performance and support experimental analysis in future work.

The first step was the setup and commissioning of a new test facility, including the definition of start-up and shutdown processes as well as the analysis of uncertainties caused by the measuring instruments used. During the uncertainty analysis, sources of uncertainties were identified and their effects on the measurement results discussed. Further, investigations were conducted to estimate the impact of thermal losses of the test facility and it was found that they represent a high uncertainty if not considered.

The focus was on the uncertainties of the measuring instruments, since the exact reproduction of an operating point due to uncertainties caused by manual intervention and changing conditions is very time consuming. During the performed experiments, an average coefficient of variation of 1.7 % for the mass flow rate and 6.0 % for the isentropic efficiency were determined. As the mass flow rate and pressure ratio increase, the coefficient of variation decreases. This is because the instrumental errors dominate and the effects decrease closer to maximum at higher conditions.

For the conduction of the performance tests, a concept for the planning of the experiments was developed and presented. Subsequently, a calculation scheme for the processing of measurement results including the identified and explained calculation steps was implemented. During the performed experiments, a comprehensive database with 87 operating points for a ROTREX C38 supercharger at superheated steam conditions were recorded and analyzed. In addition, operating experience was collected and possible further improvements to the test facility identified.

The turbo compressor of the first stage reached a maximum pressure ratio of 1.95 at an impeller speed of 81,000 rpm (90 % of the maximum speed) with a determined isentropic efficiency of 0.74. The second stage turbo compressor with an identical design reached a pressure ratio of 1.70 at an impeller speed of 72,000 rpm (80 % of the maximum speed) with a determined isentropic efficiency of 0.74. Due to the limitation

of the cooling oil temperature of the gearboxes, the maximum impeller speeds were not achievable during the experiments.

With the two-stage turbo compressor system it is possible to compress a superheated steam flow of 0.14 kg/s from atmospheric pressure at 120 °C to above 3.0 bar, where it can be condensate at a temperature of 133.5 °C. The COP of the performed investigation was 5.9 when the achievable condensation energy (299.5 kW) is compared to the total amount of energy supplied to the system (50.7 kW). For the operation of both stages near the optimum, the design of the impeller should be adjusted to the targeted pressure and volume flow conditions at each stage

For the development of object-oriented models of the turbo compressor as well as the two-stage turbo compressor system, a literature research was carried out and the Pfleiderer model was selected based on the work of (Bantle, et al., 2016). The turbo compressor model was adjusted and validated in comparison to the determined experimental results. The simulated results provided a good approximation of the experimental results in the defined operating area including the estimation of the position of the surge line. The model validation was performed with an uncertainty better than ± 5 % for the pressure ratio and mass flow range of 1.5 to 2.0 and 0.08 kg/s to 0.20 kg/s, respectively. The turbo compressor model was used to complete the determined compressor map by simulating the speed lines for higher impeller speeds. Additionally, the development of compressor maps for new impeller designs could be possible with less experimental effort by using the developed turbo compressor model.

For the evaluation of the two-stage turbo compressor system performance, a system model was developed using the turbo compressor model. This model was developed with simplified approaches and was able to estimate the experimentally determined behaviours such as the interaction between the first and second turbo compressor stage. The simulated results were used to create an operating map to control and plan further experiments and evaluate achievable pressure ratios in connection with impeller speeds. Currently, the scope of the system model is in the range of an achievable total pressure ratio up to 3.66 and an outlet mass flow rate of 0.168 kg/s to 0.235 kg/s.

With the procedures and models developed and validated in this master's thesis it is possible to test and evaluate new compressors to be developed within the boundary conditions of the turbo compressor test setup. The setup can cover mass flows up to 0.30 kg/s and pressure ratios up to 3.5 and 3.0 for the first and second stage, respectively.

## 7.2 Recommendations for further work

The conduction of the experimental performance tests at the test facility as well as the development and validation of the turbo compressor model and system model identified serval challenges and potentials for further developments. In the following, recommendations for further work are proposed based on the previous results.

A first approach for further work is the planning and conduction of new experiments up to the maximum impeller speed of the turbo compressor to verify the simulated results of the turbo compressor model and system model. For this, a solution must be found to solve the issue with the overheated cooling oil temperature for the gearbox. There are various approaches to solve this problem, such as the use of additional oil cooler to reduce the inlet oil temperature or increasing the flow rate using a larger oil pump.

In addition, experiments can be performed with various new impeller designs, which are adapted to the desired pressure and volume flow conditions at each stage. Here, the defined processes as well as the developed calculation scheme can be used for the conduction of the experiments.

Another approach is the use of the numerical models to further analyse the performance of the turbo compressor as well as the two-stage turbo compressor system by varying the defined inlet conditions. The developed turbo compressor model can also enable the simulation of newly developed impeller designs. For this, the defined input parameters must be adapted based on the impeller design. The simulated results can be verified subsequently during experiments at the test facility.

It is also conceivable to optimize the numerical models by further developments. A possible optimization of the turbo compressor model is the improvement and extension of the model calculation with focus on the determination of correct outlet temperature and isentropic efficiency. In addition, the focus could be placed on the improved representation and reduction of deviations in the choke area. The system model could be improved by extensive calculation of the pressure drop and consideration of heat losses.

# References


**Advantech Co, Ltd., 2018.** *Modular I/O System: ADAM-5000 Series.* [Online] Available at: http://www.advantech.com/products/modular-i-o-system-adam-5000-series/sub_1-368qro [Accessed 22 June 2018].

**AIT Austrian Institute of Technology GmbH, 2018.** *DryFiciency - Waste Heat Recovery in Drying Processes.* [Online] Available at: www.dry-f.eu [Accessed 15 May 2018].

**Anthoine, J., Arts, T., Boerrigter, H. & Buchlin, J.-M., 2009.** *Measurement Techniques in Fluid Dynamics.* 3rd ed. Sint-Genesius-Rode: Karman Institute for Fluid Dynamics.

**Bantle, M., 2017.** *Turbo-compressors: Prototype tests of mechanical vapour recompression for steam driers.* Rotterdam, 12th IEA Heat Pump Conference.

**Bantle, M., Eikevik, T. M. & Jokiel, M., 2016.** *Development and performance analysis of an object-oriented turbo-compressor model for steam compression cycles.* Edinburgh, 12th IIR Gustav Lorentzen Conference on Natural Refrigerants.

**Bergstrøm, J. & Leufven, O., 2007.** *Surge Modeling and Control of Automotive Turbochargers - Master's thesis,* Linköping; Sweden: Department of Electrical Engineering, Linköpings Universitet.

**Dixon, S. L. & Hall, C. A., 2014.** *Fluid Mechanics and Thermodynamics of Turbomachinery.* 7th ed. s.l.:Elsevier.

**Doebelin, E. O., 1990.** *Measurement systems: Application and Design.* 4th ed. Singapore: McGraw-Hill Publishing Company.

**Emco Controls A/S, 2018.** *EMCO Orifice Plates Series ISB/1 for RF Flanges.* [Online] Available at: www.emcocontrols.com/files/pdf/0-04-005-2e.pdf [Accessed 15 May 2018].

**EN ISO 5167-1:2003, 2003.** *Measurement of fluid flow by means of pressure differential devices inserted in circular cross-section conduits running full - Part 1: General principles and requirements (ISO 5167-1:2003-03),* Brussels: European commitee for standardization.

**EN ISO 5167-2:2003, 2003.** *Measurement of fluid flow by means of pressure differential devices inserted in circular cross-section conduits running full - Part 1: Orifice plates (ISO 5167-2:2003-03),* Brussels: European committee for standardization.

**Fister, W. & Kotzur, J., 1982.** *Conversion of Centrifugal Compress Performance Curves Considering Non-Similar Flow Conditions.* London, ASME 1982 International Gas Turbine Conference and Exhibit.

**Gasparovic, N., 1973.** Berechnung der Kennfelder Mehrstufiger Axialer Turbomaschinen. *Forsch. Ing.-Wes- Bd.,* 39(5), pp. 133-168.

**Gravdahl, J. T., 1998.** *Modeling and Control of Surge and Rotating Stall in Compressors.* Trondheim, Norway: Department of Engineering Cybernetics, NTNU.

**Gravdahl, J. T. & Egeland, O., 1999.** *Compressor Surge and Rotating Stall - Modeling and Control.* 1st ed. s.l.:Springer London.

**Hafaifa, A., Rachid, B. & Mouloud, G., 2014.** Modelling of surge phenomena in a centrifugal compressor: experimental analysis for control. *Systems Science & Control Engineering: An Open Access Journal,* Volume II, pp. 632-641.

**Huba Control AG, 2017a.** *Relative and absolute pressure transmitter type 528.* [Online] Available at: www.hubacontrol.com/fileadmin/user_upload/domain1/Produkte/EN/Datenblatt/528_pressure_sensor.pdf [Accessed 15 May 2018].

**Huba Control AG, 2017b.** *Relative and differential pressure transmitter type 692.* [Online] Available at: www.hubacontrol.com/fileadmin/user_upload/domain1/Produkte/EN/Datenblatt/692_Pressure_Sensor.pdf [Accessed 15 May 2018].

**Jensen Electric A/S, 2016.** *Thermocouple temperature sensor with B-head and screw.* [Online] Available at: www.jensenelectric.dk/temperaturfoelere-med-a-b-hoved [Accessed 15 May 2018].

**Johannesson, S. K., 2017.** *Industrial High Temperature Heat Pump Developement and Experimental Work.* Kopenhagen: Department of Mechanical Engineering - Technical University of Denmark.

**Kamstrup A/S, 2016.** *OMNIPOWER CT.* [Online]
Available at: www.kamstrup.com/en-en/products-solutions/smart-grid/electricity-meters [Accessed 15 May 2018].

**Kamstrup A/S, 2017.** *MULTICAL® 403.* [Online]
Available at: www.kamstrup.com/en-en/products-solutions/thermal-energy-meters/multical-403 [Accessed 15 May 2018].

**Kang, S.-H., Ryu, C. & S., K. H., 2016.** Analysis of performance for centrifugal steam compressor. *Mechanical Science and Technology,* 30(12), pp. 5521-5527.

**Kurzke, J., 2011.** *Correlations hidden in compressor maps.* Vancouver, ASME Turbo Expo.

**Kus, B., 2013.** *Oil-free turbocompressors for CO2 as working fluid.* Trondheim, Norway: Department of Energy and Process Engineering, NTNU.

**Modelica Association, 2018.** *Modelica.* [Online]
Available at: www.modelica.org [Accessed 10 February 2018].

**Moffat, R. J., 1988.** Describing the uncertainties in experimental results. *Experimental Thermal and Fluid Science,* I(1), pp. 3-17.

**Moran, M. J. & Shapiro, H. N., 2006.** *Fundamentals of Engineering Thermodynamics.* 5th ed. Chichester, England: John Wiley & Sons, Inc..

**Mujumdar, A. S., 2015.** *Handbook of industrial drying.* 4th ed. Boca Raton, FL: Taylor & Francis.

**Nguyen-Schäfer, H., 2015.** *Rotordynamics of Automative Turbochargers.* 2nd ed. Ludwigsburg: Springer Tracts in Mechanical Engineering.

**Parker Hannifin A/S, 2017.** *AC Variable Frequency Drives, kW Rated - AC30 Series.* [Online]
Available at: www.ph.parker.com/no/en/ac-variable-frequency-drives-kw-rated-ac30-series [Accessed 15 May 2018].

**Pfleiderer, C., 1961.** *Die Kreiselpumpen für Flüssigkeiten und Gase: Wasserpumpen, Ventilatoren, Turbogebläse, Turbokompressoren.* 5th ed. Berlin: Springer.

**Reddy, T. A., 2011.** *Applied Data Analysis and Modeling for Energy Energineers and Scientists.* 1st ed. Tempe, AZ: Springer US.

**Sannan, S., Bantle, M. & Lauermann, M., 2016.** *D1.2 Specification of performance indicators and validation requirements,* s.l.: DryF - Waste Heat Recovery in Industrial Drying Processes.

**Sidorow, A., Isermann, R., Cianflone, F. & Landsmann, G., 2011.** *Comparison of a turbocharger model based on isentropic efficiency maps with a parametric approach based on Euler's turbo-machinery equation.* Milano, 18th IFAC World Congress.

**Song, K. et al., 2016.** *A Physics-Based Control-Oriented Model For Compressor Mass Flow Rate.* Las Vegas, USA, 2016 IEEE 55th Conference on Decision and Control.

**Verein deutscher Ingenieure VDI e.V., 2013.** *VDI-Wärmeatlas.* 11 edition ed. Berlin Heidelberg: Springer Vieweg.

**Weel, M., et al., 2013.** *Energy efficient drying wirh a novel turbo-compressor based high-temperature heat pump.* Copenhagen, Denmark, 6th Nordic Drying Conference, 5.-7. June 2013.

**Weigand, B., von Wolfersdorf, J. & Köhler, J., 2013.** *Thermodynamik kompakt.* 3rd ed. Berlin Heidelberg: Springer Vieweg.

# Appendix

The appendix contains all information referred to the main part in chronological order.

## A Calculations

### Overview of performed impeller speed constellations for the first and second turbo compressor stage during the conduction of the experiments

Table A.1: Overview of performed impeller speed constellations for the first and second stage

| | Equal - 0 % difference | | Unequal - 5 % difference | | Unequal - 10 % difference | |
|---|---|---|---|---|---|---|
| Series | 1st stage | 2nd stage | 1st stage | 2nd stage | 1st stage | 2nd stage |
| 1. | 54,000 | 54,000 | 54,000 | 58,500 | 67,500 | 58,500 |
| 2. | 58,500 | 58,500 | 63,000 | 58,500 | 76,500 | 67,500 |
| 3. | 63,000 | 63,000 | 67,500 | 63,000 | 81,000 | 72,000 |
| 4. | 67,500 | 67,500 | 72,000 | 67,500 | - | - |
| 5. | 72,000 | 72,000 | 76,500 | 72,000 | - | - |

## Determined reduced compressor map data during the experiments performed

Table A.2: Performance test results reduced to reference conditions for the first stage

| # | $N_{red}$ (rpm) | $T_{hl\,in}$ (°C) | $T_{hl\,out}$ (°C) | $p_{t\,in}$ (bar) | $p_{t\,out}$ (bar) | $\Pi_t$ (−) | $\dot{m}_{red}$ (kg/s) | $\dot{V}_{red}$ ($m^3$/s) | $\eta_{isen}$ (−) | $C_{v\,\dot{m}}$ (%) | $C_{v\,\eta isen}$ (%) | $P_{el}$ (kW) |
|---|---|---|---|---|---|---|---|---|---|---|---|---|
| 1. | 54,193 | 117.2 | 152.7 | 1.01 | 1.18 | 1.17 | 0.118 | 0.208 | 0.41 | 1.74 | 8.10 | 11.85 |
| 2. | 54,223 | 116.8 | 152.5 | 1.01 | 1.20 | 1.19 | 0.116 | 0.206 | 0.45 | 1.79 | 7.50 | 11.85 |
| 3. | 54,245 | 116.5 | 152.4 | 1.01 | 1.22 | 1.22 | 0.115 | 0.203 | 0.50 | 1.86 | 6.80 | 11.61 |
| 4. | 54,263 | 116.2 | 152.4 | 1.01 | 1.26 | 1.25 | 0.110 | 0.194 | 0.58 | 2.05 | 6.08 | 11.25 |
| 5. | 54,289 | 115.8 | 152.6 | 1.01 | 1.33 | 1.32 | 0.097 | 0.172 | 0.71 | 2.65 | 5.34 | 10.16 |
| 6. | 58,845 | 115.4 | 158.2 | 1.01 | 1.21 | 1.20 | 0.130 | 0.230 | 0.40 | 1.52 | 6.81 | 14.70 |
| 7. | 58,846 | 115.4 | 158.3 | 1.01 | 1.22 | 1.21 | 0.130 | 0.229 | 0.41 | 1.53 | 6.68 | 14.82 |
| 8. | 58,949 | 114.0 | 157.1 | 1.01 | 1.24 | 1.23 | 0.129 | 0.228 | 0.44 | 1.56 | 6.24 | 14.63 |
| 9. | 58,986 | 113.6 | 156.8 | 1.01 | 1.27 | 1.26 | 0.126 | 0.223 | 0.50 | 1.63 | 5.64 | 14.49 |
| 10. | 58,994 | 113.4 | 156.9 | 1.01 | 1.32 | 1.31 | 0.121 | 0.214 | 0.58 | 1.77 | 5.02 | 13.97 |
| 11. | 59,008 | 113.3 | 157.5 | 1.01 | 1.41 | 1.40 | 0.106 | 0.188 | 0.72 | 2.33 | 4.34 | 12.70 |
| 12. | 63,262 | 116.7 | 166.9 | 1.00 | 1.24 | 1.24 | 0.141 | 0.249 | 0.39 | 1.39 | 5.85 | 17.74 |
| 13. | 63,162 | 118.0 | 168.1 | 1.01 | 1.26 | 1.25 | 0.140 | 0.249 | 0.41 | 1.39 | 5.67 | 17.86 |
| 14. | 62,658 | 124.3 | 174.5 | 1.00 | 1.26 | 1.26 | 0.136 | 0.240 | 0.43 | 1.46 | 5.50 | 17.22 |
| 15. | 63,149 | 118.1 | 168.4 | 1.01 | 1.27 | 1.26 | 0.140 | 0.247 | 0.43 | 1.41 | 5.40 | 17.78 |
| 16. | 63,139 | 118.3 | 168.6 | 1.01 | 1.30 | 1.29 | 0.138 | 0.244 | 0.47 | 1.45 | 5.02 | 17.58 |
| 17. | 63,126 | 118.4 | 169.0 | 1.01 | 1.34 | 1.32 | 0.135 | 0.238 | 0.53 | 1.51 | 4.63 | 17.36 |
| 18. | 63,107 | 118.7 | 169.8 | 1.01 | 1.42 | 1.41 | 0.125 | 0.221 | 0.64 | 1.76 | 3.99 | 16.37 |
| 19. | 67,465 | 120.4 | 178.6 | 0.99 | 1.27 | 1.28 | 0.151 | 0.267 | 0.40 | 1.29 | 5.07 | 21.24 |
| 20. | 67,413 | 121.0 | 179.4 | 0.99 | 1.29 | 1.30 | 0.149 | 0.264 | 0.43 | 1.32 | 4.77 | 20.89 |
| 21. | 67,377 | 121.4 | 180.1 | 1.00 | 1.33 | 1.34 | 0.147 | 0.260 | 0.47 | 1.36 | 4.35 | 20.68 |
| 22. | 67,334 | 121.9 | 180.9 | 0.99 | 1.40 | 1.41 | 0.142 | 0.251 | 0.56 | 1.46 | 3.83 | 20.18 |
| 23. | 67,291 | 122.4 | 182.4 | 0.99 | 1.53 | 1.54 | 0.124 | 0.219 | 0.70 | 1.90 | 3.25 | 18.28 |
| 24. | 71,942 | 120.6 | 188.0 | 1.00 | 1.30 | 1.30 | 0.163 | 0.288 | 0.37 | 1.20 | 4.60 | 25.49 |
| 25. | 71,907 | 121.0 | 188.4 | 0.99 | 1.32 | 1.33 | 0.161 | 0.285 | 0.40 | 1.22 | 4.36 | 25.49 |
| 26. | 71,878 | 121.3 | 188.9 | 0.99 | 1.36 | 1.37 | 0.160 | 0.282 | 0.45 | 1.24 | 3.94 | 25.20 |
| 27. | 71,840 | 121.8 | 189.7 | 0.99 | 1.44 | 1.45 | 0.156 | 0.276 | 0.53 | 1.30 | 3.43 | 24.55 |
| 28. | 71,755 | 122.7 | 191.6 | 0.99 | 1.60 | 1.61 | 0.138 | 0.244 | 0.68 | 1.63 | 2.86 | 22.30 |
| 29. | 717,40 | 122.9 | 193.3 | 0.98 | 1.66 | 1.68 | 0.118 | 0.209 | 0.73 | 2.19 | 2.71 | 19.76 |
| 30. | 541,51 | 117.8 | 153.2 | 0.99 | 1.13 | 1.14 | 0.121 | 0.214 | 0.33 | 1.66 | 9.77 | 12.00 |
| 31. | 541,35 | 118.0 | 153.6 | 0.99 | 1.15 | 1.15 | 0.120 | 0.212 | 0.37 | 1.69 | 8.86 | 11.85 |
| 32. | 542,23 | 116.8 | 152.6 | 0.99 | 1.18 | 1.18 | 0.119 | 0.210 | 0.43 | 1.74 | 7.72 | 11.67 |
| 33. | 542,48 | 116.4 | 152.6 | 0.99 | 1.22 | 1.23 | 0.113 | 0.200 | 0.53 | 1.93 | 6.59 | 11.29 |
| 34. | 542,59 | 116.3 | 153.0 | 0.99 | 1.30 | 1.31 | 0.100 | 0.177 | 0.69 | 2.52 | 5.47 | 10.30 |

| # | $N_{red}$ (rpm) | $T_{hl\,in}$ (°C) | $T_{hl\,out}$ (°C) | $p_{t\,in}$ (bar) | $p_{t\,out}$ (bar) | $\Pi_t$ (−) | $\dot{m}_{red}$ (kg/s) | $\dot{V}_{red}$ ($m^3$/s) | $\eta_{isen}$ (−) | $C_{v\,\dot{m}}$ (%) | $C_{v\,\eta isen}$ (%) | $P_{el}$ (kW) |
|---|---|---|---|---|---|---|---|---|---|---|---|---|
| 35. | 63,290 | 116.4 | 166.7 | 0.99 | 1.27 | 1.28 | 0.138 | 0.245 | 0.45 | 1.45 | 5.24 | 17.36 |
| 36. | 63,242 | 117.0 | 167.5 | 0.99 | 1.29 | 1.30 | 0.137 | 0.243 | 0.48 | 1.47 | 4.97 | 17.29 |
| 37. | 63,233 | 117.1 | 167.8 | 0.99 | 1.32 | 1.33 | 0.134 | 0.237 | 0.53 | 1.54 | 4.63 | 16.99 |
| 38. | 63,226 | 117.2 | 168.3 | 0.99 | 1.37 | 1.38 | 0.128 | 0.227 | 0.60 | 1.68 | 4.20 | 16.37 |
| 39. | 63,230 | 117.1 | 169.1 | 0.99 | 1.47 | 1.48 | 0.112 | 0.199 | 0.72 | 2.20 | 3.71 | 14.82 |
| 40. | 67,702 | 117.7 | 176.0 | 1.01 | 1.32 | 1.31 | 0.150 | 0.265 | 0.44 | 1.31 | 4.58 | 21.24 |
| 41. | 67,564 | 119.3 | 177.9 | 1.01 | 1.33 | 1.32 | 0.148 | 0.262 | 0.45 | 1.33 | 4.48 | 21.38 |
| 42. | 67,598 | 118.9 | 177.8 | 1.01 | 1.36 | 1.34 | 0.147 | 0.261 | 0.47 | 1.34 | 4.27 | 21.24 |
| 43. | 67,608 | 118.7 | 177.8 | 1.01 | 1.40 | 1.38 | 0.145 | 0.256 | 0.52 | 1.39 | 3.94 | 21.03 |
| 44. | 67,598 | 118.9 | 178.3 | 1.01 | 1.46 | 1.45 | 0.139 | 0.246 | 0.59 | 1.50 | 3.58 | 20.46 |
| 45. | 67,587 | 119.0 | 179.4 | 1.01 | 1.57 | 1.56 | 0.121 | 0.214 | 0.72 | 1.97 | 3.16 | 18.35 |
| 46. | 71,912 | 121.0 | 188.6 | 1.00 | 1.34 | 1.35 | 0.160 | 0.282 | 0.42 | 1.23 | 4.13 | 25.26 |
| 47. | 72,056 | 119.4 | 187.1 | 1.00 | 1.37 | 1.37 | 0.159 | 0.282 | 0.44 | 1.24 | 3.92 | 25.40 |
| 48. | 72,104 | 118.9 | 186.8 | 0.99 | 1.41 | 1.42 | 0.157 | 0.278 | 0.49 | 1.28 | 3.60 | 25.12 |
| 49. | 72,112 | 118.8 | 187.1 | 0.99 | 1.49 | 1.50 | 0.152 | 0.269 | 0.57 | 1.36 | 3.21 | 24.41 |
| 50. | 72,075 | 119.2 | 188.5 | 0.99 | 1.63 | 1.64 | 0.134 | 0.237 | 0.70 | 1.73 | 2.79 | 22.00 |
| 51. | 76,139 | 123.7 | 200.9 | 0.99 | 1.42 | 1.44 | 0.169 | 0.300 | 0.46 | 1.19 | 3.39 | 29.49 |
| 52. | 76,087 | 124.3 | 202.6 | 0.99 | 1.65 | 1.67 | 0.152 | 0.269 | 0.65 | 1.44 | 2.58 | 27.10 |
| 53. | 76,116 | 124.0 | 203.6 | 0.99 | 1.74 | 1.77 | 0.136 | 0.241 | 0.72 | 1.76 | 2.41 | 24.61 |
| 54. | 76,171 | 123.4 | 204.0 | 0.98 | 1.78 | 1.81 | 0.122 | 0.217 | 0.74 | 2.14 | 2.35 | 22.72 |
| 55. | 72,099 | 118.9 | 186.0 | 1.01 | 1.41 | 1.40 | 0.159 | 0.281 | 0.48 | 1.25 | 3.72 | 25.40 |
| 56. | 67,658 | 118.2 | 176.9 | 0.99 | 1.35 | 1.36 | 0.147 | 0.260 | 0.49 | 1.37 | 4.18 | 20.81 |
| 57. | 67,661 | 118.1 | 177.1 | 0.99 | 1.37 | 1.38 | 0.145 | 0.257 | 0.52 | 1.40 | 4.01 | 20.54 |
| 58. | 67,666 | 118.1 | 177.2 | 0.99 | 1.41 | 1.42 | 0.142 | 0.252 | 0.56 | 1.46 | 3.76 | 20.39 |
| 59. | 67,668 | 118.1 | 177.6 | 0.99 | 1.47 | 1.48 | 0.136 | 0.241 | 0.63 | 1.59 | 3.47 | 19.62 |
| 60. | 67,683 | 117.9 | 178.5 | 0.99 | 1.57 | 1.58 | 0.117 | 0.207 | 0.73 | 2.12 | 3.13 | 17.56 |
| 61. | 67,565 | 119.2 | 181.9 | 1.00 | 1.61 | 1.61 | 0.085 | 0.150 | 0.75 | 4.00 | 3.06 | 15.66 |
| 62. | 75,743 | 127.9 | 204.7 | 1.01 | 1.44 | 1.43 | 0.169 | 0.299 | 0.45 | 1.17 | 3.40 | 29.73 |
| 63. | 75,567 | 129.8 | 206.6 | 1.01 | 1.45 | 1.44 | 0.168 | 0.297 | 0.46 | 1.18 | 3.35 | 29.52 |
| 64. | 75,535 | 130.1 | 207.0 | 1.01 | 1.45 | 1.44 | 0.168 | 0.297 | 0.47 | 1.18 | 3.33 | 29.50 |
| 65. | 75,556 | 129.9 | 206.9 | 1.01 | 1.47 | 1.46 | 0.167 | 0.295 | 0.49 | 1.20 | 3.22 | 29.46 |
| 66. | 75,535 | 130.1 | 207.2 | 1.01 | 1.50 | 1.49 | 0.165 | 0.293 | 0.51 | 1.21 | 3.08 | 29.28 |
| 67. | 75,532 | 130.1 | 207.7 | 1.01 | 1.59 | 1.57 | 0.160 | 0.284 | 0.58 | 1.29 | 2.79 | 28.41 |
| 68. | 75,565 | 129.8 | 208.4 | 1.01 | 1.73 | 1.72 | 0.143 | 0.253 | 0.70 | 1.58 | 2.47 | 25.97 |
| 69. | 80,693 | 123.0 | 210.3 | 0.99 | 1.52 | 1.54 | 0.180 | 0.319 | 0.48 | 1.13 | 2.84 | 34.83 |
| 70. | 80,630 | 123.6 | 211.6 | 0.99 | 1.65 | 1.67 | 0.174 | 0.307 | 0.57 | 1.21 | 2.46 | 33.84 |
| 71. | 80,581 | 124.1 | 212.4 | 0.99 | 1.73 | 1.75 | 0.167 | 0.295 | 0.63 | 1.29 | 2.31 | 32.74 |

| # | $N_{red}$ (rpm) | $T_{hl\,in}$ (°C) | $T_{hl\,out}$ (°C) | $p_{t\,in}$ (bar) | $p_{t\,out}$ (bar) | $\Pi_t$ (−) | $\dot{m}_{red}$ (kg/s) | $\dot{V}_{red}$ (m³/s) | $\eta_{isen}$ (−) | $C_{v\,\dot{m}}$ (%) | $C_{v\,\eta isen}$ (%) | $P_{el}$ (kW) |
|---|---|---|---|---|---|---|---|---|---|---|---|---|
| 72. | 80,473 | 125.2 | 214.3 | 0.99 | 1.82 | 1.84 | 0.153 | 0.270 | 0.69 | 1.49 | 2.18 | 30.34 |
| 73. | 80,400 | 125.9 | 216.2 | 0.99 | 1.88 | 1.91 | 0.136 | 0.240 | 0.73 | 1.84 | 2.10 | 27.61 |
| 74. | 80,330 | 126.6 | 217.3 | 0.99 | 1.90 | 1.92 | 0.130 | 0.229 | 0.73 | 2.00 | 2.08 | 26.62 |
| 75. | 80,299 | 126.9 | 216.7 | 0.99 | 1.86 | 1.88 | 0.147 | 0.260 | 0.71 | 1.61 | 2.13 | 28.93 |
| 76. | 81,857 | 111.8 | 199.0 | 1.01 | 1.56 | 1.55 | 0.184 | 0.326 | 0.47 | 1.10 | 2.78 | 36.69 |
| 77. | 81,792 | 112.4 | 200.5 | 1.01 | 1.78 | 1.76 | 0.172 | 0.304 | 0.62 | 1.24 | 2.27 | 34.72 |
| 78. | 81,663 | 113.6 | 202.4 | 1.01 | 1.88 | 1.87 | 0.159 | 0.281 | 0.69 | 1.41 | 2.13 | 32.32 |
| 79. | 54,254 | 116.3 | 154.2 | 1.00 | 1.34 | 1.35 | 0.074 | 0.131 | 0.75 | 4.66 | 5.14 | 9.00 |
| 80. | 58,775 | 116.3 | 161.3 | 1.00 | 1.43 | 1.43 | 0.082 | 0.145 | 0.76 | 3.95 | 4.24 | 10.88 |
| 81. | 63,281 | 116.5 | 169.8 | 1.01 | 1.53 | 1.52 | 0.083 | 0.147 | 0.76 | 3.98 | 3.56 | 13.05 |
| 82. | 67,796 | 116.6 | 178.6 | 1.02 | 1.64 | 1.62 | 0.087 | 0.155 | 0.75 | 3.69 | 3.03 | 15.62 |
| 83. | 72,311 | 116.6 | 187.9 | 1.00 | 1.72 | 1.72 | 0.092 | 0.163 | 0.75 | 3.51 | 2.65 | 18.06 |
| 84. | 72,117 | 118.7 | 190.0 | 1.00 | 1.71 | 1.71 | 0.095 | 0.168 | 0.75 | 3.31 | 2.66 | 18.63 |
| 85. | 76,600 | 119.0 | 200.1 | 1.00 | 1.83 | 1.83 | 0.101 | 0.179 | 0.74 | 3.05 | 2.32 | 22.01 |
| 86. | 76,585 | 119.1 | 200.0 | 1.00 | 1.83 | 1.83 | 0.105 | 0.186 | 0.74 | 2.81 | 2.32 | 22.65 |
| 87. | 81,014 | 119.9 | 210.9 | 1.00 | 1.95 | 1.95 | 0.111 | 0.196 | 0.74 | 2.65 | 2.06 | 26.02 |

Table A.3: Performance test results reduced to reference conditions for the second stage

| # | $N_{red}$ (rpm) | $T_{hl\,in}$ (°C) | $T_{hl\,out}$ (°C) | $p_{t\,in}$ (bar) | $p_{t\,out}$ (bar) | $\Pi_t$ (−) | $\dot{m}_{red}$ (kg/s) | $\dot{V}_{red}$ (m³/s) | $\eta_{isen}$ (−) | $C_{v\,\dot{m}}$ (%) | $C_{v\,\eta isen}$ (%) | $P_{el}$ (kW) |
|---|---|---|---|---|---|---|---|---|---|---|---|---|
| 1. | 54029 | 119.6 | 155.5 | 1.06 | 1.24 | 1.16 | 0.115 | 0.204 | 0.39 | 1.72 | 17.09 | 12.00 |
| 2. | 54084 | 118.8 | 154.8 | 1.09 | 1.30 | 1.19 | 0.111 | 0.197 | 0.46 | 1.73 | 14.42 | 11.85 |
| 3. | 54109 | 118.4 | 154.8 | 1.12 | 1.39 | 1.24 | 0.105 | 0.186 | 0.56 | 1.75 | 11.59 | 11.75 |
| 4. | 54100 | 118.5 | 155.3 | 1.17 | 1.52 | 1.29 | 0.096 | 0.169 | 0.66 | 1.87 | 9.51 | 11.39 |
| 5. | 54027 | 119.6 | 157.3 | 1.27 | 1.71 | 1.35 | 0.079 | 0.139 | 0.75 | 2.32 | 7.89 | 10.58 |
| 6. | 59083 | 112.3 | 155.5 | 1.07 | 1.28 | 1.20 | 0.126 | 0.224 | 0.38 | 1.61 | 14.05 | 15.05 |
| 7. | 58928 | 114.3 | 157.6 | 1.07 | 1.30 | 1.21 | 0.125 | 0.220 | 0.40 | 1.61 | 13.69 | 15.10 |
| 8. | 58980 | 113.6 | 156.8 | 1.10 | 1.38 | 1.25 | 0.121 | 0.214 | 0.48 | 1.60 | 11.27 | 15.05 |
| 9. | 58949 | 114.0 | 157.4 | 1.14 | 1.50 | 1.31 | 0.117 | 0.206 | 0.57 | 1.58 | 9.18 | 14.91 |
| 10. | 58858 | 115.2 | 159.1 | 1.21 | 1.66 | 1.36 | 0.106 | 0.188 | 0.67 | 1.64 | 7.60 | 14.39 |
| 11. | 58596 | 118.7 | 163.7 | 1.34 | 1.91 | 1.43 | 0.086 | 0.151 | 0.76 | 1.99 | 6.21 | 13.12 |
| 12. | 63212 | 117.4 | 167.6 | 1.08 | 1.33 | 1.23 | 0.135 | 0.239 | 0.39 | 1.53 | 12.08 | 18.31 |
| 13. | 62821 | 122.2 | 172.2 | 1.09 | 1.35 | 1.23 | 0.136 | 0.240 | 0.40 | 1.51 | 11.94 | 18.14 |
| 14. | 63173 | 117.9 | 168.2 | 1.11 | 1.47 | 1.32 | 0.130 | 0.230 | 0.53 | 1.50 | 8.81 | 17.92 |
| 15. | 62775 | 122.8 | 173.0 | 1.11 | 1.42 | 1.28 | 0.132 | 0.233 | 0.46 | 1.50 | 10.04 | 18.20 |
| 16. | 62737 | 123.3 | 173.9 | 1.15 | 1.54 | 1.34 | 0.126 | 0.223 | 0.55 | 1.48 | 8.30 | 18.00 |

| # | $N_{red}$ (rpm) | $T_{hl\,in}$ (°C) | $T_{hl\,out}$ (°C) | $p_{t\,in}$ (bar) | $p_{t\,out}$ (bar) | $\Pi_t$ (−) | $\dot{m}_{red}$ (kg/s) | $\dot{V}_{red}$ ($m^3$/s) | $\eta_{isen}$ (−) | $C_{v\,\dot{m}}$ (%) | $C_{v\,\eta isen}$ (%) | $P_{el}$ (kW) |
|---|---|---|---|---|---|---|---|---|---|---|---|---|
| 17. | 62,717 | 123.6 | 174.6 | 1.20 | 1.67 | 1.39 | 0.118 | 0.209 | 0.62 | 1.50 | 7.07 | 17.92 |
| 18. | 62,702 | 123.7 | 175.8 | 1.32 | 1.94 | 1.47 | 0.100 | 0.177 | 0.72 | 1.65 | 5.63 | 17.08 |
| 19. | 66,944 | 126.6 | 184.1 | 1.09 | 1.39 | 1.27 | 0.144 | 0.254 | 0.40 | 1.46 | 10.30 | 21.66 |
| 20. | 66,832 | 127.9 | 185.9 | 1.12 | 1.50 | 1.34 | 0.139 | 0.246 | 0.49 | 1.43 | 8.25 | 21.59 |
| 21. | 66,750 | 128.9 | 187.3 | 1.17 | 1.66 | 1.42 | 0.130 | 0.231 | 0.59 | 1.41 | 6.60 | 21.38 |
| 22. | 66,720 | 129.2 | 188.7 | 1.26 | 1.90 | 1.51 | 0.116 | 0.206 | 0.68 | 1.46 | 5.35 | 21.17 |
| 23. | 66,677 | 129.8 | 191.4 | 1.43 | 2.28 | 1.59 | 0.090 | 0.160 | 0.75 | 1.79 | 4.30 | 19.55 |
| 24. | 72,200 | 117.8 | 184.7 | 1.08 | 1.45 | 1.34 | 0.156 | 0.277 | 0.41 | 1.40 | 8.44 | 26.34 |
| 25. | 72,161 | 118.3 | 185.4 | 1.11 | 1.58 | 1.42 | 0.151 | 0.268 | 0.50 | 1.36 | 6.80 | 26.34 |
| 26. | 72,098 | 118.9 | 186.5 | 1.17 | 1.78 | 1.52 | 0.142 | 0.251 | 0.60 | 1.33 | 5.44 | 26.19 |
| 27. | 71,967 | 120.4 | 188.7 | 1.27 | 2.06 | 1.62 | 0.127 | 0.224 | 0.68 | 1.35 | 4.45 | 25.97 |
| 28. | 71,639 | 124.0 | 194.6 | 1.49 | 2.53 | 1.70 | 0.096 | 0.171 | 0.74 | 1.63 | 3.60 | 24.13 |
| 29. | 70,917 | 132.1 | 204.3 | 1.58 | 2.66 | 1.68 | 0.081 | 0.144 | 0.73 | 1.98 | 3.48 | 21.52 |
| 30. | 59,106 | 112.0 | 154.8 | 1.00 | 1.24 | 1.24 | 0.123 | 0.217 | 0.46 | 1.71 | 12.78 | 13.97 |
| 31. | 59,045 | 112.8 | 155.9 | 1.02 | 1.31 | 1.28 | 0.120 | 0.213 | 0.52 | 1.69 | 11.06 | 13.97 |
| 32. | 59,016 | 113.2 | 156.6 | 1.06 | 1.41 | 1.33 | 0.114 | 0.203 | 0.60 | 1.70 | 9.28 | 13.78 |
| 33. | 58,968 | 113.8 | 157.6 | 1.12 | 1.55 | 1.38 | 0.104 | 0.184 | 0.69 | 1.79 | 7.85 | 13.55 |
| 34. | 58,768 | 116.4 | 161.3 | 1.24 | 1.78 | 1.43 | 0.084 | 0.149 | 0.76 | 2.19 | 6.52 | 12.42 |
| 35. | 58,493 | 120.1 | 162.3 | 1.12 | 1.32 | 1.17 | 0.129 | 0.229 | 0.35 | 1.55 | 15.30 | 15.38 |
| 36. | 58,426 | 121.0 | 163.7 | 1.15 | 1.41 | 1.22 | 0.124 | 0.219 | 0.44 | 1.53 | 12.03 | 15.52 |
| 37. | 58,425 | 121.0 | 164.0 | 1.20 | 1.54 | 1.28 | 0.116 | 0.206 | 0.55 | 1.53 | 9.46 | 15.43 |
| 38. | 58,396 | 121.4 | 165.0 | 1.27 | 1.71 | 1.35 | 0.105 | 0.186 | 0.65 | 1.59 | 7.64 | 14.96 |
| 39. | 58,280 | 123.0 | 167.7 | 1.39 | 1.98 | 1.42 | 0.084 | 0.149 | 0.76 | 1.97 | 6.13 | 13.55 |
| 40. | 62,850 | 121.9 | 171.8 | 1.15 | 1.38 | 1.20 | 0.136 | 0.242 | 0.35 | 1.47 | 12.89 | 19.26 |
| 41. | 62,254 | 129.5 | 179.1 | 1.16 | 1.39 | 1.20 | 0.139 | 0.245 | 0.35 | 1.45 | 12.99 | 19.11 |
| 42. | 62,219 | 129.9 | 179.9 | 1.19 | 1.50 | 1.26 | 0.132 | 0.234 | 0.45 | 1.43 | 10.05 | 18.99 |
| 43. | 62,204 | 130.1 | 180.6 | 1.24 | 1.66 | 1.33 | 0.124 | 0.220 | 0.56 | 1.41 | 7.79 | 18.91 |
| 44. | 62,213 | 130.0 | 181.4 | 1.32 | 1.87 | 1.41 | 0.112 | 0.198 | 0.66 | 1.46 | 6.22 | 18.49 |
| 45. | 62,194 | 130.3 | 183.3 | 1.48 | 2.22 | 1.49 | 0.087 | 0.153 | 0.75 | 1.81 | 4.96 | 16.79 |
| 46. | 67,529 | 119.7 | 178.2 | 1.14 | 1.44 | 1.26 | 0.149 | 0.263 | 0.37 | 1.40 | 10.25 | 23.00 |
| 47. | 67,629 | 118.5 | 177.1 | 1.17 | 1.57 | 1.34 | 0.143 | 0.253 | 0.47 | 1.37 | 7.99 | 23.14 |
| 48. | 67,612 | 118.7 | 177.7 | 1.23 | 1.76 | 1.43 | 0.134 | 0.237 | 0.58 | 1.34 | 6.27 | 23.14 |
| 49. | 67,475 | 120.3 | 179.9 | 1.33 | 2.03 | 1.52 | 0.120 | 0.212 | 0.68 | 1.37 | 5.02 | 22.72 |
| 50. | 67,205 | 123.5 | 184.9 | 1.52 | 2.43 | 1.60 | 0.093 | 0.165 | 0.75 | 1.65 | 4.10 | 20.93 |
| 51. | 70,493 | 137.0 | 203.6 | 1.21 | 1.71 | 1.41 | 0.148 | 0.262 | 0.51 | 1.29 | 6.53 | 27.10 |
| 52. | 70,498 | 136.9 | 206.5 | 1.51 | 2.48 | 1.64 | 0.109 | 0.194 | 0.73 | 1.37 | 3.76 | 25.54 |
| 53. | 70,664 | 135.0 | 207.5 | 1.64 | 2.75 | 1.68 | 0.090 | 0.159 | 0.72 | 1.64 | 3.40 | 23.91 |

| # | $N_{red}$ (rpm) | $T_{hl\,in}$ (°C) | $T_{hl\,out}$ (°C) | $p_{t\,in}$ (bar) | $p_{t\,out}$ (bar) | $\Pi_t$ (−) | $\dot{m}_{red}$ (kg/s) | $\dot{V}_{red}$ ($m^3/s$) | $\eta_{isen}$ (−) | $C_{v\,\dot{m}}$ (%) | $C_{v\,\eta isen}$ (%) | $P_{el}$ (kW) |
|---|---|---|---|---|---|---|---|---|---|---|---|---|
| 54. | 70,704 | 134.6 | 207.3 | 1.70 | 2.85 | 1.68 | 0.079 | 0.140 | 0.72 | 1.94 | 3.33 | 22.16 |
| 55. | 62,380 | 127.9 | 177.3 | 1.22 | 1.43 | 1.17 | 0.137 | 0.242 | 0.30 | 1.42 | 14.20 | 20.03 |
| 56. | 58,102 | 125.4 | 167.6 | 1.19 | 1.36 | 1.14 | 0.129 | 0.228 | 0.29 | 1.49 | 17.47 | 16.28 |
| 57. | 58,105 | 125.4 | 167.7 | 1.22 | 1.46 | 1.20 | 0.124 | 0.220 | 0.40 | 1.47 | 12.75 | 16.17 |
| 58. | 58,094 | 125.5 | 168.3 | 1.27 | 1.61 | 1.27 | 0.116 | 0.206 | 0.52 | 1.47 | 9.48 | 16.14 |
| 59. | 58,094 | 125.5 | 168.9 | 1.35 | 1.81 | 1.34 | 0.105 | 0.186 | 0.66 | 1.52 | 7.32 | 15.52 |
| 60. | 58,000 | 126.8 | 171.5 | 1.49 | 2.11 | 1.42 | 0.082 | 0.146 | 0.76 | 1.91 | 5.87 | 14.16 |
| 61. | 57,701 | 131.0 | 178.0 | 1.55 | 2.21 | 1.43 | 0.069 | 0.123 | 0.74 | 2.43 | 5.54 | 12.70 |
| 62. | 66,431 | 132.8 | 190.9 | 1.22 | 1.49 | 1.22 | 0.146 | 0.259 | 0.33 | 1.36 | 11.40 | 24.23 |
| 63. | 66,212 | 135.4 | 193.6 | 1.24 | 1.55 | 1.25 | 0.143 | 0.252 | 0.37 | 1.35 | 9.96 | 24.11 |
| 64. | 66,394 | 133.2 | 191.7 | 1.24 | 1.58 | 1.27 | 0.142 | 0.251 | 0.40 | 1.34 | 9.27 | 24.05 |
| 65. | 66,299 | 134.4 | 193.0 | 1.27 | 1.69 | 1.33 | 0.137 | 0.243 | 0.48 | 1.32 | 7.63 | 23.99 |
| 66. | 66,299 | 134.4 | 193.5 | 1.31 | 1.82 | 1.39 | 0.132 | 0.233 | 0.55 | 1.30 | 6.40 | 23.99 |
| 67. | 66,245 | 135.0 | 195.0 | 1.42 | 2.10 | 1.48 | 0.117 | 0.208 | 0.66 | 1.33 | 5.04 | 23.49 |
| 68. | 66,021 | 137.8 | 199.2 | 1.61 | 2.51 | 1.57 | 0.092 | 0.163 | 0.74 | 1.58 | 4.09 | 21.87 |
| 69. | 70,260 | 139.7 | 206.1 | 1.29 | 1.80 | 1.39 | 0.149 | 0.264 | 0.50 | 1.24 | 6.41 | 28.74 |
| 70. | 69,992 | 142.9 | 210.1 | 1.46 | 2.28 | 1.56 | 0.129 | 0.227 | 0.68 | 1.22 | 4.32 | 28.18 |
| 71. | 69,902 | 143.9 | 212.4 | 1.56 | 2.51 | 1.60 | 0.117 | 0.206 | 0.71 | 1.26 | 3.85 | 27.66 |
| 72. | 69,912 | 143.8 | 214.1 | 1.69 | 2.79 | 1.65 | 0.101 | 0.179 | 0.74 | 1.38 | 3.45 | 26.11 |
| 73. | 70,009 | 142.7 | 214.7 | 1.79 | 2.97 | 1.66 | 0.084 | 0.149 | 0.72 | 1.68 | 3.27 | 24.21 |
| 74. | 69,820 | 144.9 | 216.6 | 1.81 | 2.99 | 1.65 | 0.080 | 0.141 | 0.73 | 1.79 | 3.27 | 23.08 |
| 75. | 70,120 | 141.4 | 212.9 | 1.75 | 2.91 | 1.66 | 0.092 | 0.163 | 0.73 | 1.52 | 3.32 | 25.17 |
| 76. | 72,079 | 119.1 | 186.4 | 1.32 | 1.88 | 1.43 | 0.153 | 0.271 | 0.50 | 1.21 | 5.85 | 30.62 |
| 77. | 71,669 | 123.6 | 192.5 | 1.60 | 2.64 | 1.65 | 0.118 | 0.209 | 0.71 | 1.23 | 3.63 | 29.64 |
| 78. | 71,577 | 124.7 | 195.1 | 1.74 | 2.94 | 1.69 | 0.101 | 0.179 | 0.73 | 1.36 | 3.29 | 28.08 |
| 79. | 53,850 | 122.2 | 161.9 | 1.32 | 1.79 | 1.35 | 0.065 | 0.114 | 0.73 | 3.11 | 7.47 | 9.42 |
| 80. | 53,713 | 124.2 | 163.0 | 1.40 | 1.90 | 1.35 | 0.066 | 0.117 | 0.75 | 2.82 | 7.18 | 9.82 |
| 81. | 53,462 | 127.9 | 166.4 | 1.49 | 2.02 | 1.35 | 0.066 | 0.116 | 0.76 | 2.70 | 6.90 | 10.30 |
| 82. | 53,390 | 129.0 | 167.4 | 1.60 | 2.16 | 1.35 | 0.066 | 0.116 | 0.76 | 2.53 | 6.59 | 10.88 |
| 83. | 53,366 | 129.4 | 168.1 | 1.67 | 2.27 | 1.36 | 0.066 | 0.117 | 0.77 | 2.40 | 6.33 | 11.15 |
| 84. | 57,636 | 131.9 | 177.9 | 1.66 | 2.36 | 1.43 | 0.068 | 0.121 | 0.76 | 2.36 | 5.34 | 13.12 |
| 85. | 57,598 | 132.4 | 178.4 | 1.78 | 2.53 | 1.43 | 0.068 | 0.121 | 0.76 | 2.22 | 5.10 | 13.97 |
| 86. | 61,928 | 133.7 | 187.5 | 1.77 | 2.66 | 1.50 | 0.072 | 0.127 | 0.75 | 2.10 | 4.35 | 16.71 |
| 87. | 61,800 | 135.4 | 189.6 | 1.88 | 2.82 | 1.50 | 0.072 | 0.127 | 0.75 | 1.98 | 4.19 | 17.44 |

## Speed corrected test results for the discussed operating points reduced to the reference conditions at equal and unequal impeller speeds

Table A.4: Speed corrected test results at equal impeller speeds

| Stage | | $N_{set}$ (rpm) | $\dot{m}_{rel}$ (kg/s) | $\dot{V}_{rel\ in}$ (m³/s) | $T_{hl\ in}$ (°C) | $T_{hl\ out}$ (°C) | $p_{t\ in}$ (bar) | $p_{t\ out}$ (bar) | $\Pi_{rel}$ (–) | $\eta_{isen}$ (–) |
|---|---|---|---|---|---|---|---|---|---|---|
| 1. | 1st | 72,000 | 0.163 | 0.288 | 120.6 | 188.0 | 1.00 | 1.30 | 1.31 | 0.37 |
| | 2nd | 72,000 | 0.156 | 0.276 | 117.8 | 184.7 | 1.08 | 1.45 | 1.34 | 0.41 |
| 2. | 1st | 72,000 | 0.160 | 0.283 | 121.3 | 188.9 | 0.99 | 1.36 | 1.37 | 0.45 |
| | 2nd | 72,000 | 0.142 | 0.251 | 118.9 | 186.5 | 1.17 | 1.78 | 1.52 | 0.60 |
| 3. | 1st | 72,000 | 0.138 | 0.244 | 122.7 | 191.6 | 0.99 | 1.60 | 1.62 | 0.68 |
| | 2nd | 72,000 | 0.097 | 0.172 | 123.98 | 194.55 | 1.49 | 2.53 | 1.71 | 0.74 |

Table A.5: Speed corrected test results at unequal impeller speeds

| Stage | | $N_{set}$ (rpm) | $\dot{m}_{rel}$ (kg/s) | $\dot{V}_{rel\ in}$ (m³/s) | $T_{hl\ in}$ (°C) | $T_{hl\ out}$ (°C) | $p_{t\ in}$ (bar) | $p_{t\ out}$ (bar) | $\Pi_{rel}$ (–) | $\eta_{isen}$ (–) |
|---|---|---|---|---|---|---|---|---|---|---|
| 1. | 1st | 72,000 | 0.123 | 0.217 | 123.4 | 204.0 | 0.98 | 1.78 | 1.82 | 0.74 |
| | 2nd | 72,000 | 0.080 | 0.142 | 134.6 | 207.3 | 1.70 | 2.85 | 1.71 | 0.72 |
| 2. | 1st | 72,000 | 0.131 | 0.231 | 126.6 | 217.3 | 0.99 | 1.90 | 1.94 | 0.73 |
| | 2nd | 76,500 | 0.082 | 0.146 | 144.9 | 216.6 | 1.81 | 2.99 | 1.70 | 0.73 |
| 3. | 1st | 72,000 | 0.118 | 0.209 | 122.9 | 193.3 | 0.98 | 1.66 | 1.69 | 0.73 |
| | 2nd | 81,000 | 0.083 | 0.146 | 132.1 | 204.3 | 1.58 | 2.66 | 1.71 | 0.73 |

# B Additional results

## Measured operating points displayed in the compressor map structure

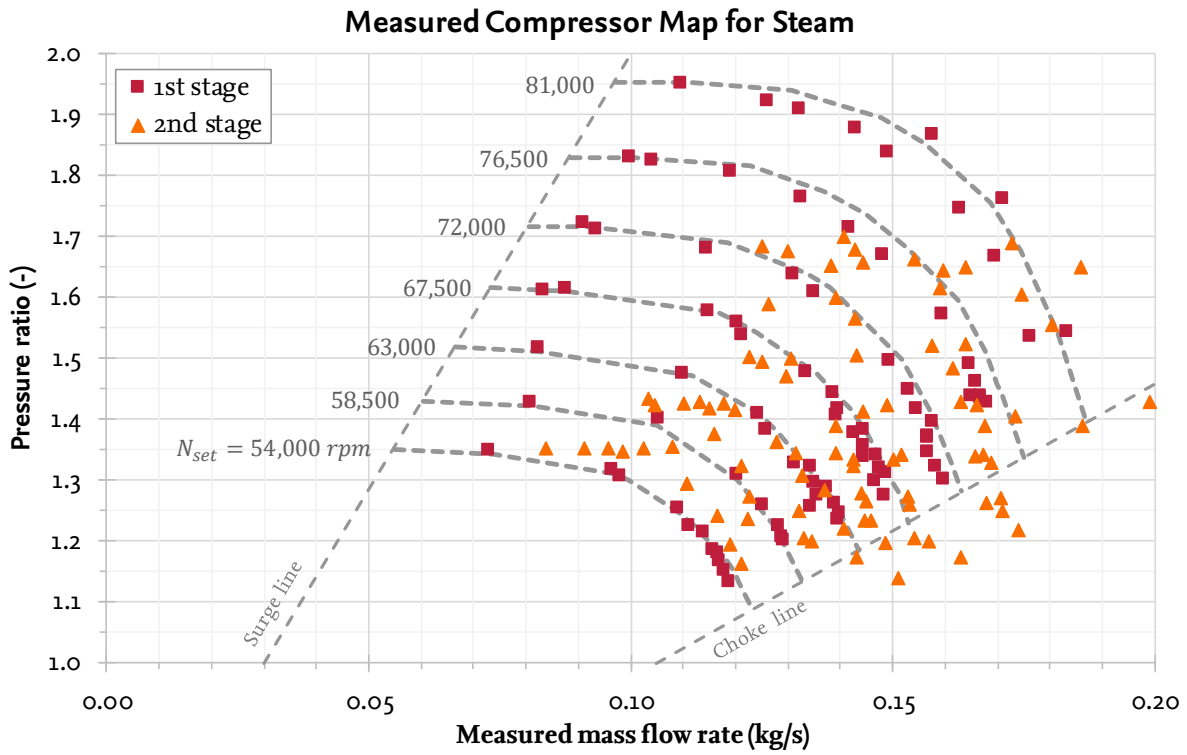


Figure B.1: Measured compressor map - Mass flow rate including operating points

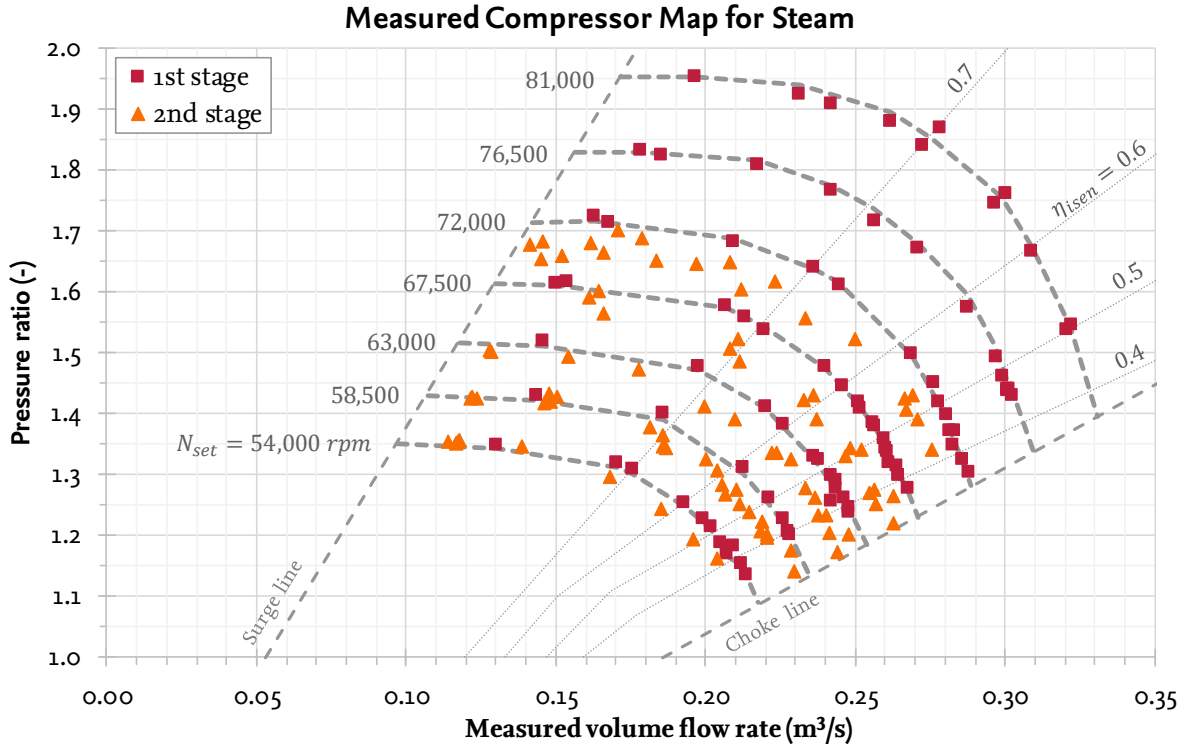


Figure B.2: Measured compressor map - Volume flow rate including operating points

## Operating points reduced to the defined reference conditions

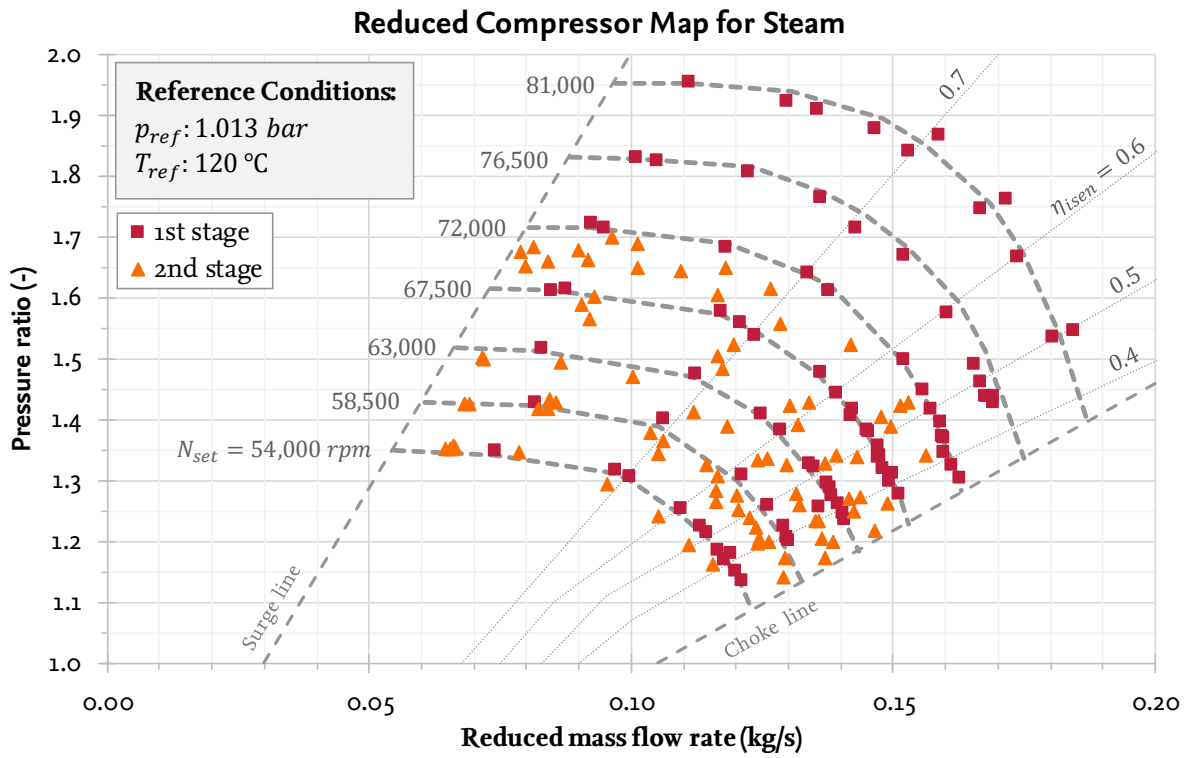


Figure B.3: Reduced compressor map - Mass flow rate including operating points

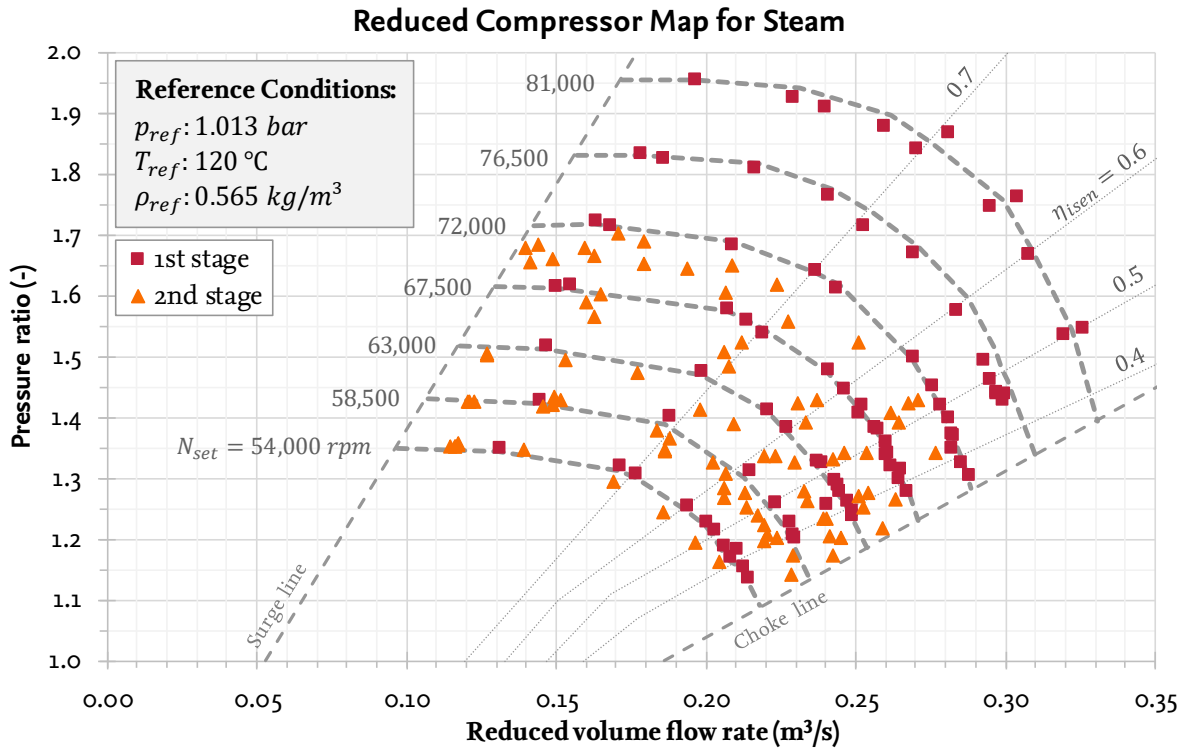


Figure B.4: Reduced compressor map - Volume flow rate including operating points

## Operating points speed corrected and reduced to the defined reference conditions

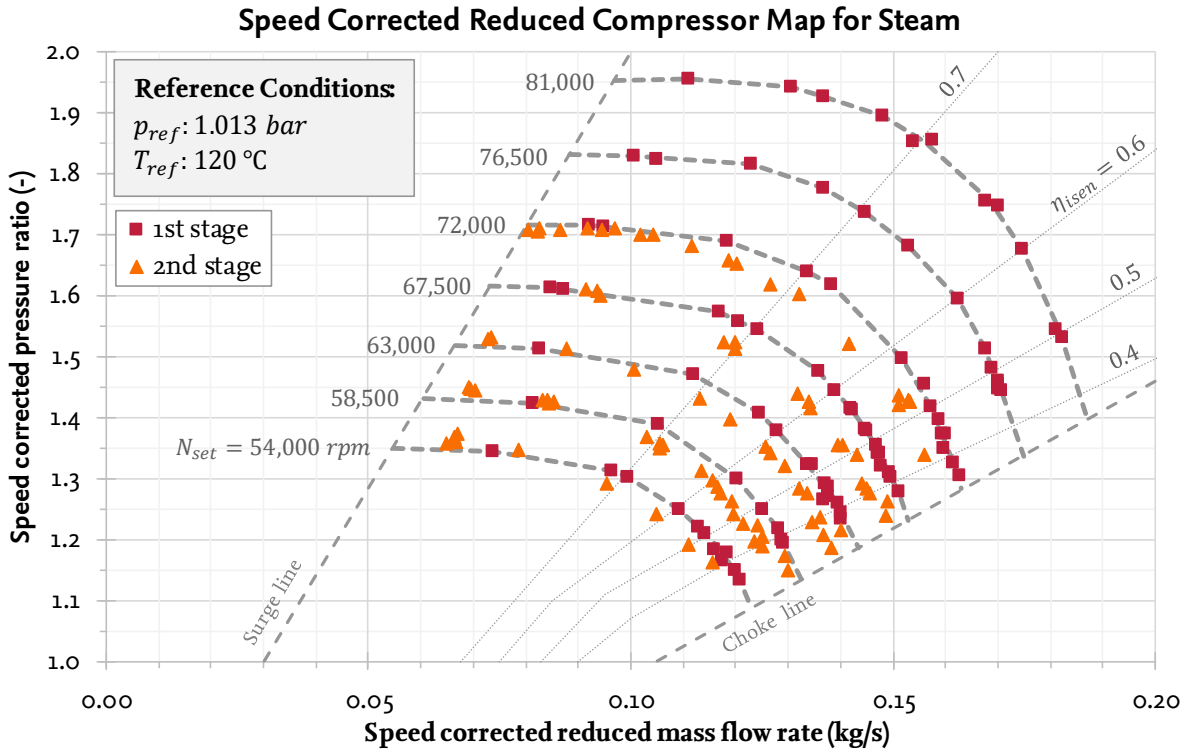


Figure B.5: Speed corrected reduced compressor map - Mass flow rate including operating points

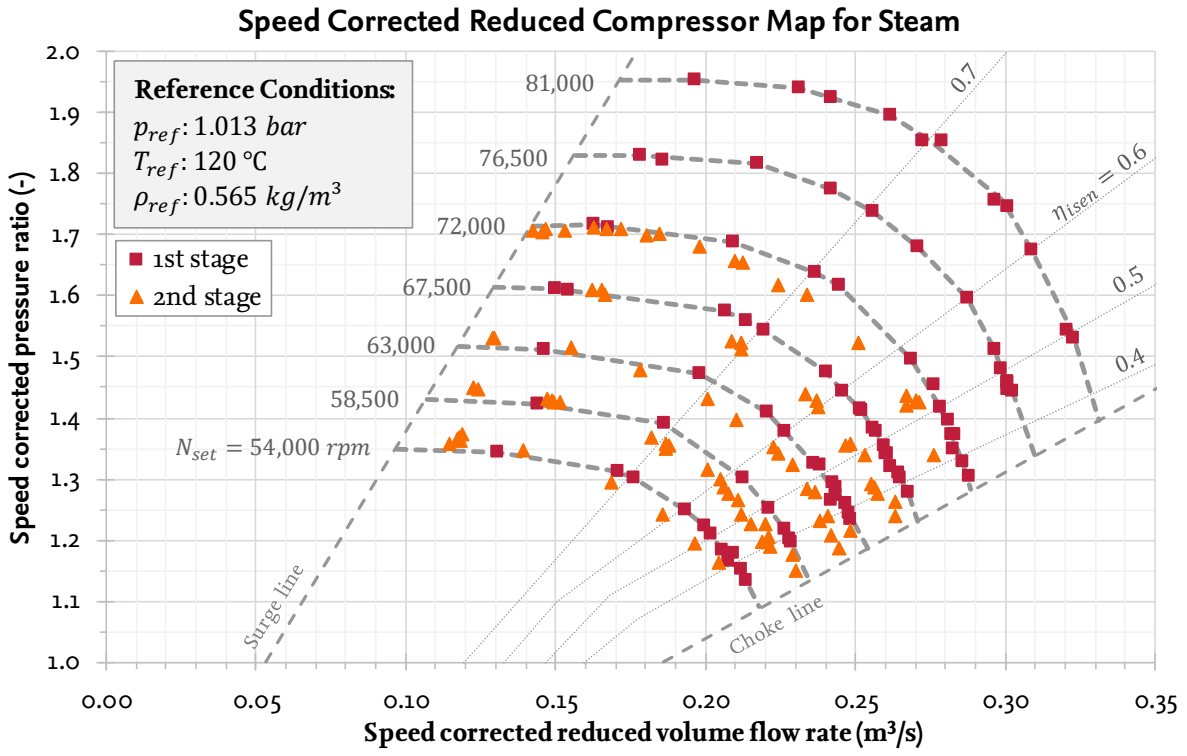


Figure B.6: Speed corrected reduced compressor map - Volume flow rate including operating points

# C Conference Paper

The following conference paper was published for the 13th IIR GUSTAV LORENTZEN CONFERENCE ON NATURAL REFRIGERANTS 2018, Valencia, Spain.

DOI: 10.18462/iir.gl.2018.1157

# Performance evaluation of two stage mechanical vapour recompression with turbo-compressors

**Michael Bantle[(a)], Christian Schlemminger[(a)], Ignat Tolstorebrov [(b)],Marcel Ahrens[(a)], Kjetil Evenmo[(c)]**

[(a)] SINTEF Energi AS, Department of Thermal Energy

7465 Trondheim, Norway, Christian.Schlemminger@sintef.no & Michael.Bantle@sintef.no

[(b)] Norwegian University of Science and Technology, Department of Energy and Process Technology

[(c)] Epcon Evaporation Technology, 7079 Flatåsen, Norway, ke@epcon.org

## ABSTRACT

Mechanical Vapour Recompression (MVR) is an open loop heat pump system using water (R718) as working fluid, one of the most abundant and safest refrigerant on the planet. The concept can significantly reduce the energy consumption for steam based processes like drying, pasteurization, evaporation or distillation but also for steam production itself. However, the compression technology is commonly not cost efficient especially for small scale productions in the capacity range from 500 kW to 4 MW.

A two stage turbo-compression system was developed and tested based on mass produced automotive turbocharger technology. The turbo-compressor of the first stage reached a pressure ratio of 1.69 and is designed for a mass flow of 400-600 kg/h superheated steam. The second stage turbo-compressor had an identical design and achieved the same pressure ratio. Between compression stage one and two de-superheating is applied by water injection. With the developed system it is possible to compress superheated steam from atmospheric pressure to above 2.8 bar, where it can be condensed at a temperature of 131°C. The COP of the performed investigation was 7.8, when the achievable condensation energy is compared to the total amount of energy supplied to the system. The compressor efficiency is around 70% of the Carnot efficiency.

**Keywords:** R718, Energy Efficiency, Superheated Steam Drying, Turbomachinery, COP

## 1. INTRODUCTION

The limitation of global warming and the related reduction of greenhouse gas emission forces the thermal process industry to consider alternative, preferable renewable, energy sources in order to substitute fossil energy carriers. This development is, among others, driven by the outcome of the Paris climate conference in 2015 and the expected impact on legislative and national regulation. With this background the market potential of high temperature heat pumps is increasing, however industrial phase in of this technology is currently limited by the low technological readiness level of heat pumps operating with a heat sink of higher than 100°C (Elmengaard et al, 2017, IEA, 2014) and the relative high investments costs (when compared with fossil driven boiler/burner technology). The potential for implementing high temperature heat pumps at process temperatures between 100 °C and 150 °C was estimated to be 175 TWh for just Europe (Wolf, 2014).

Mechanical Vapour Recompression (MVR) is a special sub-application of heat pumps in which the evaporator is replaced by a thermal process which supplies low-pressure excess steam. This excess steam is then compressed to a higher pressure so that its condensation energy can be utilized at a higher temperature level so that it can be used re-heat a process fluid. Distillation columns, Evaporators, pasteurization processes and steam-driers are ideal processes for the MVR implementation. The concept is illustrated on the example of a superheated steam drier in Figure 1.

The application of MVR for these processes can reduce the specific energy consumption by over 75%. However, MVR technology is normally only applied for thermal capacities higher than 10 MW (Bantle et al, 2017), because the specific investment costs (per kW installed capacity) for smaller systems can be as high as 1000€/kW. It is outlined in Elmegaard (2017) that heat pump systems require investment costs between 100 – 200 €/kW in order to be an economic feasible alternative for the industry. The steam compressor technology

DOI: 10.18462/iir.gl.2018.1157

is currently the main cost component in MVR and for thermal process with an capacity between 500 kW – 4 MW a cost efficient compressor technology is not available at the market (Elmegaard, 2017).

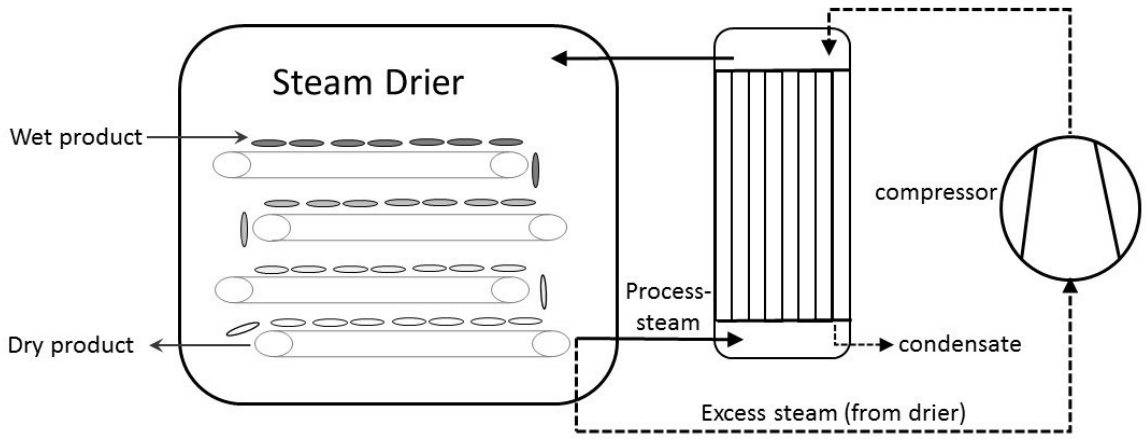


Figure 1: Simplified schematic layout for superheated steam drier with energy recovery through mechanical vapour recompression.

The turbo-compressors technology is considered as a potentially cost-effective and efficient alternative to conventional compressors (Bantle et al., 2014; Weel et al., 2013). Turbo-compressors are used in nearly every diesel vehicle for air compression. Bantle et al. (2017) demonstrated that the operating conditions were stable for steam compression. At a rotational speed of 90 000 rpm a standard automotive unit of a turbo-compressor achieved a pressure ratio of 2.4 with an isentropic efficiency of 72% and a mass flow of 450 kg/h. The measured efficiency was close to) the expected performance (3%-points lower) at the design point of the unit. The COP of MVR equipped with this prototype would be 11.5, however the temperature increase (between thermal process and the condenser) would be limited to around 23 Kelvin. It must be outlined that such a performance could be also achieved with conventional compressor technology, but the return of investment for the turbo-compressor system will be less than a year even for countries with a high price ratio between electricity and fossil fuel/gas (e.g. Germany).

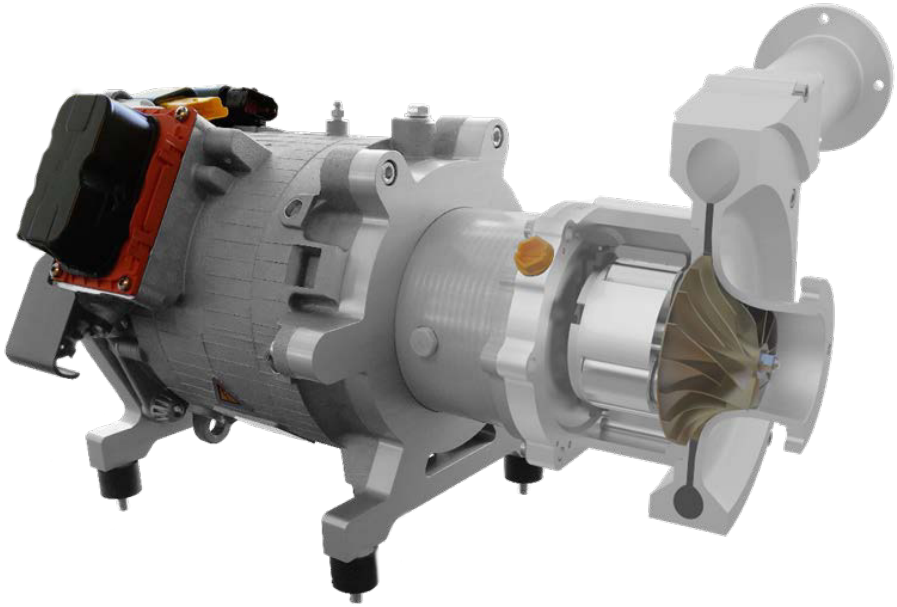

Figure 2: Section view through the prototype of the turbo-compressor including motor and gearbox.

For this study a two stage turbo-compressor system was investigate with the aim to demonstrate the performance of two identically constructed prototypes when operated in series. The basic structure of the

prototype is described in this article, the experimental setup and the results of the test are included and future challenges are discussed.

## 2. METHODS

### 2.1 Design of the turbo-compressor prototype

The turbo-compressors used in this experiment are a further development of a conventional radial turbocharger from the automotive industry. The patented design has been adapted by the manufacturer (Rotrex A/S, Copenhagen, Denmark) for use in steam compression (see Figure 2). For this purpose, the impeller was designed in titanium; the rest of the casting is done in alumina. The carbon sealing between the compression chamber and the planetary traction drive was reinforced to ensure a better sealing. The aim of these modifications was to increase the achievable pressure ratio at a high efficiency and to improve the durability for long-term, continuous operation. At the design point $N_{ref}$ =68000 rpm, the volume flow of air on the low-pressure side is $Vc_{ref} = 0.27 m^3/sec$ at $T_{ref} = 288.15$ K and $p_{ref} = 1.013$ bar. The compression ratio achieved is $PR_{ref} = 2.72$.The isentropic efficiency of the compressor was calculated to be 74.5%. Depending on the temperature and pressure of the steam on the low-pressure side, it will be possible to achieve a thermal capacity of up to 300 kW while achieving a temperature lift of approximately 25 Kelvin (between high and low-pressure saturation temperatures).

A planetary traction gearbox is mounted on the drive shaft of the turbo-compressor that enables a high transmission ratio. The transmission ratio is 7.5 at a mechanical efficiency of 98% under full load. The planetary gearbox is lubricated by means of an internal oil pump and at the same time cooled by an external oil cooler.

A 650 Volt DC-motor which can deliver up to 12 000 rpm is placed directly on the drive shaft of the gearbox, thus a rotational speed of up to 90 000 rpm can be achieved at the impeller. The motor is driven by an inverter that delivers 59 kilowatts. The total weight of the complete unit (turbo-compressor, gearbox, DC-motor) is about 40 kg and the dimensions are 50 cm in length, 40 cm in width and 35 cm in height, which illustrates the compact and light weighted design.

Two identical turbo-compressors were installed in series in order to achieve a 2-stage compression with the aim to reach a pressure ratio of 3. The theoretical design conditions can be found in Table 1 and the aim to investigation was to evaluate if these conditions can be achieved using identical impeller designs.

Table 1: Operation parameter for first and second stage with identical impeller design.

| | Impeller 1: Low stage | Impeller 2: High stage |
|---|---|---|
| Inlet conditions: | $\dot{m}_{\text{in}} = 0.081 - 0.116$ kg/s<br>$\dot{V}_{\text{in}} = 499 - 734$ m$^3$/h<br>$p_{\text{in}} = 1.02$ bar ± 0.01<br>$T_{\text{in}} = 115 - 120$ °C | $\dot{m}_{\text{in}} = 0.085 - 0.125$ kg/s<br>$\dot{V}_{\text{in}} = 401 - 497$ m$^3$/h<br>$p_{\text{in}} = 1.36 - 1.65$ bar ± 0.01<br>$T_{\text{in}} = 120 - 130$ °C |
| Rotational speed: | $n = 54000 - 72000$ rpm | $n = 54000 - 72000$ rpm |
| Pressure ratio (max): | PR = 1.7 | PR = 1.7 |
| Expected isentropic efficiency: | $\eta_{\text{is}} = 0.80 - 0.75$ | $\eta_{\text{is}} = 0.74 - 0.70$ |

### 2.2 Test-setup for the experiments

The two turbo-compressors were installed in an MVR heat pump unit in which it was possible to by-pass the condenser (see Figure 4). The inlet of the first stage turbo-compressor is connected to an MVR-condenser which is operated as steam supply unit. The pressure in the condenser is approximately at atmospheric condition since the purge valve is open to the ambient. Temperature, pressure, mass flow and oxygen content is measured at the inlet and outlet of each compressor. Between the first and second stage a controlled amount of water is injected in order to de-superheat the working fluid. Water injection is also used to de-superheat after the expansion valve in order to reduce the thermal stress to the condenser. All piping work was constructed in a way that the thermal expansion is compensated during start-up and operation, so that the mechanical stress to the compressor is reduced to a minimum. The piping is insulated by 50mm mineral wool (k=0.05 W/m·K).

Both compressors are controlled by DC-Inverters, seperate 3-phase power meters were installed upstream each DC-Inverter. Gearbox and motor of the turbo-compressors are cooled by water and an energy-flow meter monitored the required cooling. An internal steam cooler in the MVR-condenser cooled the total system by de-superheating the working fluid before the inlet to the first stage. Also, here the energy flow is recorded. The

DOI: 10.18462/iir.gl.2018.1157

inlet temperature to the first and second turbo-compressor was controlled to 10 K superheat, depending on the pressure. The system is fully automated and controlled by a self-developed software program.

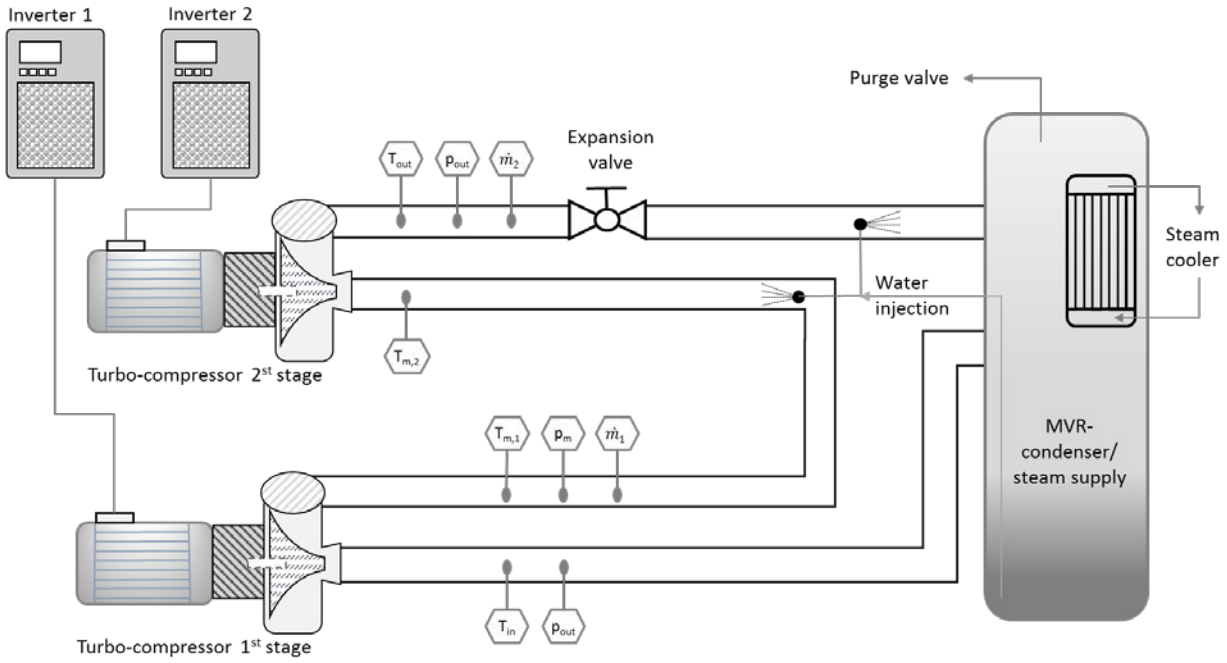


Figure 3: Principle setup of the 2 stage turbo-compression test son the MVR heat pump system.

### 2.3 Start-up of the system

The impeller of the turbo-compressor is quite sensitive to particle or droplet impact at higher speed and the inlet conditions of the working fluid need therefore to be superheated in order to avoid liquid droplets. Hence the system cannot be started with saturated steam and needs therefore to be heated to above 100°C (at atmospheric pressure) before water/steam is injected. Since the turbo-compressors are originally designed for air the start-up or preheating of the system can therefore be performed with air as working fluid. The turbo-compressors are hereby started when the system is dry and filled with ambient air. The system is then heated up the excess heat of the compressors until the coldest point (inlet to first compressors) reaches a stable temperature above 100°C. Then water is injected through the de-superheaters which is immediately evaporated and filling the system with superheated steam by replacing the air through the purge valve of the MVR-condenser. The start-up procedure takes around 45 minutes and after that the system is completely filled with steam (oxygen content <0.1%).

### 2.4 Performed tests

For this study the turbo-compressor speed in both units was set to 54000 rpm, 63000 rpm and 72000 rpm in order evaluate and achieve an overall pressure ratio of 3. In order to compare the conducted tests with the performance predicted the following correction were performed:

Relative flow correction:

$$V_C = \frac{\dot{V}_{in}\sqrt{ZRT/Z_{ref}R_{ref}T_{ref}}}{\dot{V}c_{ref}\ (p/p_{ref})}$$

Reduced ratio:

$$PR_C = \frac{PR - 1}{PR_{ref} - 1}$$

Relative speed correction:

$$N_C = \frac{N\sqrt{ZRT/Z_{ref}R_{ref}T_{ref}}}{N_{ref}}$$

DOI: 10.18462/iir.gl.2018.1157

Here the reference conditions as described in paragraph 2.1 were applied. The air gas constant and compressibility was $R_{air}$=287.05 J/kgK and $R_{air}$=1, respectively. The relevant superheated steam properties were calculated using REFPROP version 9.

## 3. RESULTS

The MVR heat pump with the turbo-compressor was operated for several days under various operating conditions. The initial tests were carried out at low capacity (about 50% of the maximum capacity) in order to make sure that the system was stable and to make the necessary fine adjustment. Then the compressor was operated at full load (60-80% of maximum capacity). In Table 2 the operation conditioned are summarized.
Figure 4 shows the achieved operational conditions of the turbo-compressors during the pilot tests. The points illustrated in the figure were held for at least 2 hours and the isentropic efficiency is based on the average compressor performance during this time. The achieved mass flow at the highest capacity was 420 kg/h in the first stage and the isentropic efficiency of the turbo-compressor was constant at 73%. In the second stage the mass flow increased by the water injection from approximately 306 kg/h at 54000 rpm to 450 kg/h at 75000 rpm; here the isentropic efficiency decreased from 75% to 70%.

Table 2: Operating conditions of two stage MVR heat pump

| | Impeller 1: Low stage | Impeller 2: High stage |
|---|---|---|
| 60% | | |
| Inlet conditions: | $\dot{m}_{\mathrm{in}} = 0.081\ \mathrm{kg/s}$<br>$\dot{V}_{\mathrm{in}} = 499\ \mathrm{m^3/h}$<br>$p_{\mathrm{in}} = 1.02\ \mathrm{bar} \pm 0.01$<br>$T_{\mathrm{in}} = 115\ °\mathrm{C}$ | $\dot{m}_{\mathrm{in}} = 0.085\ \mathrm{kg/s}$<br>$\dot{V}_{\mathrm{in}} = 401\ \mathrm{m^3/h}$<br>$p_{\mathrm{in}} = 1.36\ \mathrm{bar} \pm 0.01$<br>$T_{\mathrm{in}} = 120\ °\mathrm{C}$ |
| Outlet conditions: | $p_{\mathrm{out}} = 1.41\ \mathrm{bar} \pm 0.02$<br>$T_{\mathrm{out}} = 152\ °\mathrm{C}$ | $p_{\mathrm{out}} = 1.87\ \mathrm{bar} \pm 0.02$<br>$T_{\mathrm{out}} = 161\ °\mathrm{C}$ |
| Rotational speed: | $N = 54000\ \mathrm{rpm}$ | $N = 54000\ \mathrm{rpm}$ |
| Pressure ratio: | $\mathrm{PR} = 1.38$ | $\mathrm{PR} = 1.38$ |
| Isentropic efficiency: | $\eta_{\mathrm{is}} = 0.78$ | $\eta_{\mathrm{is}} = 0.75$ |
| Electric power consumption: | $P_{\mathrm{el}} = 9.6\ kW$ | $P_{\mathrm{el}} = 9.9\ kW$ |
| 70% | | |
| Inlet conditions: | $\dot{m}_{\mathrm{in}} = 0.098\ \mathrm{kg/s}$<br>$\dot{V}_{\mathrm{in}} = 613\ \mathrm{m^3/h}$<br>$p_{\mathrm{in}} = 1.02\ \mathrm{bar} \pm 0.01$<br>$T_{\mathrm{in}} = 116\ °\mathrm{C}$ | $\dot{m}_{\mathrm{in}} = 0.105\ \mathrm{kg/s}$<br>$\dot{V}_{\mathrm{in}} = 455\ \mathrm{m^3/h}$<br>$p_{\mathrm{in}} = 1.48\ \mathrm{bar} \pm 0.01$<br>$T_{\mathrm{in}} = 121\ °\mathrm{C}$ |
| Outlet conditions: | $p_{\mathrm{out}} = 1.55\ \mathrm{bar} \pm 0.02$<br>$T_{\mathrm{out}} = 168\ °\mathrm{C}$ | $p_{\mathrm{out}} = 2.26\ \mathrm{bar} \pm 0.02$<br>$T_{\mathrm{out}} = 180\ °\mathrm{C}$ |
| Rotational speed: | $N = 63000\ \mathrm{rpm}$ | $N = 63000\ \mathrm{rpm}$ |
| Pressure ratio: | $\mathrm{PR} = 1.53$ | $\mathrm{PR} = 1.53$ |
| Isentropic efficiency: | $\eta_{\mathrm{is}} = 0.76$ | $\eta_{\mathrm{is}} = 0.69$ |
| Electric power consumption: | $P_{\mathrm{el}} = 14.3\ kW$ | $P_{\mathrm{el}} = 15.1\ kW$ |
| 80% | | |
| Inlet conditions: | $\dot{m}_{\mathrm{in}} = 0.116\ \mathrm{kg/s}$<br>$\dot{V}_{\mathrm{in}} = 734\ \mathrm{m^3/h}$<br>$p_{\mathrm{in}} = 1.02\ \mathrm{bar} \pm 0.01$<br>$T_{\mathrm{in}} = 120\ °\mathrm{C}$ | $\dot{m}_{\mathrm{in}} = 0.125\ \mathrm{kg/s}$<br>$\dot{V}_{\mathrm{in}} = 497\ \mathrm{m^3/h}$<br>$p_{\mathrm{in}} = 1.65\ \mathrm{bar} \pm 0.02$<br>$T_{\mathrm{in}} = 130\ °\mathrm{C}$ |
| Outlet conditions: | $p_{\mathrm{out}} = 1.73\ \mathrm{bar} \pm 0.01$<br>$T_{\mathrm{out}} = 191\ °\mathrm{C}$ | $p_{\mathrm{out}} = 2.79\ \mathrm{bar} \pm 0.02$<br>$T_{\mathrm{out}} = 205\ °\mathrm{C}$ |
| Rotational speed: | $N = 72000\ \mathrm{rpm}$ | $N = 72000\ \mathrm{rpm}$ |
| Pressure ratio: | $\mathrm{PR} = 1.69$ | $\mathrm{PR} = 1.69$ |
| Isentropic efficiency: | $\eta_{\mathrm{is}} = 0.73$ | $\eta_{\mathrm{is}} = 0.70$ |
| Electric power consumption: | $P_{\mathrm{el}} = 21.0\ kW$ | $P_{\mathrm{el}} = 22.5\ kW$ |

DOI: 10.18462/iir.gl.2018.1157

The compressor map in Figure 4 shows the corrected pressure ratio as a function of the relative corrected volume flow. For both stages an almost linear trendline of the performance from 52000 rpm to 72000 rpm is achieved. The trendline in the second stage has a larger gradient compared to the first stage. This is caused by the high-density change of water-vapor with increased pressure.

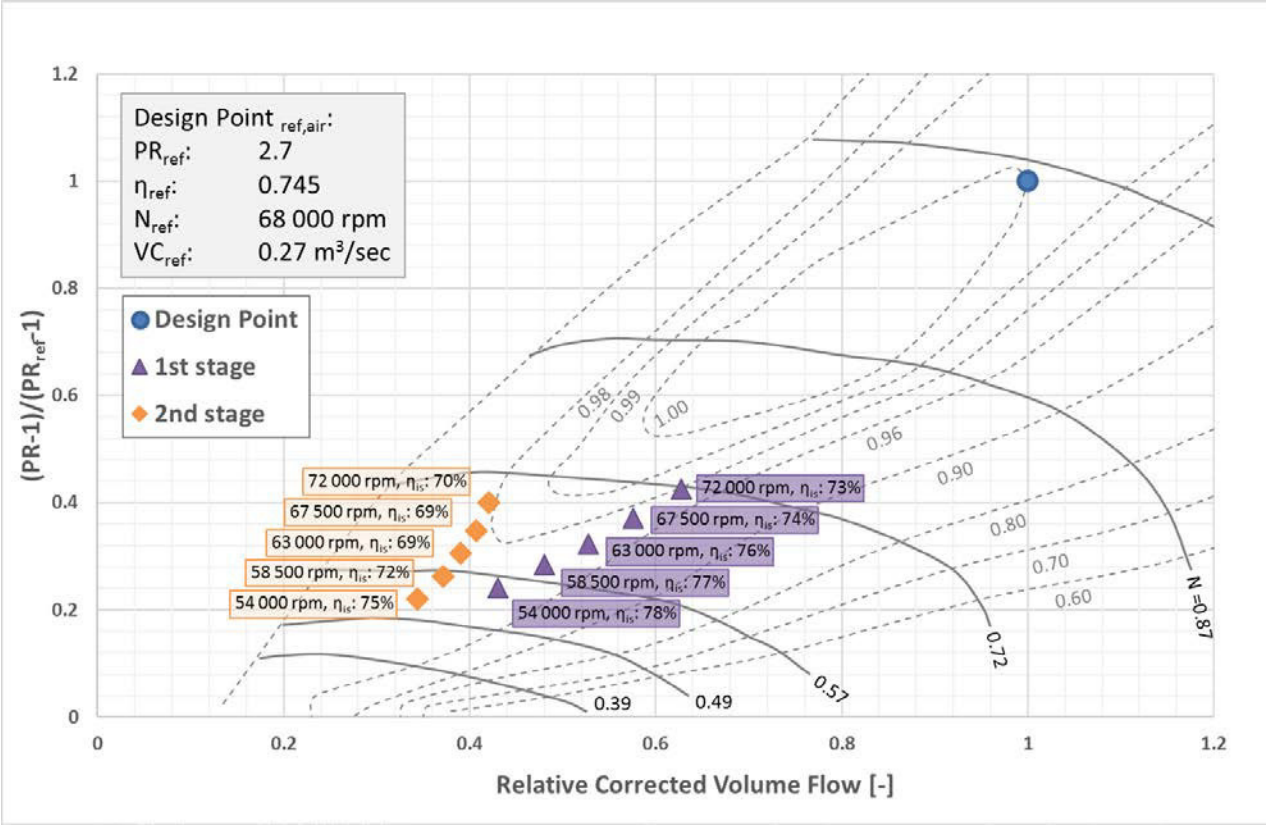


Figure 4: Achieved, stable operational conditions of the turbo-compressors in the first and second stage during the pilot-tests.

## 4. DISCUSSION

The performed tests demonstrated that it is possible to achieve stable operation conditions in the investigated setup and with the used of identical turbo-compressors. The impeller speed was the same for both turbo-compressors and was never higher than 80% of the maximum design speed. The achieved overall pressured ratio was around 2.8 and resulted from pressure ration of 1.69 and 1.69 in the first and second stage respectively. It must be noted that the volume flow in the second stage was significantly lower compare to the first stage even when the mass flow was increased by water injection after the first stage. This is a result of the specific volume of steam which is reduced with increased pressure. As a consequence, the second turbo-compressor operated closer to the surge line of the unit. Ideally the design of the impeller should be adjusted to the targeted pressure and volume flow in each stage. However, that would require a more modular construction of the turbo-compressors.

The performance of each compressor from 54000 rpm to 72000 rpm seems to have a clear trendline in the compressor map. However, it is difficult to predict a trend based on five points only. On the other hand, the identified trend helps to predict if the system would be able to operate stable at high speed. It seems reasonable to assume that the system could be also operated at a speed of 81000 rpm or even 90000rpm. At this point a pressure ratio of 4 (at 81000 rpm) and a pressure ratio 5.5 (at 90000 rpm) could be achieved. That would also mean that the second stage turbo-compressor would operate close to the surge condition of the system and it is currently difficult to estimate if the system can be operated stable at such a high-pressure ratio.

The achieved pressure ratios were almost identical in stage one and stage two, since no pressure control device is installed between the two units. The energy input in the second stage was on the other hand slightly higher (up to 10 % increased) when compared to the energy consumption of the first stage. This might be caused by the fact that the two turbo-compressors were operation at different areas in the compressor map and that the second compressor had an increase mass flow due to the water injection.

In the compressor map it can be seen that the constant speed lines of the turbo-charger are flat and almost horizontal in some parts of the map. This results in a quite sensitive surge-behaviour of the turbo-compressors even when they are operated in a stable point "in the middle" of the map. Slight pressure change can cause the system to turn fast into surge-operation in which the turbo-compressors no longer operate stable. It is therefore good advice to operate the system closer to the choke area of the compressor map.
The applied de-superheating concept was based on the injection of water and required a precise control of the added amount of water in order to prevent sub-cooling and droplet formation. The disadvantageous of such water spraying systems is that the evaporation time of the water droplets require a relative long pipe length. Hence the system has special space requirements in industrial applications and while the turbo-compressors are compact and small the required pipe work could limit the industrial implementation. For an industrialized solution it might therefore be necessary to investigate more compact but still cost effective de-superheating concepts.
The used cooling oil (Rotrex, SX 150) in the gearbox has a maximum allowed temperature of 140°C. In the investigation operation the oil temperature never exceeded 130°C in the second compressor. However, with increased impeller speed it will be possible to increase the performance of the system even more, but currently it seems that the limiting factor of the turbo-compressor system is the oil temperature. Improved oil cooling could be achieved by a larger oil pump.
During the operation of the turbo-compressors a very small amount of steam was penetrating into the gearbox of the turbo-compressor. This created an emulsion of the cooling oil and could potentially result in system failure. However, since the temperature of the cooling oil reaches more than 100 °C the water was evaporated out of the emulsion in the oil container. It was also observed that the cooling was improved once a small amount of water was present in the oil. The pure oil was analysed after the test and did not show degradation or other negative impact. Fur future applications it must therefore be evaluated if it is necessary to improve the sealing between gearbox and impeller room even more or if a certain water penetration can be accepted. The performed investigation indicate that a certain steam penetration is acceptable.
The COP of the performed investigation is 7.8, when the achievable condensation energy is compared to the total amount of energy supplied to the inverters. This COP value includes the losses in the inverter, motor and gearbox. Without these losses the COP is 9.4, which is the COP when only the isentropic losses of compression are considered. The ideal Carnot COP for the investigated temperature range is 13.4, which means that the isentropic efficiency is around 70% of the Carnot efficiency and the system efficiency (including losses of inverter, motor and gearbox) is still 58% of the Carnot efficiency This outlines of course also the general advantage of R718 as working fluid.
Cost estimations for industrial systems based on the presented technology are at the current technological readiness level only rough estimates and need to be verified further. However, the investments costs in the turbo-compressor systems are dominated by the costs for inverter and motor. Based on the unit costs for this investigation the compressor costs can be estimated to around 50€/kW installed condenser capacity. The costs for the complete MVR heat pump can be estimated to be approximately 200 €/kW; this estimation is based on the costs for the current investigation. Further developments will focus on increasing the size of the turbo-compressor and it is expected that investment costs for a complete heat pump system can be reduced further, when more standardized technology (e.g. for de-superheating) is implemented. However, even with the current cost situation the technology results in acceptable return of investment periods also for countries with high electricity to gas prize ratios.

## 5. CONCLUSIONS

Two identical turbo-compressor prototypes were used to test two stage vapor compression for the application in an MVR heat pump. The development has the potential to be a very cost-efficient compression technology for industrial high temperature heat pumps. The turbo-compressor of the first stage reached a pressure ratio of 1.69 and is designed for a mass flow of 400-600 kg/h superheated steam. The second stage turbo-compressor had an identical design and achieved a pressure ration of 1.69. Between compression stage one and two de-superheating is applied by water injection. With the developed system it is possible to compress superheated steam from atmospheric pressure to 2.8 bar, where it can be condensed at a temperature of 131°C. The COP of the performed investigation was 7.8, when the achievable condensation energy is compared to the total amount of energy supplied to the system. The compressor efficiency is around 70% of the Carnot efficiency.

The investigation showed that the two turbo-compressors were operated at different areas in the compressor map and each compressor showed a clear trendline. Based on this it seems reasonable to assume that a higher performance can be achieved with the current prototype system. However, the limiting factor is the danger of unstable operation especially of the second compression stage close to the surge condition. Another limitation might be the temperature limitations and stability of the cooling oil in the gearbox.
The costs for the complete MVR heat pump can be estimated to be approximately 200 €/kW; this estimation is based on the costs for the current installation. Further developments will focus on increasing the size of the turbo-compressor and it is expected that investment costs for a complete heat pump system can be reduced further, when more standardized technology (e.g. for de-superheating) is implemented. However, even with the current cost situation the technology results in acceptable return of investment periods also for countries with high electricity to gas prize ratios.

## ACKNOWLEDGEMENTS

The project has received funding from the European Union's Horizon 2020 programme for energy efficiency and innovation action under grant agreement No. 723576.

## REFERENCES

Bantle, M., I. Tolstorebrov, and A. Hafner, Energierückgewinnung mittels Brüden-Kompression in Trocknungssystemen mit überhitztem Dampf in DKV-Tagungsbericht 2014 Düsseldorf - 19. – 21. November 2014 2014, DKV - Deutscher Kälte- und Klimatechnischer Verein: Düsseldorf/Germany.

Elmegaard, B., Zühlsdorf, B., Reinholdt, L., Bantle, M. (Eds.), 2017. International Workshop on High Temperature Heat Pumps, in: Book of Presentations of the International Workshop in High Temperature Heat Pumps. Copenhagen.

IEA Heat Pump Centre, 2014. Annex 35: Application of Industrial Heat Pumps - Final Report (No. Report HPP-AN35-1&2). Borås, Sweden.

Madsboell, H., Weel, M., Kolstrup, A., 2015. Development of a Water Vapor Compressor for High Temperature Heat Pump Applications, in: Proceedings of International Congress on Refrigeration. IIR, Yokohama, Japan, p. Paper ID 845.

Weel, M., et al. Energy efficient drying with a novel turbo-compressor based high-temperature heat pump. in 6th Nordic Drying Conference, 5.-7. June 2013. 2013. Copenhaben, Denmark.

Wolf, S., et al. (2014). Analyse des Potenzials von Industriewärmepumen in Deutschland (in German) Forschungsbericht. Universität Stuttgart, Institut für Energiewirtschaft und Rationelle Energieanwendung